Neural Oscillations
and the Decoding of Sensory Information

Thesis by

Javier Perez-Orive

In Partial Fulfillment of the Requirements

for the Degree of

Doctor of Philosophy

California Institute of Technology

Pasadena, California

2004

(Defended May 7, 2004)

This dissertation is dedicated

to my daughters Claudia and Daniela,

for the infinite love and happiness they make me feel

Acknowledgments

I would like to thank my advisor Gilles Laurent, for his ideas and for introducing me into this fascinating area of science. I would also like to thank my Thesis Committee Members: John Allman, Mark Konishi, Pietro Perona and Thanos Siapas, for all their time and interest in this project. I am also grateful to the Alfred P. Sloan Foundation and the Swartz Foundation, who provided me with financial support for my Ph.D.

I also need to thank all the past and present members of the Laurent Lab, and particularly Stijn Cassenaer, Sarah Farivar, Vivek Jayaraman, Roni Jortner, Ofer Mazor and Ben Rubin, for all those discussions, scientific and otherwise, and for making my Ph.D. experience a very enriching and enjoyable one. Thanks also to my fellow CNS-1st-year classmates, for making my first year at Caltech a really interesting and exciting one.

I would also like to acknowledge here great teachers I have had the good fortune of learning from throughout my life and who have had decisive influences in shaping my academic path to Caltech: Angelica Takahashi de Mestre and Asdrubal Ayala (each of whom inspired in me the great love of biology and mathematics, respectively, that led me to study Biomedical Engineering), Raul Ulloa, Alejandro Navarrete, Ruth Mayagoitia (who introduced me into the fascinating field of Neural Prostheses that led to my M.S. degree) and Hillel Chiel (whose outstanding course on Computational Neuroscience sparked the interest which ultimately led to my Ph.D. at Caltech).

Of course I need to thank my mother, my father and my brother Joaquin, to whom I owe all that I am. And finally, I need to give the biggest 'thank you' of all to my wife Claudia, my teammate in life, who not only provided me with the emotional and intellectual support that made possible this Ph.D., but who also gave me Claudia and Daniela, the biggest joys one could possible have. Las amo a las tres con todo mi corazón.

Abstract

An important problem in neuroscience is to understand how the brain encodes information. A hypothesis is that differences in the timing of action potentials, reflecting synchronization changes among neuronal ensembles —often occurring in the context of oscillations— can be meaningful to downstream neurons detecting coincident input. Several properties, such as active conductances, feedforward inhibition and oscillatory input, could potentially influence whether a neuron acts as a coincidence detector. Although different neural circuits in various animal groups will use different strategies to solve somewhat varying problems, there will also be many powerful solutions to coding problems that will be used repeatedly across diverse processing stages and animal phyla. The insect olfactory system, sharing many design similarities with other systems while having a reduced complexity, provides an excellent model in which to study the functional interactions of all these coding features.

This dissertation focuses on the decoding of olfactory information by the mushroom body (MB), the second relay of the insect olfactory system, which receives oscillating input from the antennal lobe (the first relay, analogous to the vertebrate olfactory bulb). Kenyon cells (KCs), the intrinsic neurons of the MB, are found to respond very specifically to odors. These responses typically consist of one or two reliable action potentials, phase-locked to the global oscillations, over extremely low baseline firing rates. This leads to a dramatic sparsening of the olfactory representation in the MB. Several circuit and intrinsic properties are found to take part in this transformation.

Feedforward inhibition contributes to odor specificity and sparseness: blocking inhibitory input to the KCs broadened their odor tuning and abolished their phase-locking, supporting the idea that feedforward inhibition limits the temporal window over which KCs integrate their inputs. Voltage-dependent conductances contribute to a supralinear summation of coincident postsynaptic potentials and a reduction of their half-widths, indicating that KC intrinsic properties further contribute to coincidence detection. Taken together, these results indicate that oscillations serve as a framework on which KCs act as coincidence detectors and sparsen the olfactory representation. Abolishing the input oscillations disrupts KC odor responses, decreasing their specificity and the sparseness in the MB.

The work in this dissertation describes a mechanism for decoding timing information and indicates that not all spikes are equally relevant to downstream neurons, their specific relevance depending on whether they are correlated, within a specific phase of an oscillation cycle, with other input spikes. These general features can also provide useful insights into neural coding in more complex neural systems, where all the mechanisms described here have been separately observed. This work illustrates how these mechanisms can interact to code sensory information and bring about drastic transformations of neural representations, increasing our understanding of how nervous systems can process information.

Table of Contents

Abbreviations

AL	antennal lobe
AN	antennal nerve
ATP	adenosine triphosphate
cAMP	cyclic adenosine monophosphate
CAP	compound action potential
CBL	cell body layer
EEG	electroencephalogram
EPSP	excitatory postsynaptic potential
FFT	fast Fourier transform
GABA	γ-aminobutyric acid
GTP	guanosine triphosphate
IPSP	inhibitory postsynaptic potential
KC	Kenyon cell
LFP	local field potential
LH	lateral horn
LHI	lateral horn interneuron
LN	local neuron
LP	lateral protocerebrum
MB	mushroom body
MC	mitral cell

OB	olfactory bulb
OR	olfactory receptor
ORN	olfactory receptor neuron
PC	pyramidal cell
PCT	picrotoxin
Ped	pedunculus
PN	projection neuron
PSTH	peristimulus time histogram
SA	electrical stimulus amplitude
shi^{ts1}	temperature-sensitive *shibire* transgene

1 Introduction

1.1 Neural Coding

An important issue concerning neuroscience today is to understand the way in which the brain encodes, processes and transforms sensory information. A way of approaching this problem is to study what aspects of a train of action potentials sent from a given neuron to another convey information about a particular sensory stimulus. In other words, how do neurons communicate? And what information do they select or filter out of their communications? In all likelihood, the answers to these questions will be somewhat different for different sensory modalities, stages in the processing of the information and animal groups. However, there will also be many powerful solutions to coding problems that will be used repeatedly by nervous systems across diverse information processing tasks and animal phyla.

Several studies of sensory systems have found that the mean firing rate of neurons contains information about the stimulus [e.g., (Adrian, 1926; Hubel and Wiesel, 1962; Britten et al., 1992; Parker and Newsome, 1998)]. An underlying assumption in these studies is that a downstream neuron receiving this information conducts simple spatial or temporal averaging of its inputs, disregarding any precise correlations between them (Shadlen and Newsome, 1994). On the other hand, as will be discussed below, there is evidence from different systems and sensory modalities suggesting that relevant information can be conveyed by the synchronized firing of neuronal ensembles, and that

small differences in the timing of action potentials can be meaningful to downstream neurons.

Local field potential (LFP) and electroencephalogram (EEG) measurements reflect the summed activity of populations of neurons. Oscillatory activity has been observed in LFP and EEG recordings obtained under different conditions in a wide variety of animal groups and reveals the ubiquitous existence of synchronization in groups of neurons (Adrian, 1942; Steriade et al., 1993; Laurent and Naraghi, 1994; Bragin et al., 1995; Siapas and Wilson, 1998; Rodriguez et al., 1999; Csibra et al., 2000; Lam et al., 2000; Fries et al., 2001; Buzsaki, 2002). Although correlated neural activity is not necessarily periodic, most cases of neural synchronization that have been studied involve oscillations (possibly because this oscillatory activity is easier to detect than non oscillatory synchronizations).

A number of roles have been proposed for neuronal synchronization. For example, gamma oscillations (typically considered to be in the 30-90 Hz frequency band) have been linked to attention (Fries et al., 2001) and processes involved in managing expectations and predictions about coming sensory stimuli (Engel et al., 2001; Salinas and Sejnowski, 2001), binding of distributed representations of perceptual objects (von der Malsburg and Schneider, 1986; Gray et al., 1989; Engel et al., 1991; Singer and Gray, 1995; Rodriguez et al., 1999; Csibra et al., 2000), episodic (Sederberg et al., 2003) and working (Pesaran et al., 2002; Howard et al., 2003) memories; hippocampal place cells are known to phase-lock to theta oscillations (O'Keefe and Recce, 1993), and internally

generated synchronized spikes have been linked to cognitive motor processes (Riehle et al., 1997) and specific behavioral events (Abeles et al., 1993; Vaadia et al., 1995; Prut et al., 1998). However, a thorough understanding of the functional role of oscillatory synchronization has remained lacking due to the immense complexity of the mammalian nervous systems in which the previous studies have been performed.

Several studies have focused on studying the emergence of larger increases in synchronization than would be expected by chance, and correlating those synchronous episodes with cognitive or behavioral events [e.g., (Vaadia et al., 1995; Riehle et al., 1997; Steinmetz et al., 2000)]. Yet in order to fully understand how information is transmitted and processed by neurons it is necessary to study the downstream neurons which are using that information. Only by establishing how downstream neurons decode their inputs, that is, what are the specific properties of the incoming signal that they are responsive to, can we know where the relevant information is actually contained. (Just as the width of an action potential contains information about the temperature of the brain, this feature is apparently not used to decode temperature by neurons. Thus, it is important to distinguish information that is actually relevant to the downstream decoders from that available to an ideal observer.)

In this sense, a critical question to determine is the temporal window in which a neuron integrates its inputs. Neurons that have a strong preference for responding only to inputs that are received during a relatively short interval [for instance, compared to their average interspike interval (Konig et al., 1996)], will act as "coincidence detectors." Conversely,

"temporal integrator" neurons are insensitive to precise coincidences, integrating their inputs during longer intervals. Whether a neuron acts as a coincidence detector or a temporal integrator will have important implications on the nature of the code that it uses. Neurons integrating over long intervals will be insensitive to correlated inputs, and will only respond to the firing rate averaged over their integration window. On the other hand, if neurons respond selectively to coincident input, it implies that the relevant conveyor of information will be the correlated firing of its inputs. Several theoretical studies have proposed that cortical neurons act as coincidence detectors (Abeles, 1982; Softky and Koch, 1993; Konig et al., 1996), whereas others have argued that they effectively behave as temporal integrators (Shadlen and Newsome, 1994, 1998). Yet, in large part due to the complexity of mammalian cortex, there is still a lack of experimental evidence to conclusively settle this issue. More realistically, one can imagine that all possibilities exist and that specific neural circuits, under specific conditions, can behave as either coincidence detectors or integrators. In this sense, what is important to determine is how each coding-decoding mode actually works, and what computation it accomplishes.

Different intrinsic and circuit properties can potentially determine whether a neuron is sensitive to coincident input. Theoretical studies have demonstrated that the membrane time constant of a neuron can have a critical influence on its preference for coincident input, specifically relating the half-width of an excitatory postsynaptic potential (EPSP) to the minimal temporal structure it can resolve in its input [(Kempter et al., 1998); see also (Abeles, 1982; Softky and Koch, 1993; Konig et al., 1996)]. Active dendritic depolarizing and repolarizing conductances can greatly reduce the duration of EPSPs,

limiting the temporal window over which inputs are integrated [(Laurent, 1990; Fricker and Miles, 2000; Galarreta and Hestrin, 2001; Ariav et al., 2003); see also (Johnston et al., 1996; Fricker and Miles, 2001)] and provoking a supralinear summation of coincident input (Margulis and Tang, 1998). The circuit that a neuron belongs to can also have a strong influence on its integrative properties. For instance, feedforward inhibitory input can limit the window available for temporal summation, as has been shown experimentally in hippocampal and medial superior olive brain slices (Grothe and Sanes, 1994; Pouille and Scanziani, 2001), and suggested for other auditory systems (Fujita and Konishi, 1991; Wehr and Zador, 2003).

Although several of the coding issues mentioned above (oscillatory activity, sensitivity to correlated spiking through coincidence detection, intrinsic and circuit integrative properties) have been considered in isolation in the past, the way in which all of them may act in concert to convey a neural system with important functional properties has not been studied. As will be discussed below, the insect olfactory system provides an excellent model to address these issues: its reduced complexity affords greater opportunities of achieving a thorough understanding of the way it encodes and processes sensory information, making possible a mechanistic comprehension of neural computation within and between local circuits.

1.2 Insect Olfactory System

Olfactory system designs share many characteristics across phyla: odor-evoked oscillatory activity has been observed in mollusks (Gelperin and Tank, 1990), arthropods (Laurent and Naraghi, 1994), and chordates (Adrian, 1942; Ottoson, 1959; Satou, 1990; Lam et al., 2000), including primates (Hughes and Mazurowski, 1962); olfactory receptor neurons (ORNs) exhibit remarkably precise and convergent projection patterns to the olfactory bulb (OB) in vertebrates (Mombaerts et al., 1996) and to the antennal lobe (AL) in insects (Gao et al., 2000; Vosshall et al., 2000); in both animal groups there is significant convergence and divergence around this relay (OB or AL), which contains many fewer neurons than its input (ORNs from nose or antenna) or its output (piriform cortex or mushroom body, MB) (see Table 1-1). These important commonalities imply that olfactory circuits have been either conserved or, alternatively, that strong functional constraints have forced them to converge to a common design. In either case this suggests similar coding mechanisms of olfactory information across animal phyla.

What makes insect olfaction very attractive as a model system is that it presents researchers with the important advantage of having a significantly reduced complexity, in terms of the fewer types and smaller number of cells it contains (for instance compared with the mammalian olfactory system, Table 1-1). Within insects, the locust *Schistocerca americana* has several additional advantages, particularly the fact that it is a relatively large and robust insect, which greatly facilitates conducting electrophysiological experiments. Studying this model system presents the opportunity to gain a more complete understanding of how information is processed, and of the mechanisms

underlying this processing, than would be possible by tackling more complex systems.

Considering the apparent similarity in design principles of olfactory systems, it seems

likely that some or many of the coding rules uncovered in insect olfaction will apply to

most animal groups, including mammals.

	Fruit fly	**Locust**	**Mouse (*Rat)**
OR genes	*ca.* 41	?	*ca.* 1000
ORNs	1,000-1,200	50,000-90,000	*ca.* 5,000,000
Glomeruli	*ca.* 43	*ca.* 1,000	*ca.* 1,800
PNs / MCs	200	830	50,000*
KCs / PCs	2,500	50,000	>1,000,000*

Table 1-1. Current estimates for the number of components of different model olfactory systems. For mouse (*rat): MCs, mitral cells, PCs pyramidal cells in piriform cortex. References: fruit fly (Technau and Heisenberg, 1982; Stocker et al., 1990; Vosshall et al., 2000); locust (Ernst et al., 1977; Leitch and Laurent, 1996); mouse (*rat) (Mombaerts et al., 1996; Haberly, 1997; Zou et al., 2001).

1.2.1 Anatomy of the insect olfactory system

The antennae are the olfactory organs of insects. ORNs are found in small groups within

sensilla, cuticular structures existing in different forms and sizes on the antennae (Lee

and Strausfeld, 1990; Masson and Mustaparta, 1990). Each sensillum typically contains

two or more ORNs, surrounded by three auxiliary cells (Keil, 1989). The outer branches

of ORN dendrites penetrate the lumen of the sensillum, where they are reached by

odorants through pores or spoke channels in the sensillum walls (Steinbrecht, 1980; Keil,

1982) [for reviews of insect peripheral olfaction see (Masson and Mustaparta, 1990; Hildebrand and Shepherd, 1997)]. Genetic work in fruit flies has discovered a family of genes encoding the complete repertoire of olfactory receptor proteins (Clyne et al., 1999; Vosshall et al., 1999). Each ORN seems to express only a single OR gene, whose spatial expression patterns in the antennae are conserved among individuals (Vosshall et al., 1999; Vosshall et al., 2000). A receptor from this gene family has been shown to localize to the dendritic membrane of ORNs and to be required for olfactory function *in vivo* (Dobritsa et al., 2003). In the fruit fly, all ORNs expressing a given OR send axons via the antennal nerve that project, bilaterally, onto one or two spatially invariant glomeruli in the AL (Gao et al., 2000; Vosshall et al., 2000). In the locust, ORNs appear to project to a few ipsilateral glomeruli (Ernst et al., 1977; Hansson and Anton, 2000).

There are two types of AL neurons: inhibitory local neurons (LNs) and excitatory projection neurons (PNs). Both LNs and PNs receive direct synaptic input from ORNs (Hansson and Anton, 2000). In the locust there are about 300 LNs, which are axonless nonspiking neurons with dense arborizations throughout the AL making dendrodendritic GABAergic synapses onto PNs (Leitch and Laurent, 1996; MacLeod and Laurent, 1996). While there are some differences in LN morphology and physiology among insect species[1], LNs have shown GABA-like immunoreactivity throughout all species studied,

---

[1] For instance, in bees (Flanagan and Mercer, 1989), moths (Anton and Hansson, 1995), and fruit flies (Wilson et al., 2004) LNs do produce action potentials, and while branching patterns of LNs in locusts (MacLeod and Laurent, 1996), fruit flies (Stocker et al., 1990) and moths (Anton and Hansson, 1994) are

consistently supporting their inhibitory role [e.g., (Schafer and Bicker, 1986; Distler, 1989; Hansson and Anton, 2000)].

Locust PNs are multiglomerular cholinergic spiking cells, sending axons via the antennoglomerular tract into the MBs and the lateral protocerebrum (Ernst et al., 1977; Oleskevich, 1999; Hansson and Anton, 2000). There is, however, some variability across insect species in the branching patterns of PN dendrites. For instance, in moths (Homberg et al., 1988), ants (Masson and Mustaparta, 1990) and fruit flies (Stocker et al., 1990), PNs are uniglomerular, while bees seem to have both uniglomerular and multiglomerular PNs (Fonta et al., 1993). Furthermore, a careful anatomical study of the cockroach has identified six classes of PNs: two of them are uniglomerular, two are sex-specific macroglomerular and yet another two are multiglomerular (Strausfeld and Li, 1999a). In the fruit fly, genetical tools have revealed that the targeting of PN dendritic projections to a specific glomerulus appears to be determined early in development before contact with ORN axons is established, or OR genes expressed (Jefferis et al., 2001), suggesting PNs are predetermined to carry specific olfactory information.

The next stage in the olfactory pathway is the MB. The intrinsic cells of the MB are the Kenyon cells (KCs). As can be seen in Figure 1-1, KCs have stereotyped branching patterns that give MB neuropils their characteristic shape: their somas are clustered above the calyx in a cell body layer; a primary neurite extends from the soma and sends

---

homogeneously distributed throughout the AL, in other species, such as bees (Flanagan and Mercer, 1989; Fonta et al., 1993) and cockroaches (Ernst and Boeckh, 1983), LNs arborize in only some glomeruli.

dendritic arborizations into the calyx neuropil and an axon which travels down the pedunculus and bifurcates into the α- and β-lobes [(Kenyon, 1896); see also (Mobbs, 1982; Laurent and Naraghi, 1994; Strausfeld, 2002)]. While KCs and MBs throughout insect species share this general structure, some variability in the number of calyces and lobes exists[2] [for a review of MB comparative anatomy see (Strausfeld et al., 1998)]. Studies on cultured honey bee KCs have identified several K^+ (delayed rectifier, rapidly inactivating A-type, Ca^{2+}-dependent), Na^+ (rapidly activating and inactivating, persistent) and Ca^{2+} (voltage-dependent) conductances (Schafer et al., 1994; Grunewald, 2003). As PN axons reach the MB calyx, they send collaterals which synapse onto KC dendrites. The main PN axon then proceeds to the lateral protocerebrum. Molecular biology work in fruit flies suggests that axonal projections from PNs innervating the same AL glomerulus have similar patterns of spatial branching in the lateral protocerebrum, and that these patterns are conserved throughout individuals (Marin et al., 2002; Wong et al., 2002). In the fruit fly MB, PN axons have been described to project to one of three stereotyped calycal zones, while the dendrites of an individual KC can project to all of these zones, thus receiving convergent input from all groups of PNs (Tanaka et al., 2004).

---

[2] For instance, while locusts and fruit flies have only one calyx per MB, bees, wasps and cockroaches have two calyces per MB, and some anosmic insects such as dragonflies have no calyx at all. Locusts, bees and cockroaches have two lobes, α and β, but fruit flies have five: α, α', β, β' and γ (Mobbs, 1982; Laurent and Naraghi, 1994; Strausfeld et al., 1998; Strausfeld and Li, 1999b; Ehmer and Hoy, 2000; Rein et al., 2002; Tanaka et al., 2004).
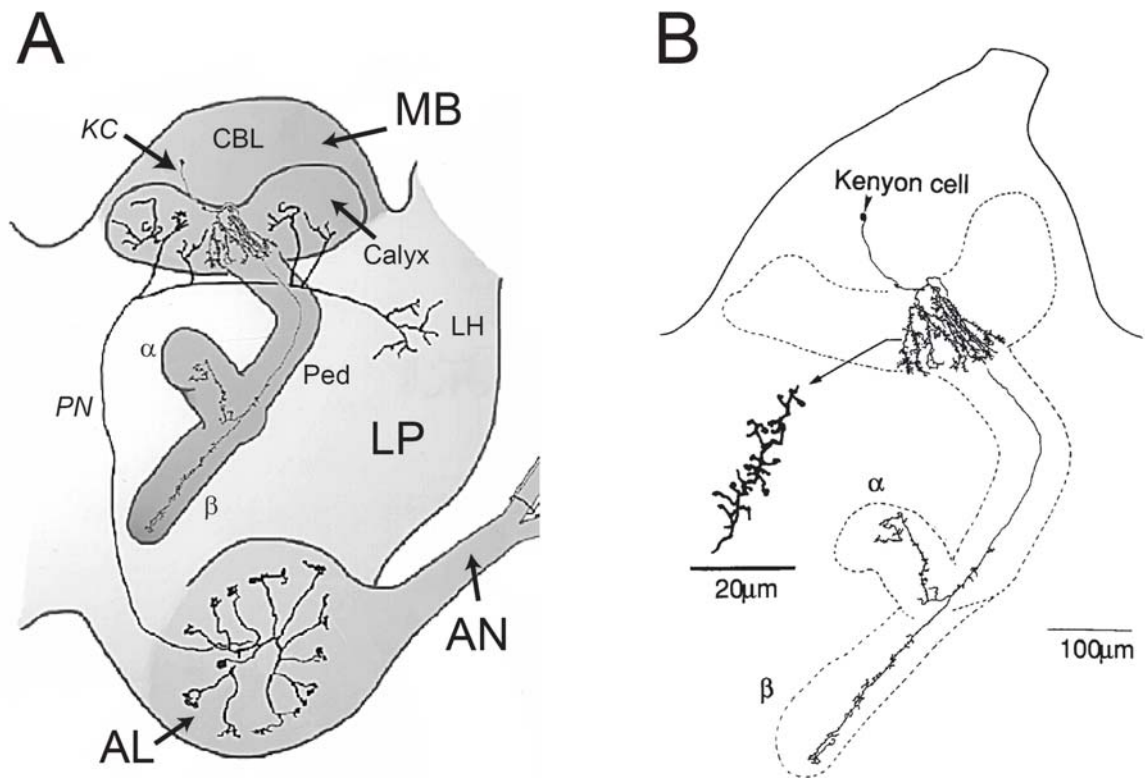
Figure 1-1. Locust olfactory system. (A) Main structures: AN, antennal nerve; AL, antennal lobe; MB, mushroom body; LP, lateral protocerebrum. MB substructures: CBL, cell body layer; calyx; Ped, pedunculus; α, α-lobe; β, β-lobe. Within the lateral protocerebrum: LH, lateral horn. **(B)** Close-up of KC showing the soma, the primary neurite, the spiny dendritic branches in the calyx and the relatively unbranched axonal terminals in the α- and β- lobes. Figures adapted from (Laurent and Naraghi, 1994; Wehr and Laurent, 1999).

The axons of KCs project down the pedunculus of the MB, where they are tightly packed and make axoaxonic synapses with other KCs (Leitch and Laurent, 1996). In the pedunculus and lobes, KC axons synapse onto dendrites of MB extrinsic neurons, which are typically considered to be the output of the MB. These extrinsic neurons often arborize profusely across specific cross-sections of the pedunculus or lobes and send projections to the protocerebrum or back into the calyx (MacLeod et al., 1998; Mizunami

et al., 1998b; Grunewald, 1999a; Li and Strausfeld, 1999). Very little is known about the neural processing of information in the lateral protocerebrum; it is generally assumed that this brain area is linked to descending pathways supplying motor neuron circuits in the thoracic and abdominal ganglia (Li and Strausfeld, 1999), but evidence is scarce and circumstantial.

1.2.2 Coding of information in the locust olfactory system

Electrophysiological experiments during the past several years have increased our understanding of the way olfactory information is processed in the insect brain. LFP recordings from the MB calyx reveal the appearance of 20-30 Hz oscillations upon presentations of olfactory stimuli to the antennae (Laurent and Naraghi, 1994). These LFP oscillations in the MB are driven by oscillatory input from the AL (Laurent and Davidowitz, 1994; MacLeod and Laurent, 1996; Wehr and Laurent, 1999) and are thought to be generated by E- and IPSPs in the KCs. Intracellular recordings of PNs and LNs reveal that their subthreshold membrane potentials oscillate upon odor presentations, and that both these oscillations and the action potentials of the PNs (locust LNs do not spike) become correlated to the LFP oscillations during specific epochs of the response (Laurent and Davidowitz, 1994; Laurent et al., 1996). Furthermore, these transient synchronization episodes were shown to be cell- and odor-specific. In parallel with these fast synchronization events, occurring in the time frame of an oscillation cycle (30-50 ms), the odor responses of PNs were shown to present slower temporal patterns of excitation and inhibition, evolving throughout several hundreds of milliseconds (Laurent

et al., 1996). Taken together, these results suggested that oscillatory synchronization allows olfactory information to be represented in a spatio-temporal code in which both time and space are used as coding dimensions in a combinatorial manner (Laurent, 1996; Laurent et al., 1996; Wehr and Laurent, 1996).

To test the effects that oscillatory synchronization may have on this system, it was necessary to uncover a way of abolishing these oscillations without disrupting other components of the odor response. It was therefore very important to discover that fast GABAergic inhibition from the LNs is required for the oscillatory activity to emerge in the AL: injecting picrotoxin (PCT), an antagonist of ionotropic GABA-receptor-gated chloride channels, into the AL blocks fast GABAergic inhibition from the LNs, and this inhibition proved to be required for the emergence of odor-evoked oscillatory dynamics in the AL circuit (MacLeod and Laurent, 1996). Furthermore, this intervention does not have a significant effect on PN average firing rate during the response, on odor-evoked slow temporal patterns or on response tuning. The fact that the slow temporal patterns (together with their longer periods of inhibition) persist after PCT injection indicates that PCT does not block slower inhibitory receptors, which seem to be involved in maintaining the response profiles and average firing rates of PNs (MacLeod and Laurent, 1996; MacLeod et al., 1998; Bazhenov et al., 2001a).

This intervention made it possible to test the physiological and behavioral effects of abolishing oscillatory synchronization. Honey bee experiments demonstrated that there is a behavioral impairment of odor discrimination under PCT-induced desynchronization

(Stopfer et al., 1997). Specifically, bees could not discriminate anymore between similar odors (1-hexanol and 1-octanol), even though they could still discriminate between dissimilar odors (geraniol and either alcohol). These experiments were significant because they provided a first demonstration that oscillatory synchronization is functionally relevant. At the same time, they raised the issue of identifying the physiological correlates of this behavioral deficit, in other words, of identifying the cellular and circuit processes which require oscillatory synchronization.

β-lobe neurons, which have dendritic processes in the β-lobe of the MB and are postsynaptic to KC axons, are a likely output of the early olfactory system. Electrophysiological recordings from these MB extrinsic neurons revealed that they lose specificity in their responses when oscillatory synchronization is abolished with PCT (MacLeod et al., 1998). This loss of specificity was caused both by the appearance of new responses (a broadening of the response profile of individual β-lobe neurons), and by the fact that spike trains evoked by different odors were more similar, indicating a further loss in the information carried by each response. These results are consistent with the loss of discriminability of similar odors observed behaviorally under PCT (Stopfer et al., 1997). Interestingly, however, there was no loss of specificity observed in the PN responses under these conditions (MacLeod et al., 1998). This raises the possibility that the loss of specificity observed behaviorally involves the KCs, and that it is at this intermediate stage of processing (between PNs and β-lobe neurons), that oscillatory synchronization is required for the proper decoding of olfactory information. It thus becomes important to record the electrophysiological responses of KCs before and after

oscillatory synchronization is blocked by PCT (motivating some of the experiments presented in Chapter 3 of this dissertation).

1.2.3 Mushroom bodies

Given that the MBs, and specifically their intrinsic cells, the KCs, will be the focus of the work presented in this dissertation, I will now present a brief background of what is known about their connectivity, inputs and presumed functional roles.

A current estimate of PN to KC divergence is 1:2000 (on the order of 100 synaptic varicosities per PN axon, with each varicosity contacting approximately 20 distinct KCs; S. Farivar and G. Laurent, personal communication). Assuming the PN to KC synapses are uniformly distributed among the 50,000 KCs, this would give an approximate convergence ratio of 30 PNs onto each KC. If only half of the KCs receive olfactory input, the mean convergence would be 60:1. There is no data yet on the variance of this ratio but it seems unlikely that it varies by more than a few fold across the population.

Comparative evolutionary analyses suggest that the MB calyces evolved mainly as a means to process olfactory information coming from the ALs: the MBs of primitive anosmic insects which lack ALs (e.g., odonates: dragonflies, damselflies, etc.) have greatly reduced or no calyces at all (Strausfeld et al., 1998). However, there is also evidence for inputs from other sensory modalities converging onto the MB calyces: direct connections from the optic lobes to the calyx have been observed in crickets (Honegger

and Schurmann, 1975), bees (Mobbs, 1982), and ants (Gronenberg, 1999). In cockroaches there is some evidence as well for mechanosensory and auditory afferents (in addition to olfactory and visual) supplying the calyces (Strausfeld and Li, 1999a). In some insect species, the inputs from these sensory modalities tend to be segregated into discrete calycal zones. For example, calyces in bees and ants are subdivided into three zones, each apparently receiving a specific modality of sensory input: the lip receives olfactory input from the AL, the collar visual input from the optic lobe and the basal ring receives input from both areas (Mobbs, 1982; Gronenberg, 1999). In the locust, however, branches from PN axons seem to branch uniformly throughout the main calyx (S. Farivar, personal communication). It is not yet understood how these different sensory modalities interact in the MB, but the fact that MBs receive this type of multimodal input has led researchers to hypothesize that a possible role of the MBs could be to place olfactory information in a wider multimodal context (Strausfeld, 2002).

Some experimental attempts to assign specific functional roles to MBs have implicated them in place memory (Mizunami et al., 1998a) and in making choices with conflicting cues (Tang and Guo, 2001) but so far the most evidence that has accumulated indicates that MBs are required for olfactory learning and memory [for a review, see (Heisenberg, 2003)]. Initial experiments in mutant flies lacking complete MBs (*mushroom bodies deranged* and *mushroom bodies miniature*) showed that these flies were deficient in olfactory learning (Heisenberg et al., 1985). Further experiments testing olfactory classical conditioning in a T-maze (Tully and Quinn, 1985) on wild-type flies whose

MBs were ablated (by feeding them hydroxyurea when the MB neuroblasts are dividing)
also show that olfactory learning is impaired (de Belle and Heisenberg, 1994).

Several lines of evidence have implicated the cAMP signaling pathway in these MB-
related learning deficits. For instance, a constitutively activated G-protein targeted to the
MB abolished olfactory learning (Connolly et al., 1996). Rescue experiments involving
genes whose products are involved in the cAMP pathway also support this idea (Waddell
et al., 2000; Zars et al., 2000). *Rutabaga* is a mutant fly with impaired olfactory learning.
The *rutabaga* gene encodes a Ca^{2+}/calmodulin-dependent adenylyl cyclase and restoring
rutabaga expression specifically to the MBs rescues olfactory learning in these mutants
(Zars et al., 2000). The product of the *amnesiac* gene has been linked to cAMP synthesis
and *amnesiac* mutants show impaired olfactory memory. Restoring *amnesiac* expression
in two cells which express it strongly in wild-type flies and project profusely to the MB
lobes rescues olfactory memory (Waddell et al., 2000). A common problem with these
experiments, however, is that the promoters are often less specific than advertised,
leading to some doubt about the causal link between the deficit and the neural locus of
genetic intervention.

Further experiments using a temperature-sensitive *shibire* transgene (shi^{ts1}) have focused
on distinguishing between the role of KCs in three different stages of olfactory
conditioning: acquisition, storage and retrieval (Dubnau et al., 2001; McGuire et al.,
2001; Schwaerzel et al., 2002; McGuire et al., 2003). The *shibire* gene encodes a
dynamin GTPase thought to be essential for synaptic vesicle recycling and thus, for

synaptic transmission; the temperature-sensitive transgene renders dynamin inactive when temperatures are raised above 29°C. By expressing shi^{ts1} exclusively in KCs, and raising the temperature at different stages of the conditioning trials, experimenters are able to evaluate whether KC synaptic transmission is required for these stages. Although some of these results are not totally clear (e.g., regarding secondary effects the expression of shi^{ts1} may be having on the flies performance, both at and above the permissive temperature; and whether shi^{ts1} expression is truly specific to the KCs in some of the fly lines), they all seem to suggest that KC output is required for retrieval of olfactory memories, but not for their acquisition or storage.

As can be seen from the above descriptions, there have been numerous genetic and anatomical studies of MBs [starting with the accounts of Dujardin and Kenyon in the XIX century (Dujardin, 1850; Kenyon, 1896)]. However, even though it is an area that has elicited so much interest, there is little physiological data on its intrinsic cells, the KCs (Laurent and Naraghi, 1994). This is partly explained because KCs are very small and fragile cells and have proven difficult to record from. Several important questions remain unanswered, for instance: how do KCs respond to odors? how are odors represented in the MB? what components of PN odor-evoked firing are relevant for KC decoding of olfactory information?

Questions like these are not only important for understanding the specific function of KCs and MBs within the insect nervous system, but can also provide valuable insights into other neurobiological issues of wider relevance such as oscillations and correlated

neuronal activity, as discussed in Section 1.1. Insect olfaction, and specifically the transfer of information from the AL to the MB, is an ideal model system in which to approach these broader neural coding questions because in this system, which seems to be a nearly pure feedforward network (for there is no evidence of feedback projections from the MB neurons back to the AL), we already know who does the encoding of information (the AL), who does the decoding (the MB), and a significant amount about the code that seems to be used (Laurent, 1996, 1999; Laurent et al., 2001).

1.3 Specific Issues to Be Addressed

In this dissertation I will focus on addressing two related questions: 1. How is olfactory information decoded by the KCs, the intrinsic neurons of the MBs? 2. What is the role served by neural oscillations in the transfer of information between the AL and MB?

With respect to MB decoding, the work in this dissertation will study the following questions: Which are the relevant components in the AL activity that influence or modulate KC responses? What are the mechanisms that make KCs selective to these components? What is the time frame in which KCs integrate their inputs? In other words, do they act as "temporal integrators" or "coincidence detectors"? Which is the representation of olfactory information in the MBs that arises from these decoding properties?

The other important issue this dissertation will focus on (and one which is intimately related to the decoding questions mentioned above) will be to understand how the oscillations generated in the AL underlie the processing of information by downstream components. We believe this is particularly important because understanding the role that oscillations play in the processing of information in this system might shed light on their role in other, more complex, systems. Identifying the transformation of representations between AL and MB circuits can provide insights on the potential computational advantages that oscillatory synchronization can serve for the representation, perception and memory processes performed by various nervous systems.

2 Oscillations and Sparsening of Odor Representations in the Mushroom Body

2.1 Introduction

Electroencephalogram (EEG) and local field potential (LFP) oscillations generally indicate periodic coherent synchronization of neuronal assemblies (Adrian, 1942; Steriade et al., 1993; Bragin et al., 1995; Gelperin, 1999; Rodriguez et al., 1999; Csibra et al., 2000). Although the occurrence of macroscopic oscillations has now been correlated with various sensory, behavioral or cognitive states in mammals (Eckhorn et al., 1988; Gray et al., 1989; Patel and Balaban, 2000; Fries et al., 2001), the functional significance of such observations is debated (Abbott and Dayan, 1999; Shadlen and Movshon, 1999). Many hypotheses based on temporal correlations have been proposed (von der Malsburg and Schneider, 1986; Abbott and Dayan, 1999; Diesmann et al., 1999; Engel et al., 2001; Brody and Hopfield, 2003); among others, one proposes that cortical neurons might act as coincidence detectors instead of integrators and thus select for correlated input (Abeles, 1982; Konig et al., 1996). Most hypotheses, however, remain tentative for lack of a direct experimental test. The olfactory nervous system, in which molecular design (Mombaerts et al., 1996; Clyne et al., 1999; Gao et al., 2000; Vosshall et al., 2000), circuit architecture (Mombaerts et al., 1996; Vosshall et al., 2000) and oscillatory dynamics (Adrian, 1942; Hughes and Mazurowski, 1962; Laurent and Naraghi, 1994; Gelperin, 1999; Lam et al., 2000) appear common across phyla, offers a rare opportunity to study some of these coding issues.

The insect antennal lobe (AL) is the analog of the vertebrate olfactory bulb. In locusts, each AL receives input from about 50,000 olfactory receptor neurons (ORNs) and contains about 1,130 densely interconnected neurons (300 local inhibitory neurons, LNs; 830 excitatory, multiglomerular projection neurons, PNs) (Leitch and Laurent, 1996; MacLeod and Laurent, 1996). Each AL sends distributed projections to the ipsilateral mushroom body (MB), an area involved in olfactory memory (Heisenberg et al., 1985; de Belle and Heisenberg, 1994; Zars et al., 2000; McGuire et al., 2001) (Figure 2-1). PNs are the only channel for olfactory input to the MB. Conversely, there is no evidence for feedback from the MB to the AL. Each locust MB contains about 50,000 small neurons (Kenyon cells, KCs) (Kenyon, 1896; Laurent and Naraghi, 1994; Leitch and Laurent, 1996), whose spiny dendrites receive direct input from PNs (Laurent and Naraghi, 1994).

Odor-evoked PN responses exhibit globally coherent 20-30 Hz oscillations and stimulus- and PN-specific slow modulation of firing rate, both shaped in great part by LN-mediated inhibition (Laurent and Davidowitz, 1994; Laurent et al., 1996; MacLeod and Laurent, 1996; Wehr and Laurent, 1996). Hence, during a stimulus, the AL output consists of barrages of spikes from an evolving PN assembly. Although individual PN spike timing during one oscillation cycle can be phase-locked, this locking does not occur for all PNs active during that cycle. At what time(s) a PN locks to others depends on both the odor and the PN. To understand the decoding of PN output by KCs, we examine the firing behavior of both populations at rest and in response to odors.
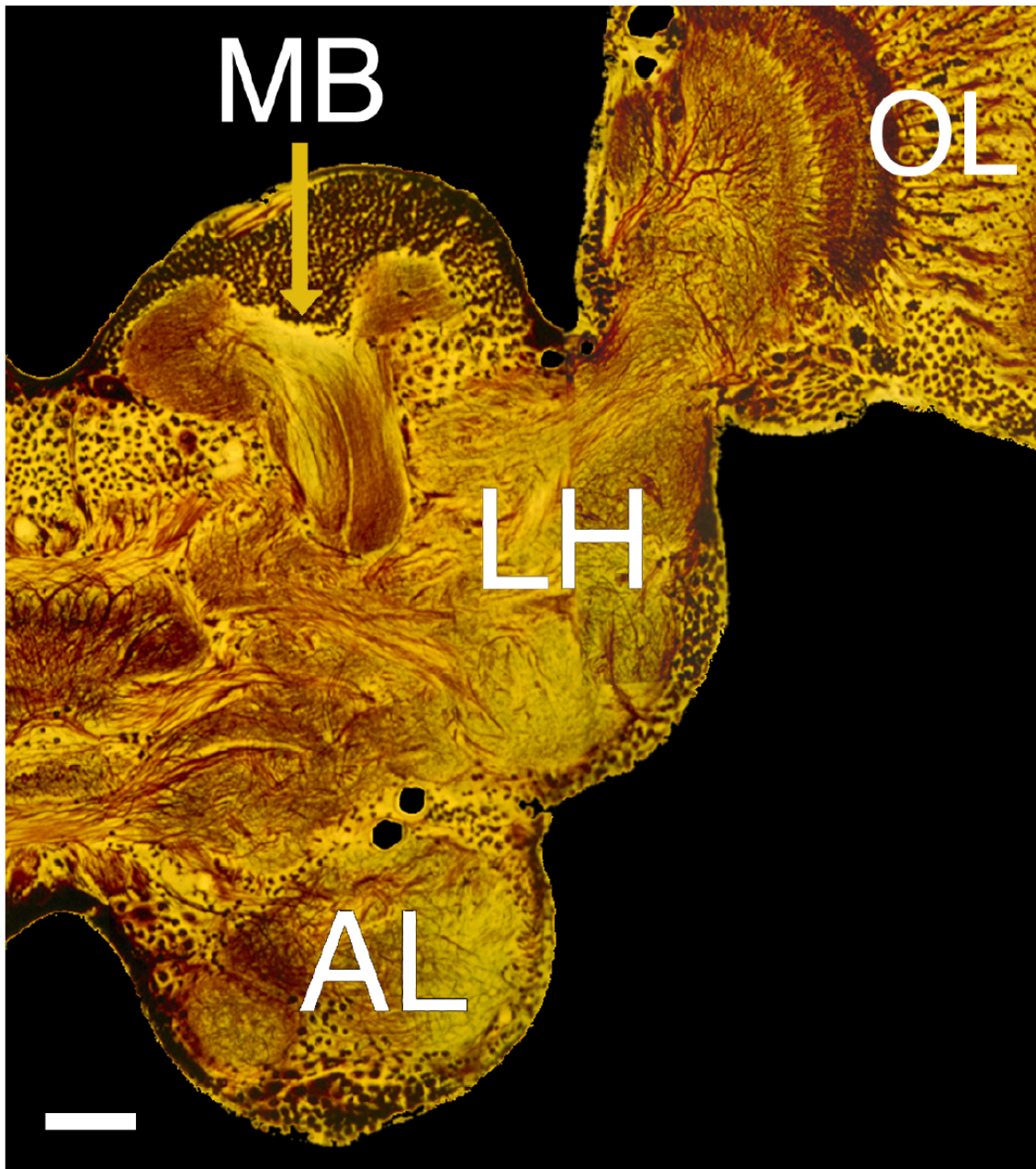
Figure 2-1. Olfactory circuits: Transverse section of the locust brain (left half, Bodian stain).
Olfactory input originates from ORNs on the antenna. ORN axons terminate in the AL, where PNs act as relays, with projections to the MB and the lateral horn (LH). OL: optic lobe. Calibration: 80 μm.

2.2 Results

2.2.1 Resting activity

Baseline activity profiles of PNs and KCs were measured over several-minute-long stretches of uninterrupted recording in naïve animals, with multiple tetrode recordings (see Methods Sections 2.4.1, 2.4.2, 2.4.3). At rest, the PN population fired at a mean rate of 3.87 ± 2.23 spikes/s per PN (range: 0.49 to 10.4; $n = 35$ PNs). Baseline firing was >100 times lower in KCs (median: 0.025 spike/s; interquartile range: 0.088 spike/s; $n = 23$ KCs) (Figure 2-2). Hence, despite a constant excitatory drive from PNs, KCs at rest remained remarkably inactive.
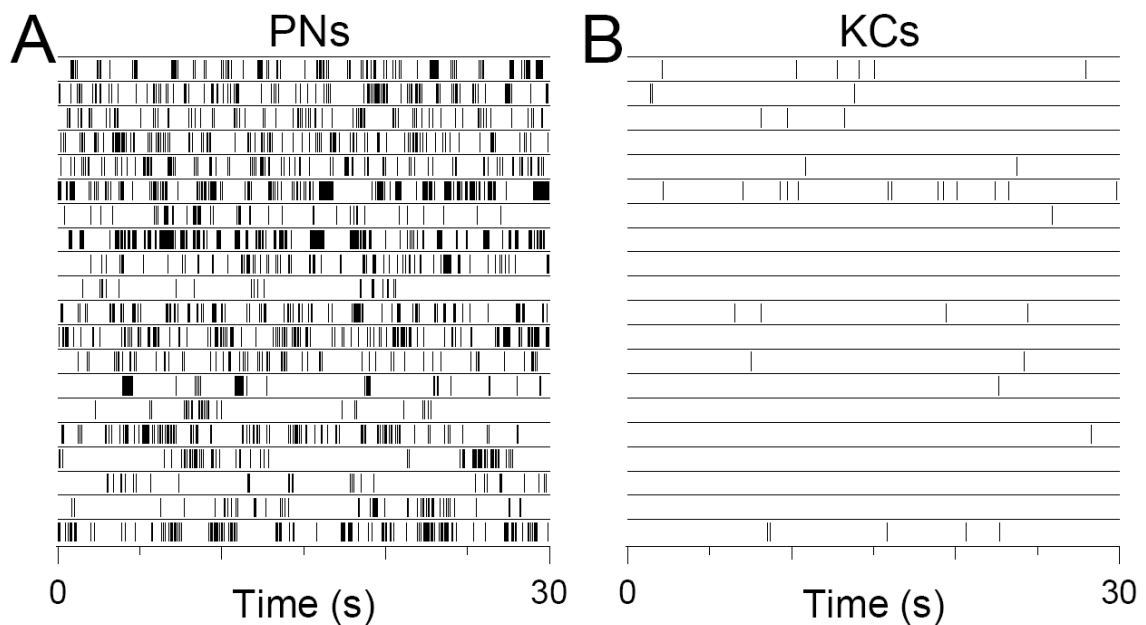

Figure 2-2. PN and KC baseline firing in the absence of odor stimulation. Thirty second rasters of 20 PNs **(A)** and 20 KCs **(B)** recorded with tetrodes. Note the exceedingly low baseline activity of KCs. Empty rasters denote absence of action potentials during the randomly selected segment chosen for display. These

rasters, however, of course originate from identified KCs, whose action potentials occurred at other times during the recording period. [PN data (A): O. Mazor & S. Cassenaer; KC data (B): J. Perez-Orive.]

2.2.2 Response selectivity

PNs and KCs were challenged in awake animals with a panel of odors (typically 17; range: 5-24; 5-25 trials per odor; 1s pulses; 20-30 s between trials). Experimental conditions were identical for PN and KC recordings.

Spiking response probability. The probability of observing a stimulus-evoked change in firing behavior was different across the two populations (Figure 2-3). Most PNs exhibited a reliable change in firing behavior within the first few seconds after stimulus onset. They showed complex temporal patterning (with increases and decreases in instantaneous firing rate) that often greatly outlasted the stimulus itself (Figure 2-3 A). Many of these responses were inhibitory, and many of these inhibitory periods were followed by a period of increased firing, up to five seconds after stimulus offset. We analyzed excitatory response probabilities across PNs (and KCs) quantitatively, by a variety of methods and analysis windows. We show here the results obtained with Method A (see Methods Section 2.4.4; results obtained with the other methods are nearly identical Table 2-1, Figure 2-10). The distribution of response probabilities for PNs was broad (Figure 2-4 A), with a mean over all cells of 0.64 (median: 0.74; interquartile range: 0.57; $n = 58$ PNs, 1,140 PN-odor pairs). KC responses to these same odors were extremely rare: over all KCs ($n = 74$ KCs, 1,101 KC-odor pairs), 58% failed to show any detectable response to any of the odors presented (Figure 2-4 A). The distribution of response probabilities

was heavily skewed towards low values (Figure 2-4 A), even when only those KCs that

produced at least one response were considered. The mean response probability, after

averaging all the individual response probabilities of the KCs (Figure 2-4 A) (median:

0.00; interquartile range: 0.12) was 0.11. Figure 2-3 B shows three typical responsive

KCs. Among all recorded KCs, only two responded to all odors presented (8 and 10

odors, respectively). To avoid possible sampling bias, recordings were made from all

regions and depths of the KC cell body layers. Responsive and unresponsive KCs were

found everywhere, which is consistent with the anatomy of PN axonal projections in the

MB (Laurent and Naraghi, 1994). Similarly, no selection bias toward strong responses

existed, for the great majority of them were extremely brief and were rarely detected

during the recording. Selective and promiscuous KCs could occur simultaneously on the

same tetrode, which indicates that differences in tuning width were not caused by global

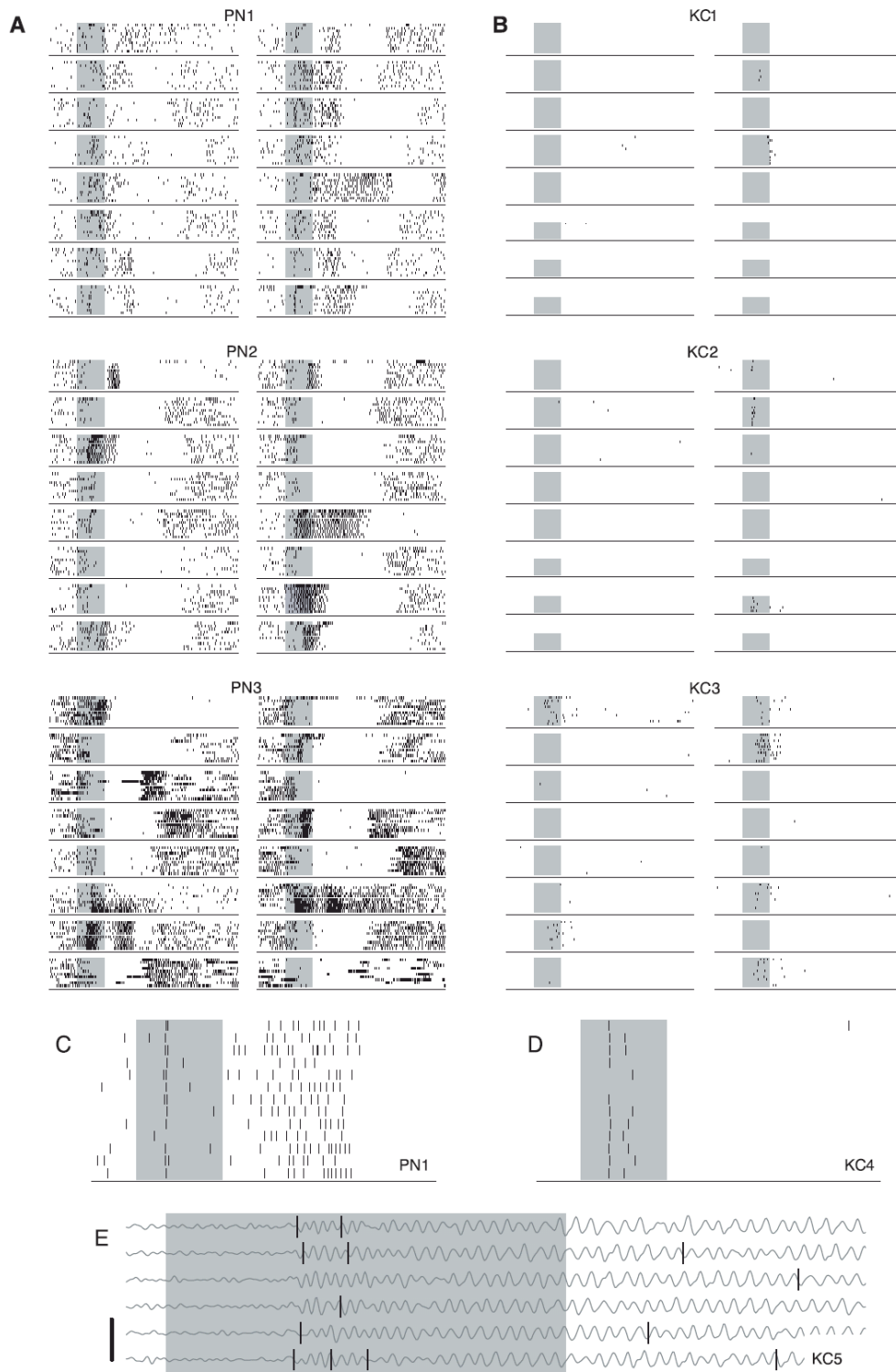modulation of excitability over time.

Figure 2-3. *In vivo* **tetrode recordings of odor responses in PNs (A and C) and KCs (B, D, and E).**
Shaded area, odor puff (1 s). **(A)** Responses of three simultaneously recorded PNs (PN1 to PN3) to 16

different odors (first 10 trials with each stimulus displayed, top to bottom). Odors from top, left column: hpo, don, che, hx3, unn, min, oca, pnn; right column: chx, oco, nnn, thx, 2hp, nna, 3hp, hxo. Abbreviations are as follows: 1-hexen-3-ol (hx3), trans-2-hexen-1-ol (thx), cis-3- hexen-1-ol (chx), 1-hexanol (hxo), 1-heptanol (hpo), 1-octanol (oco), hexanal (hxa), heptanal (hpa), octanal (oca), nonanal (nna), 3,7- dimethyl-2,6-octadiene-nitrile (don), 3-pentanone (pnn), 2-heptanone (2hp), 3-heptanone (3hp), 5-nonanone (nnn), 6-undecanone (unn), cherry (che), mint (min), geraniol (ger), vanilla (van), citral (cit), apple (app), strawberry (str), amyl acetate (ama), benzaldehyde (bnh), methyl salicylate (mts), eugenol (eug), L-carvone (lca), D-carvone (dca), dihydro-myrcenol (dhm). **(B)** Responses of 3 KCs to the same 16 odors. Conditions are the same as in (A) with the following exceptions: for six of the odors, KC1 and KC2 have only five trials; in KC2, the seventh odor in the right column is hxa. **(C)** Expanded view of PN1 rasters in response to hxo (trials 3 to 15). Note alignment of spikes. **(D)** Response of a fourth KC to hx3 (trials 3 to 15). Note low baseline activity and alignment of first spike in the response across trials. **(E)** Response of a fifth KC with superimposed LFP, recorded in the MB (10-55 Hz bandpass). Note phase-locking of KC spikes. LFP = 400 μV. [PN data (A and C): O. Mazor & S. Cassenaer; KC data (B, D and E): J. Perez-Orive.]

Response intensity. Response patterns and intensities differed in PNs and KCs. Whereas PN responses often lasted several seconds (Figure 2-3 A), KC responses were brief and lacked the slow temporal patterning typical of PNs (Figure 2-3 B). Using responsive cell-odor pairs, we counted action potentials produced by PNs and KCs over the 3 s window after stimulus onset. The distribution of PN spike counts over that period was broad, with a mean of 19.53 ± 10.67 spikes. KCs responded with 2.32 ± 2.68 spikes (Figure 2-4 A)[3]. We found a negative correlation between KC spike count and response selectivity (Spearman ranked correlation coefficient: -0.567, $p < 0.05$).

---

[3] Most KC spikes occurred in the beginning of the response: response intensity was 2.33 ± 2.02 spikes over the first 1.4 s; PNs produced 12.84 ± 7.29 spikes on average in that period.
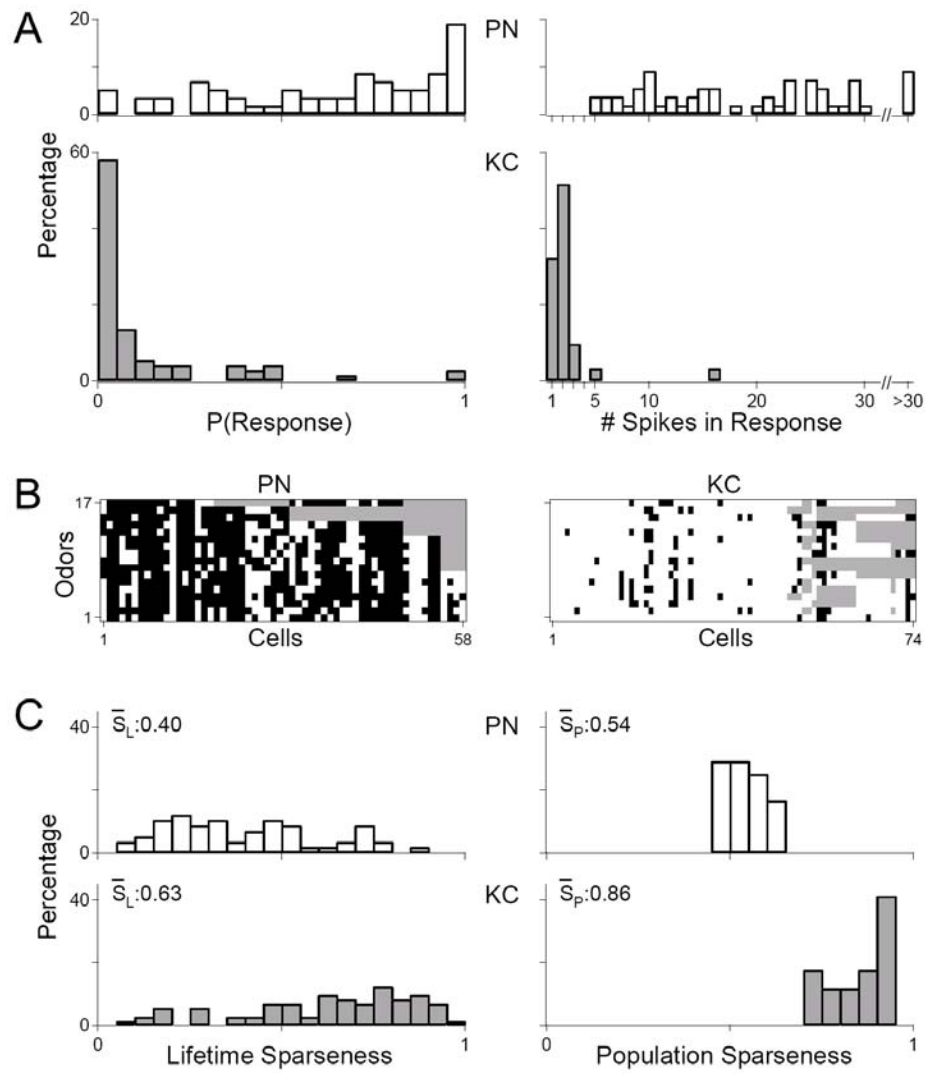
Figure 2-4. Statistics and sparseness of PN and KC odor responses (see Methods Sections 2.4.4, 2.4.5).
(A) (Left) Frequency distribution of cell response probabilities; note opposite skew in PN and KC
distributions. (Right) Frequency distributions of response intensities (1 spike per bin, measured over a 3 s
window). Spike counts were computed only from cell-odor pairs with a detected excitatory response. **(B)**
Excitatory responses (filled squares) of individual PNs and KCs (columns) (n = 58 PNs, 74 KCs) to 17
different odors (rows: hx3, thx, chx, hxo, hpo, oco, nna, nnn, don, pnn, 2hp, 3hp, oca, unn, che, min, hxa).
Abbreviations are as in Figure 2-3. Open squares denote inhibition (PNs only) or absence of a response.
Gray squares indicate not tested. **(C)** Distributions of lifetime (left) and population (right) sparseness,
computed across all cells and all tested odors. S_L and S_P are significantly different across PNs and KCs (p <
0.001, t test for S_P, z statistic for S_L). [PN data: O. Mazor & S. Cassenaer; KC data: J. Perez-Orive.]

Temporal precision. PN spike probability and precision is PN-, odor- and time-specific (Laurent and Davidowitz, 1994; Laurent et al., 1996; Wehr and Laurent, 1996). Time-locked PN spikes were easily detected when they occurred in isolation (e.g., Figure 2-3 C), but they were also found within sustained responses, which is consistent with previous intracellular results. In KCs, individual responses typically contained about two spikes (Figure 2-4 A), at least one of which could be precisely locked to stimulus onset with a fixed delay. Stimulus-locked spikes were often the first ones in the response of the KCs but could occur at any cycle. The first spike in the response of KC4 (Figure 2-3 D), for example, had a jitter of only ± 4 ms relative to stimulus onset. Stimulus-locked spikes with such small jitter, however, were not commonly observed. Another measure of precision, more relevant to this system, is the timing of each action potential relative to its LFP oscillation cycle (phase) (Figure 2-3 E). The mean phase of KC spikes was $83^{o} \pm 77^{o}$ (n = 18 KCs; 0° is oscillation peak, Figure 2-6 F). Mean spike phase was the same in the most and in the least specific KCs ($90^{o} \pm 67^{o}$ vs. $86^{o} \pm 81^{o}$; n = 5 cells each). The spikes within a doublet (or triplet) were typically separated by one to a few oscillation cycles (e.g., Figure 2-3 E). This indicates that appropriate PN drive to individual KCs lasted several oscillation cycles and that, when a KC spike was fired, it occurred preferentially at the same phase of its oscillation cycle.

2.2.3 Sparseness of odor representations across PNs and KCs

Figure 2-4 B compresses the responses of 58 PNs and 74 KCs to the same 17 odors and illustrates the contrast between the two population representations[4]. A simple estimate of population sparseness (S_P) is the proportion of cells unresponsive to each stimulus, averaged over all stimuli. It thus represents the sparseness of the representation of each odor across the population, averaged over all odors, but ignores the strength of each response. S_P was 0.90 in KCs and 0.33 in PNs. S_P can also be calculated without relying on how a response is defined by using firing rate distributions for each tested stimulus, whether we detected a response or not (Rolls and Tovee, 1995)[5] (see Methods Section 2.4.5). Applied to PNs and KCs, this measure of S_P was again always greater in KCs (Figure 2-4 C). Finally, sparseness can be calculated for each cell across all the stimuli it has experienced. This measure, called lifetime sparseness, S_L, approximates the mean tuning width of each neuron averaged over all neurons. Again, S_L was significantly higher in KCs than in PNs ($p < 0.001$, t' test, Figure 2-4 C). S_L and S_P were also calculated by using the other response analysis windows, or by using only the odor responsive cells. By all measures, odor representations were always significantly sparser across KCs than across PNs (Table 2-1 and Figure 2-10).

---

[4] Responses were determined here according to Method A (see Methods Section 2.4.4). Nearly identical results were obtained if responses were assessed by different criteria adapted to each population (Table 2-1 and Figure 2-10).

[5] This sparseness measure had its origin in (Treves and Rolls, 1991). The measure was developed from this idea to its current form in (Rolls and Tovee, 1995) and the normalizations we use here were those applied by (Vinje and Gallant, 2000). (Willmore and Tolhurst, 2001) discuss these and other lifetime and population sparseness measures.

2.2.4 Mechanisms underlying sparsening

Subthreshold KC activity during odor stimulation. Sharp electrode recordings (see

Methods Section 2.4.6) from KCs ($n = 29$) revealed odor-evoked, subthreshold activity

made up of periodic synaptic potentials (Figure 2-5 A). These were locked to the LFP

(Figure 2-5 B) and superimposed on a noisy and irregular synaptic background, away

from the firing threshold. Appropriate odor-KC combinations revealed reliable and time-

specific EPSPs and/or action potentials. The response of the KC in Figure 2-5 C, for

example, contained a train of prominent EPSPs late within the stimulus. One of these

EPSPs led to an action potential in half of all trials with that odor. A different KC

responded to the same odor with at least two reliable action potentials, at cycles 1 and 3

of the response, whether the neuron was at rest (Figure 2-5 D) or was held depolarized by

current injection. In all tested KCs, the existence, timing and reliability of these firing

events were odor specific. We noted that a large component of the odor-evoked activity

in KCs was inhibitory: if the KC was held depolarized by current injection, periodic

hyperpolarizing potentials could be seen during a response; if the KC was held above

firing threshold, odor-evoked inhibition interrupted this tonic firing (Figure 2-5 A and C).

Thus, odor stimulation also causes synaptic inhibition of KCs. Finally, the amplitude of

odor-evoked EPSPs paradoxically increased when the KC was held in a depolarized state

(Figure 2-5 A), which suggests active membrane properties. We examined the possibility

that synaptic inhibition and KC active conductances work together to make KCs
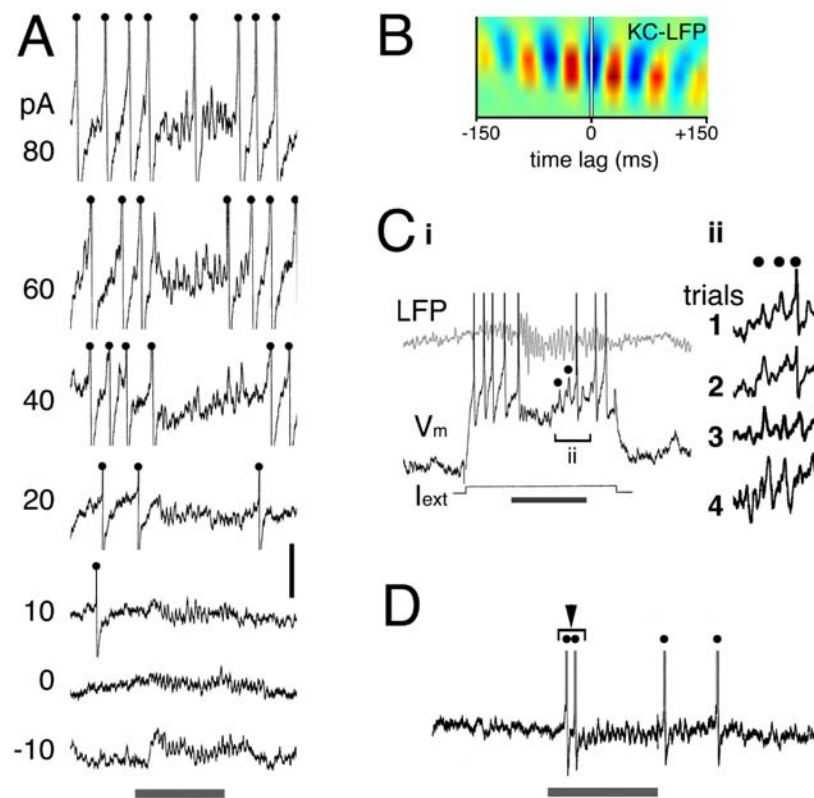
coincidence detectors of PN input.

Figure 2-5. *In vivo* **sharp electrode intracellular records from different KCs during odor stimulations.** All action potentials are clipped. **(A)** Responses obtained while resting voltage was set by holding currents between -10 and +80 pA. Horizontal bar, odor (cherry) delivery (800 ms). This KC never produced any action potential in response to this odor at resting potential. Note oscillating membrane potential at rest (0 pA), interruption of direct current-evoked firing by odor delivery (+20 to +80 pA traces), and amplification of many discrete depolarizing potentials at most depolarized holding potentials. **(B)** Sliding crosscorrelation of KC V_m and simultaneous LFP during hexanol odor puff [different KC from that in (A)]. Red, maxima; blue, minima. *y* axis: time, 0.5 s. Note locking of signals during odor puff. **(C)** Third KC recording, showing interruption of current-evoked firing by cherry odor response and prominent, late EPSPs (•); 800 ms odor delivery (i). Repeated trials (1 to 4) show precise reoccurrence of these EPSPs during the same epoch of the response; time calibration, 500 ms (ii). **(D)** Fourth KC and its spiking response to cherry odor at cycles 1 and 3; 800 ms odor pulse. Vertical calibrations: KC, 10 mV (A and D), 8 mV (Ci), 6 mV (Cii); LFP, 300 µV, 1-40 Hz bandpass (C). [Intracellular traces of KC odor responses (A, C and D): G. Laurent; cross-correlogram (B): G. C. Turner.]

Source of masked odor-evoked inhibition. Because direct effects of PNs are excitatory

and because locust PNs do not contain GABA (Leitch and Laurent, 1996), the source of

odor-evoked KC inhibition should be downstream of PNs. In addition to sending

collaterals into the MB, PN axons terminate in the lateral horn (LH) (Ernst et al., 1977;

Hansson and Anton, 2000). We identified among their targets there a cluster of about 60

GABA-immunoreactive neurons (lateral horn interneurons, LHIs), with direct axonal

projections to the MB (see Methods Section 2.4.7; Figure 2-6 A). Intracellular staining of

individual LHIs showed profuse axonal collaterals, overlapping with KC dendrites

(Figure 2-6 B). KC dendrites receive GABAergic input (Leitch and Laurent, 1996). LHIs

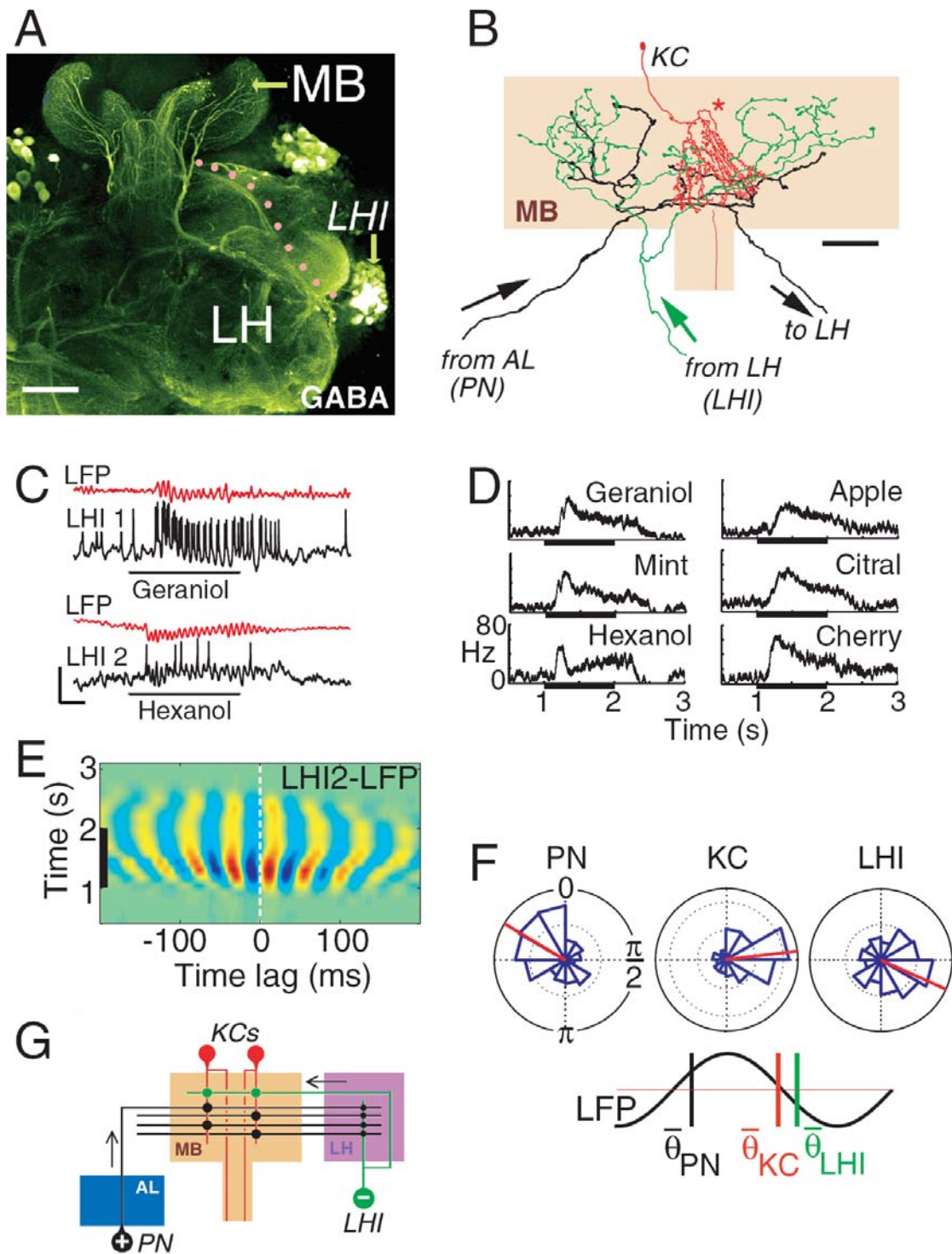thus are well suited to be a source of the odor-evoked inhibitory inputs.

Figure 2-6. Feedforward inhibition of KCs by LHIs. (A) Immunolabeling by antibody to GABA (see Methods Section 2.4.7). Cluster of about 60 reactive somata (LHI) and tract of LHI axons running to the MB (stipples) are shown. The terminals of one of these axons in the MB are shown in (B). Bar, 100 μm.

(B) PN axon (black) projects to the MB calyx (orange) and to the LH (Ernst et al., 1977; Hansson and Anton, 2000). LHI axon (green) projects to the calyx (this study). PN and LHI axons terminate on KC dendrites (red). Neurons were stained by iontophoresis of cobalt hexamine (KC, PN) or neurobiotin (LHI) in separate preparations and were drawn with a camera lucida. Note varicosities in LHI and PN axon collaterals. Asterisk, KC axon. Bar, 50 μm. **(C)** Representative odor-evoked responses of two LHIs and simultaneously recorded LFPs (5-40 Hz bandpass). Note membrane potential oscillations, locked to the LFP. Identity and delivery (1 s long) of stimulus indicated by black bar. LHI, 20 mV; LFP, 400 μV; 200 ms. **(D)** Instantaneous firing rate of LHI1 [in **(C)**] in response to various odors. Lower edge of profile shows mean instantaneous rate averaged across trials; profile thickness, SD. All LHIs responded to all odors tested, with response profiles that varied little across different odors. **(E)** Sliding cross-correlation between LFP and LHI2 traces (spikes clipped). Red, maxima; blue, minima. Strong locking is present throughout the response (odor delivery, vertical bar). Lower edge of correlation stripes just precedes stimulus onset due to width of the correlation window (200 ms). **(F)** Phase relationships between PN, KC, and LHI action potentials, and LFP. (Upper) Polar plots. LFP cycle maxima defined as 0 rad, minima as π rad (PNs: 3 cell-odor pairs, 388 spikes; LHIs: 17 cell-odor pairs, 2632 spikes; KCs: 18 cells, 862spikes). Mean phases are shown in red. Gridlines are scaled in intervals of 0.10 (probability per bin). (Lower) Schematic diagram showing LFP and mean firing phases. **(G)** Circuit diagram. [LHI anatomy and physiology (A to F): G. C. Turner; PN recording (F): M. Westman; KC phase-locking (F): J. Perez-Orive.]

LHI responses to odors. LHIs responded vigorously and reliably to odors (Figure 2-6 C and D). LHI membrane potential oscillated in phase with the LFP (Figure 2-6 E), and, when sufficiently excited, LHIs fired one or a short burst of action potentials at each oscillation cycle (Figure 2-6 C). In each cycle, LHI mean firing time lagged 173° behind that of PNs (Figure 2-6 F). LHI firing phase was independent of odor identity. Synaptic drive to KCs thus likely consists of EPSPs from PNs alternating with IPSPs from LHIs, occurring preferentially in opposite halves of each oscillation cycle (Figure 2-6 F and G). PN and LHI inputs to KCs differ in one important respect: because each KC on average receives inputs from a very small fraction of the PNs and because the firing probability and phase-locking of each PN typically evolves during a response, the probability that

many of the PNs presynaptic to a given KC fire together within the same half of one

oscillation cycle is low. By contrast, individual LHIs showed sustained responses to all

odors presented (Figure 2-6 D), consistent with the fact that 830 PNs converge onto only

about 60 LHIs. Because LHI axons diverge profusely in the MB (Figure 2-6 B),

individual KCs should receive periodic input composed of consistent IPSPs, alternating

with EPSPs whose total strength strongly depends on the stimulus.

Sharpening of KC response to direct PN stimulation. We next tested more directly

whether both synaptic inhibition and intrinsic active conductances assist coincidence

detection in KCs. To study single EPSP-IPSP cycles in isolation, we used direct electrical

stimulation of PNs instead of odors. Evoked postsynaptic potentials in KCs dramatically

changed shape and duration when we varied stimulus strength (Figure 2-7 A). At high

stimulus intensities, a sharp "spikelet" rode atop the depolarizing potential, suggesting

active conductances (Figure 2-7 A, top trace). This spikelet was not an artifact of

unusually strong stimuli: when a weak stimulus was used to elicit a smaller EPSP and

holding current was adjusted so that the KC was near firing threshold, spikelets could

also be observed (see Methods Section 2.4.8; Figure 2-7 B)[6] (Schafer et al., 1994). Next,

we tested the idea that GABAergic feedforward inhibition also shapes PN-evoked

postsynaptic potentials. At voltages below spikelet threshold, EPSP shape remained

strongly voltage-dependent (Figure 2-7 C). Local injection of picrotoxin (PCT), a

---

[6] Although we have not characterized this spikelet pharmacologically its shape and all-or-none waveform suggest the involvement of voltage-dependent conductances (possibly Na^+ or Ca^{2+} for depolarization and K^+ for repolarization), consistent with previous patch-clamp studies *in vitro* (Schafer et al., 1994).

GABA$_A$-like chloride channel blocker, into the MB calyx (see Methods Section 2.4.9) broadened the EPSP and decreased the voltage-dependence of EPSP shape (Figure 2-7 C). This indicates that the LHI-mediated IPSP normally contributes to the shape and duration of PN-evoked EPSPs. Blocking inhibition in the calyx increased the scatter of KC spike times after PN stimulation (Figure 2-7 D). LHI-mediated IPSPs thus contribute to shortening the epoch during which a KC remains depolarized after each volley of PN excitation; it could also explain why KC action potentials are so precisely phase-locked during responses to odors (Figure 2-6 F). Hence, the tendency of each KC to convert its excitatory input from PNs into an action potential can be facilitated in the early phase of the compound EPSP by voltage-dependent depolarizing nonlinearities, and it can be antagonized shortly thereafter by feedforward inhibition. The remaining voltage dependence of the EPSP after PCT injection (Figure 2-7 C) suggests the existence of an active repolarizing conductance. Thus, both active and synaptic properties probably contribute to making KCs prefer coincident input, on a cycle by cycle basis.
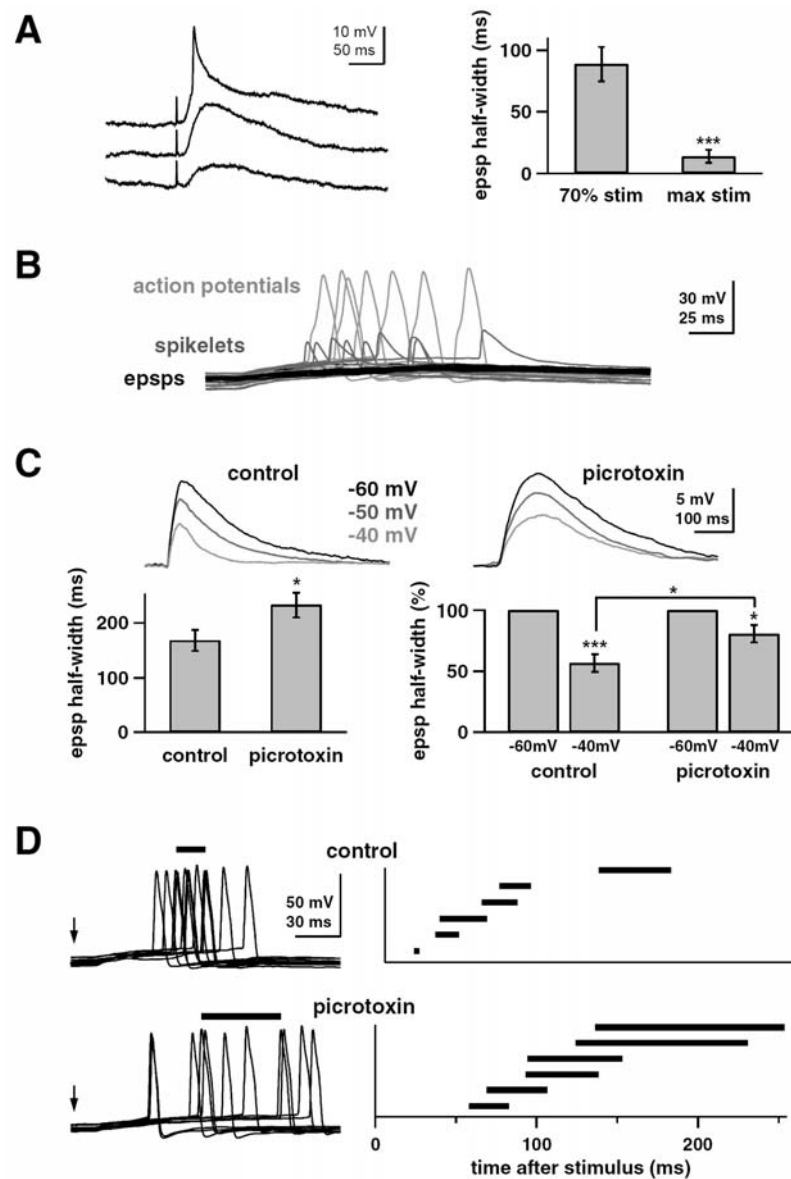
Figure 2-7. KC responses to electrical stimulation of PNs. (A) PNs were stimulated directly with an electrode placed in the AL and evoked EPSPs were recorded with a sharp electrode intracellularly from KCs. Three traces show EPSPs recorded at progressively stronger stimulus intensities (bottom to top). Note positive inflexion during rising phase of the top EPSP and sharp repolarization. Bar graph compares EPSP half-width at the maximum stimulus intensity that was still below action potential threshold versus halfwidth at 70% (± 5%) of this maximum intensity. EPSP half-width was significantly different at these two stimulus intensities ($P < 0.001$, paired *t* test, $n = 11$ KCs). **(B)** Intrinsic active conductance amplifies and sharpens EPSPs near threshold. KC was held near threshold with a constant holding current; PN stimulus amplitude was constant. Successive trials elicited full-blown sodium spikes (light gray), subthreshold EPSPs (black), or intermediate spikelets. Sample traces were collected in PCT; similar

spikelets were observed in control conditions (A). **(C)** Synaptic inhibition shortens KC EPSP. At progressively depolarized holding potentials, EPSP half-width significantly decreased (half-width at -40 mV was significantly smaller than half-width at -60 mV; P < 0.0005, paired *t* test, $n = 10$ KCs); all analyzed data were below threshold for spikelet activation. After PCT injection in MB, EPSPs became broader (-60 mV half-width significantly increased in PCT; P < 0.05, *t* test, $n = 9$). EPSP shape was less dependent on postsynaptic voltage (-40 mV half-width as percent of -60 mV half-width significantly increased in PCT; P < 0.05, *t* test, $n = 9$) but was still voltage dependent (P < 0.05, *t* test, $n = 9$). Sample traces are shown from two KCs in the same brain. **(D)** Synaptic inhibition narrows the window in which KCs can fire after PN stimulation. Stimulus intensity was adjusted to elicit an EPSP of 5 to 10 mV (when KC is held at -60 mV), and then holding current was adjusted so that this EPSP elicited a spike on 30% to 60% of trials. Representative traces (left) show those sweeps where spikes were elicited (arrows mark stimulus, bars mark interquartile range of spike times). Sample traces are shown from two KCs in the same brain. Group data (right) show the interquartile range for each cell. PCT significantly increased the magnitude of the interquartile ranges (P < 0.05, *t* test, $n = 6$ control KCs, 6 KCs in PCT). [Sharp microelectrode recordings (A): J. Perez-Orive; whole-cell recordings (B to D): R. I. Wilson.]

2.2.5 Influence of feedforward inhibition on KC responses to odors

If feedforward inhibition competes with and resets the periodic excitation of KCs by PNs, antagonizing LHI-mediated inhibition should decrease KC specificity to odors. KCs recorded *in vivo* with tetrodes were tested with up to 17 odors (ten trials per odor) and retested immediately after PCT injection (see Methods Section 2.4.9) into the MB (Figure 2-8). PCT caused no significant change in the KC baseline firing rate (medians: 0.018 spikes/sec after PCT vs. 0.005 before, $n = 12$ KCs, $p = 0.19$, nonparametric sign test). PCT caused a broadening of KC tuning, characterized by greatly reduced odor selectivity (Figure 2-8 A to C). Even in KCs that responded to none of the odors presented in controls, responses to these same odors appeared after PCT (Figure 2-8 A to C). Individual KCs did not become responsive to all odors but rather to a larger subset of all tested odors. The mean population and lifetime sparseness calculated over this KC subset

was significantly decreased after PCT (S_P = 0.70 to 0.41, n = 11 odors, p < 0.001, paired t test; S_L = 0.47 to 0.30, n = 12 KCs, p < 0.05, nonparametric Wilcoxon signed-rank test). Individual KC response intensity after PCT treatment was not significantly different from control (control: 1.96 ± 0.81 spikes; PCT: 1.82 ± 0.47 spikes), but KC action potentials after PCT lost their locking to the LFP[7] (PCT: Figure 2-8 D; controls: Figure 2-6 F). This confirms earlier experiments (Figure 2-7 C and D) which suggest that LHI-mediated IPSPs normally constrain KC integration and spike timing.

---

[7] PCT application to the MB did not abolish the LFP oscillations recorded there, for the principal source of these oscillations —synchronized, periodic synaptic input drive from PNs— was excitatory and cholinergic (nicotinic) (MacLeod and Laurent, 1996; Oleskevich, 1999).
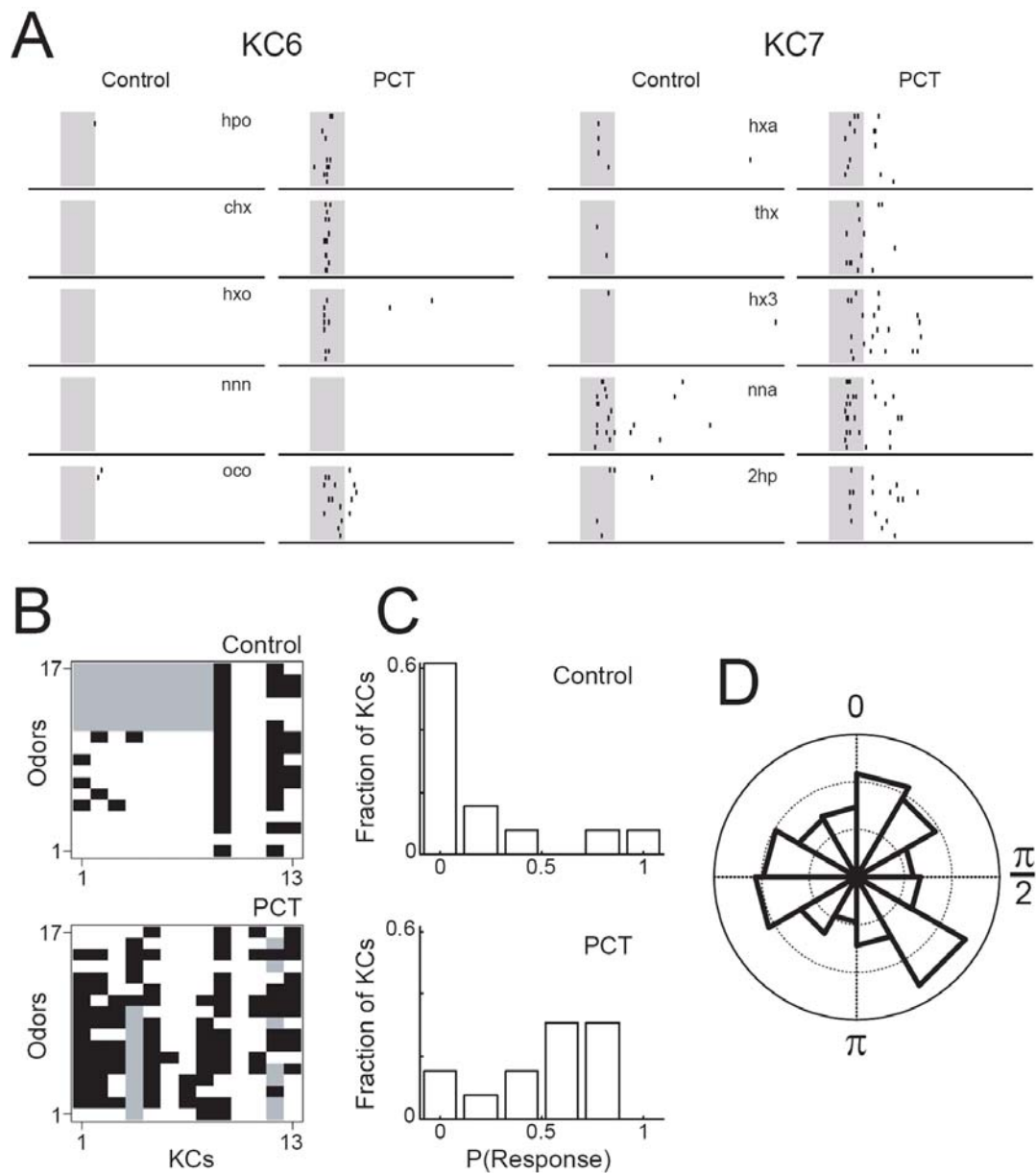
Figure 2-8. Influence of feedforward inhibition on KC odor tuning and phase-locking (*in vivo*, wire tetrode recordings). (A) Two KCs (6 and 7) and their responses to five odors before and after local PCT injection into the MB (see Methods Section 2.4.9). Odor pulses (shaded area): 1 s; 10 trials per odor, top to bottom. Abbreviations are as in Figure 2-3. **(B)** Comparison of KC response profiles before and after PCT. Filled, response; open, no response; gray, not tested (more odors were generally tested after PCT treatment). In a vast majority of KCs, PCT broadened tuning profiles. Odors, 1 to 17: oca, hxa, thx, hx3, oco, unn, nna, 2hp, che, chx, hxo, don, nnn, 3hp, hpo, pnn, min. **(C)** Frequency distribution of response probabilities (across all odors tested) before and after PCT treatment (*n* = 13 KCs). Note dramatic reduction

of proportion of specific KCs (leftmost bin) after PCT treatment. Median response probabilities: 0.09 (control), 0.59 (PCT). **(D)** Phases of KC spikes relative to LFP during odor-evoked responses (0 rad, max; π, min of LFP voltage). Vector strengths: 0.03 (PCT) versus 0.41 (Figure 2-6 F, control). Gridlines are in intervals of 0.05 (probability per bin). [J. Perez-Orive.]

2.3 Discussion

In the AL, individual odors are represented by a large fraction of the 830 PNs: baseline activity is high, sparseness is low and individual PN responses are sustained. In the MB, the same odors activate a small proportion of neurons in a larger population (50,000 KCs): baseline activity is close to 0, sparseness is high and individual KC responses are rare and typically contain only two action potentials. KC action potentials thus each carry much more information than those of PNs.

2.3.1 How does sparsening arise?

We propose that KCs act as selective coincidence detectors on periodic PN input: because individual KCs receive inputs from only a small fraction of PNs, because the patterned responses of individual PNs are staggered in time and because EPSP summation by KCs occurs best within a fraction of each oscillation cycle, the conditions appropriate for bringing a KC to threshold are rarely met. During odor stimulation, each oscillation cycle contains both locked and unlocked PN spikes (Laurent et al., 1996). Periodic IPSPs, caused in KCs by LHIs whose mean firing is in antiphase with the discharge of the synchronized PNs, antagonize the action of inappropriately timed PN action potentials. When LHI-mediated inhibition is blocked, this normally antagonized

excitatory drive to KCs can now summate over a longer time window: KCs lose much of their specificity. Time-locked feedforward inhibition thus helps define very short but renewed (once per oscillation cycle) integration windows for each KC, akin to a periodic reset, with critical consequences for KC specificity.

None of the features uncovered so far (oscillatory patterning, feedforward inhibition, fan-in and fan-out, active properties) are unusual ones (Contreras et al., 1997; Haberly, 1997; Fricker and Miles, 2000; Galarreta and Hestrin, 2001; Pouille and Scanziani, 2001). In particular, distributed and partly overlapping projection patterns of mitral cells have been seen in rodent prepiriform cortex (Zou et al., 2001) and local feedforward inhibitory circuits are common (Contreras et al., 1997; Pouille and Scanziani, 2001; Brand et al., 2002). Nonlinear intrinsic properties have been seen in some cortical and hippocampal cells among others and hypothesized to underlie coincidence detection (Margulis and Tang, 1998; Fricker and Miles, 2000; Galarreta and Hestrin, 2001). We show here that all these properties exist together in the same circuit and that their concerted use in the context of oscillatory activity results in a major transformation of sensory codes.

2.3.2 How could sparsening be useful?

Because the MB is a likely site for formation and retrieval of olfactory memories (Heisenberg et al., 1985; de Belle and Heisenberg, 1994; Zars et al., 2000; McGuire et al., 2001), we must ask why sparse codes might be advantageous there. Although it is clear that extremely sparse codes ["grandmother" schemes, (Barlow, 1969)] may be

undesirable because they confer sensitivity to damage and low capacity, representations carried by small subsets of neurons offer many theoretical advantages. First, overlaps between individual representations are less likely than if each representation used a large proportion of the available neurons, limiting interference between memories. This system's memory capacity can still be very high, because the total population size is large and sparseness is not extreme. Second, comparisons between stimulus-evoked patterns and stored memories are simpler if they invoke fewer elements. Similarly, associations (for example, between odors and images) are facilitated. Third, representations become more synthetic or "high level." Every KC action potential compresses the signals carried by several PNs that are each potentially more informative about stimulus composition. Sparsened representations thus contain less explicit detail. This conclusion agrees with behavioral and psychophysical observations in humans, rats and insects that odor perception has a prevalent synthetic quality (Cain and Potts, 1996; Livermore and Laing, 1996; Linster and Smith, 1999).

2.3.3 Significance for neural coding

Our results have implications for understanding neural codes. First, single-neuron responses can be exquisitely specific, extremely short (one or two spikes only), and temporally precise (both within and across oscillation cycles). Studies of frontal, motor and olfactory cortices show rare and very brief firing events, consistent with some of our results (Tanabe et al., 1975; Nemitz and Goldberg, 1983; Vaadia et al., 1995; Duchamp-Viret et al., 1996; Riehle et al., 1997). Second, subtle yet highly relevant activity patterns

may go undetected with many large-scale brain activity monitoring techniques: sparse and brief activity is unlikely to be reflected in most macroscopic signals. Yet, as we show here, this may sometimes be all there is. Lastly, to measure the relevant information content of an action potential, one must know how downstream targets interpret it. For example, we showed previously that PN action potentials typically phase lock to the LFP only during certain (stimulus- and PN-specific) epochs of a response (Laurent et al., 1996). Our results indicate that KCs will be more sensitive to phase-locked PN action potentials than to those that occur closer to each LHI-mediated IPSP, whose timing is itself determined by the locked PN population. PN spikes, therefore, are not all equally meaningful to a KC. Even in cases in which firing rates are high, many spikes may be of minimal significance to a target, because they are improperly timed. Here, relevance is determined by interneuronal correlation. Hence, deciphering brain codes requires evaluating these correlations and their consequences on the channeling of information. Conversely, macroscopic oscillations may indicate the existence of neural filters, whose properties will determine the interpretation one should make of a spike train.

2.4 Methods

2.4.1 Preparation and stimuli

Results were obtained from locusts (*Schistocerca americana*) in an established, crowded colony. Young adults of either sex were immobilized, with one or two antennae intact for olfactory stimulation. The brain was exposed, desheathed and superfused with locust saline, as previously described (Laurent and Naraghi, 1994). Odors were delivered by

injection of a controlled volume of odorized air within a constant stream of dessicated air.

Teflon tubing was used at and downstream from the mixing point to prevent odor

lingering and cross-contamination. Odors were used at 10% vapor pressure (all PNs, 85%

of KCs) or 100% vapor pressure (15% of KCs, all LHIs), further diluted in the dessicated

air stream. Electrical stimulation of PNs was performed in the AL: typical stimulus

amplitudes 20-100 µA; 300 µs pulses; 25 µm tungsten wire bipolar electrodes; WPI

A360 stimulus isolator.

2.4.2 Tetrodes

Two types of tetrodes were used for extracellular recordings: silicon probes for PNs and

wire tetrodes for KCs. Silicon probes were generously provided by the University of

Michigan Center for Neural Communication Technology

(www.engin.umich.edu/facility/cnct/). Wire tetrodes were constructed with 0.0005" and

0.0004" (12.7 and 10.2 µm, respectively) insulated nichrome wire (REDIOHM wire with

PAC insulation, H.P. Reid). Four strands of wire were twisted together and heated to

partially melt the insulation. The tip was cut with fine scissors and each channel tip was

electroplated with gold solution to reduce the impedance to between 200 and 350 kΩ at

1kHz. The same custom-built 16-channel preamplifier (unitary gain) and amplifier

(10,000X) were used for both types of tetrodes. Data from each tetrode were filtered (in

custom-built amplifiers, bandpass 300-6,000 Hz) acquired continuously (15 kHz/channel,

12 bits) and stored. Two to four tetrodes were used simultaneously. Because of low

baseline activity and low response probability in KCs (see results), fewer KCs than PNs

were usually isolated in a typical recording session. Tetrodes were placed within the AL

or MB soma clusters, peripheral to the neuropils at depths less than 200 μm. Cell

identification was unambiguous because PNs are the only spiking neurons in the locust

AL, (LNs do not produce sodium action potentials) (Laurent and Davidowitz, 1994), and

because all the somata located above the MB calyx belong to KCs.

2.4.3 Extracellular data analysis

Tetrode recordings were analyzed as described in (Pouzat et al., 2002). Briefly, events

were detected on all channels as voltage peaks above a pre-set threshold (usually 2.5-3.5

times each channel's signal SD). For any detected event on any channel, the same 3 ms

window (each containing 45 samples) centered on that peak was extracted from each one

of the four channels in a tetrode. Each event was then represented as a 180-D vector (4 x

45 samples). Noise properties for the recording were estimated from all the recording

segments between detected events, by computing the auto- and cross- correlations of all

four channels. A noise covariance matrix was computed and used for noise whitening.

Events were then clustered using a modification of the expectation maximization

algorithm. Because of noise whitening, clusters consisting of, and only of, all the spikes

from a single source should form a Gaussian ($SD = 1$) distribution in 180-D space. This

property enabled us to perform several statistical tests to select only units that met

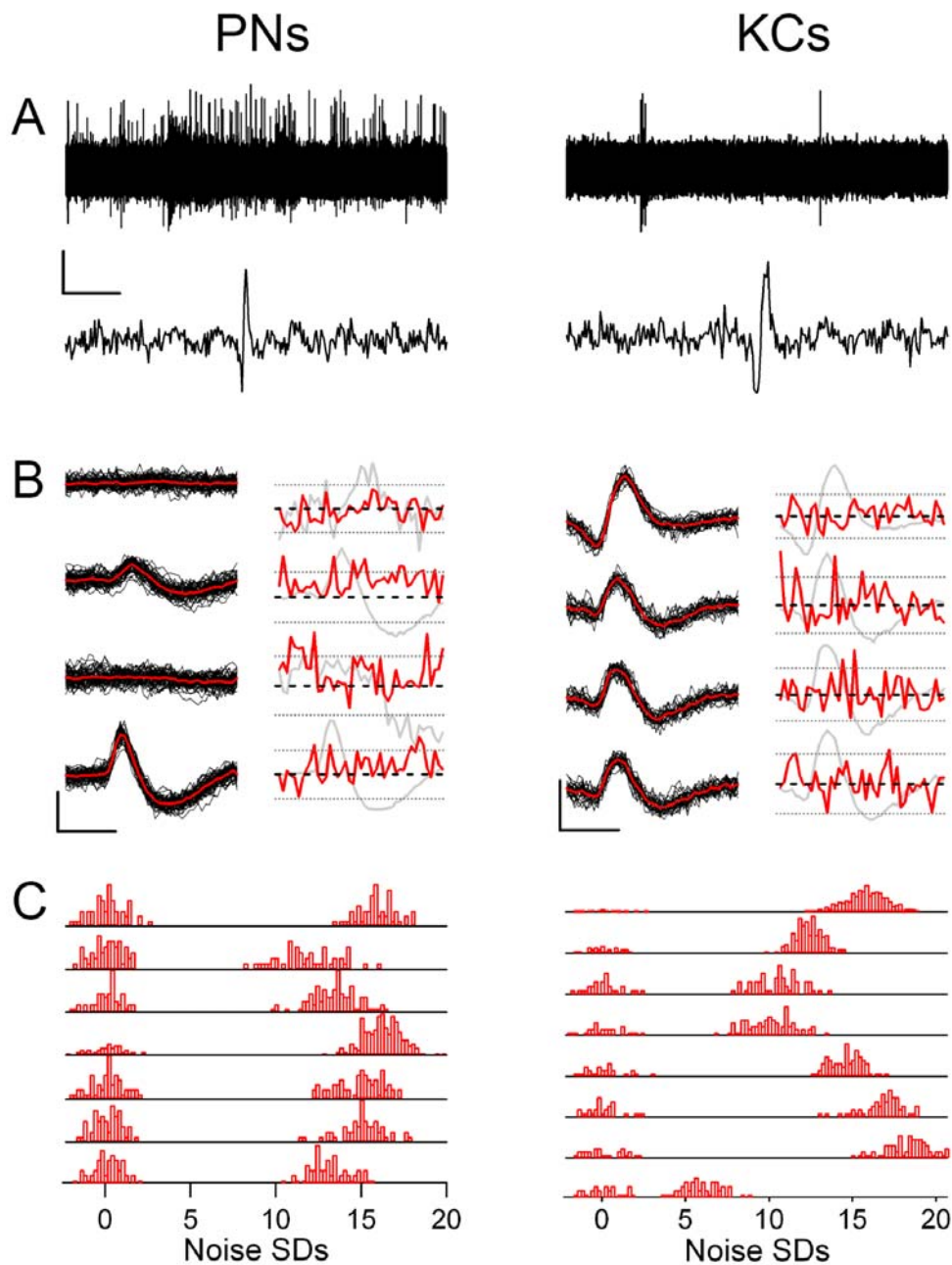rigorous quantitative criteria of isolation (Figure 2-9).

Figure 2-9. Extracellular tetrode recordings and spike sorting. (A) Raw data traces with PN action potentials recorded in the AL (left), and KC action potentials recorded in the cell body layer of the MB (right). Calibrations: 50 μV, 3 s (top traces), 3 ms (bottom traces). **(B)** Examples of two clusters: PN (left panel) and KC (right panel). In each panel the traces on the left show the superimposed events classified for that cluster (black) for each of the four tetrode channels, together with the average waveform (red). Calibration: 100 μV, 1 ms. Two of the statistical tests used to evaluate the isolation of the cells in the model are shown in (B) and in (C): on the right side of each panel in (B) is the variance around the mean for each

of the four channels, together with 95% confidence intervals which are based on the noise model. **(C)** Projection tests in which each pair of clusters in the model in 180-D space is projected onto the line connecting the cluster centers so as to evaluate their degree of isolation. All cluster centers are separated by at least 5 times the noise SD. All analyzed data were selected on these separation criteria. [PN data: O. Mazor & S. Cassenaer; KC data: J. Perez-Orive.]

2.4.4 Response definitions

Defining what constitutes a response quantitatively and equally accurately for PNs and KCs requires careful consideration. For example, a conventional mean firing rate measure applied to the entire "response period" is not appropriate, because PN responses are patterned; a typical PN response, such as one composed of subsequent excitatory and inhibitory epochs, often produces a mean rate no different from baseline, yet clearly constitutes an odor-specific response; reliability across trials thus needs to be taken into account. In addition, PNs and KCs have very different baseline firing statistics, implying that response criteria based on a change from baseline might not apply equally well to both populations.

We thus analyzed the data using a variety of methods and display, in our paper, the results of one (Method A), applied identically to KCs and PNs. The analyses using other methods, summarized in Table 2-1, yielded nearly identical results. Our methods go as follows. First, for all methods, we used one of two response windows: short (0-1.4 s) and long (0-3 s after stimulus onset), with stimulus on for 1 s in all cases. Method A used a 3 s window. Second (Method A), a PN or KC was classified as responding if its firing behavior during the window met two independent criteria of response *amplitude* and

reliability: *a*. Amplitude: the neuron's firing rate (measured in successive 200 ms bins, averaged across all trials) had to exceed *n* SDs of the mean baseline rate in at least one bin within the response window. Baseline rate was measured for each cell-odor pair over a period of 3 to 5 s preceding stimulus onset and over all trials with that odor. We explored values of *n* from 2 to 4. If *n* was low (e.g., *n* = 2 SDs) the rate of false responses detected in PNs prior to stimulation was unacceptably high (> 35%). If *n* was high (*n* = 4 SDs), the proportion of missed responses (as judged by visual inspection of PN rasters and peristimulus time histogram, PSTHs) during odor presentation was unacceptably high (> 10%). Values of *n* of 3 or 3.5 gave low rates of both false positives (during baseline) and false negatives (during stimulation) in PNs. Values of *n* between (and including) 2 and 4 made no significant difference with KCs. We show the results with *n* = 3.5 (Method A, Figure 2-4); those obtained with other values of *n* are summarized in Table 2-1. *b*. Reliability: to ensure that responses detected were reliable even at low firing rates (characteristic of KCs), we required that more than half of all trials with each odor contain at least one spike during the response window. We also analyzed the same data sets using different criteria for PNs and KCs, each adapted to each population's baseline firing statistics. Despite this difference, the results (Table 2-1 and Figure 2-10) are nearly identical to those shown in Figure 2-4.

Method	A	B	C	D	E	F	G	H
Threshold	**3.5SD**	2SD	3SD	4SD	3.5SD			
Window	**3s**	3s	3s	3s	1.4s	3s	3s	3s
PN *P(R)*	**0.64**	0.73	0.68	0.61	0.51	0.64	0.65	–
False Pos. (%)	**2.23**	35.98	6.16	0.80	0.89	2.14	3.57	–
Overlap (%)	–	90.71	96.34	96.79	87.41	99.73	99.55	–
KC *P(R)*	**0.11**	0.12	0.12	0.11	0.09	0.11	–	0.11
False Pos. (%)	**0.09**	1.46	0.18	0.00	0.00	0.09	–	0.00
Overlap (%)	–	99.27	99.82	99.91	97.46	100.00	–	99.46

Table 2-1. Quantitative comparison of different methods of response detection. For each method, three statistics are computed for PNs and KCs. Response probability (P(R)) indicates the probability of a detected response, computed over all cell-odor pairs. The false positives value (False Pos.) is the percentage of responses detected when the method was applied to a window of baseline activity prior to odor onset (computed for all cell-odor pairs). The final statistic (Overlap), is a measure of similarity between a particular method and Method A (see Section 2.4.4), defined as the percentage of cell-odor pairs for which the two methods either both detected or both did not detect a response. Methods B-D are identical to Method A, but use a different response amplitude threshold, ranging from 2 SDs to 4 SDs above baseline. Method E is the same as Method A, but uses only a 1.4 s response window (0-1.4 s after odor onset). Method F is based on Method A, but it uses a different reliability criterion that adapts to the baseline statistics of the cell (as opposed to using one action potential as in Method A). In this method, an odor response was deemed reliable if more than half of all trials contained at least one 200 ms bin with a spike count higher than a threshold, specified as 1 SD above the mean baseline rate. Methods G and H are the methods of response detection for PNs and KCs, respectively, described in Figure 2-10. [PN data: O. Mazor & S. Cassenaer; KC data: J. Perez-Orive.]
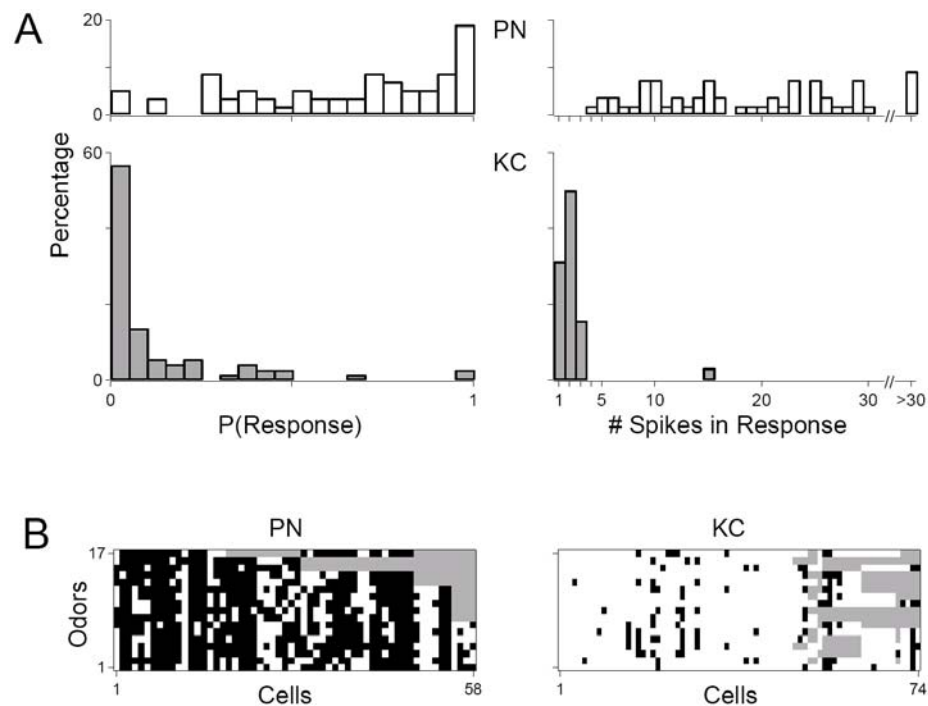
Figure 2-10. Population responses and sparseness across PNs and KCs, calculated using different response criteria for PNs and KCs: a PN qualified as responding during the 3 s following odor onset, if its firing rate increased to above 3.5 SDs of the pre-odor baseline rate (measured by a PSTH with 200 ms nonoverlapping bins). In contrast, a KC response occurred when over 50% of individual trials for a particular odor showed an increase from baseline activity anywhere in the 3 s window. An increase in activity was defined as at least one 200 ms bin with a spike count higher than 3 SDs above baseline (computed from the pre-odor period over all trials). **(A)** Left: Histograms displaying PN and KC response probability distributions. Response probabilities measured across all odors tested. Note opposite skews in KC and PN distributions. Right: Histograms displaying distributions of spike numbers in a response. Spike counts were computed only from cell-odor pairs with a significant excitatory response during the analysis window. **(B)** Excitatory responses (filled boxes) of individual PNs and KCs. Open squares denote inhibitory response (PNs only) or absence of a response; gray squares: not tested (same odors as those in Figure 2-4). Note similarity to Figure 2-4 A and B. [PN data: O. Mazor & S. Cassenaer; KC data: J. Perez-Orive.]

2.4.5 Sparseness

Data were analyzed using Matlab (The Mathworks) and Igor Pro (Wavemetrics, Inc.).

The sparseness measures are taken from (Treves and Rolls, 1991; Rolls and Tovee, 1995;

Vinje and Gallant, 2000; Willmore and Tolhurst, 2001). In brief:

$$S_P = (1 - [\ [\Sigma^N_{j=1}\ r_j/N]^2 / \Sigma^N_{j=1}\ [r_j^2/N]\ ]\ ) / (1\text{-}1/N),$$

where N is the number of units and r_j is the response of unit j. Lifetime sparseness, S_L, is

calculated in the same way, except that index j now corresponds to each odor and N to the

total number of odors tested with each cell. Analog response intensities for a given cell-

odor pair were computed by first segmenting the recording into 200 ms bins and

computing the mean spike count in each bin, averaged over all trials with that odor. We

then subtracted from all bin measures within the analysis window (1.4 or 3 s), the mean

baseline rate. All values calculated in this way greater than 0 over the window (7 or 15

bins) were then added. S_P and S_L vary between 0 and 1 (1 = sparsest).

2.4.6 Sharp pipette recordings and staining

Sharp electrode recordings of KCs (Figure 2-5, Figure 2-7 A) were made with

borosilicate glass micropipettes (DC R > 300 MΩ) filled with 0.2 or 0.5 M K-acetate or

patch electrode solution (see Section 2.4.8). KC input resistance at the soma was usually

around 1 GΩ. Signals were recorded with an Axoclamp–2B (Axon Instruments) and

acquired (10 kHz, 12 bits) with a PCI-MIO-16E-4 data acquisition board and LabVIEW

software (National Instruments). Intracellular recordings of LHIs (soma or dendritic

impalement, Figure 2-6) were made with borosilicate glass micropipettes filled with 0.5

M K-acetate (DC R:100-300 MΩ). Intracellular staining of LHIs (Figure 2-6 B) was

carried out by iontophoretic injection of 2% neurobiotin in 0.5 M K-acetate (0.5 s current

pulses of -2.5 to -3.5 nA at 1 Hz for 30-60 min). Injected neurons were visualized in

whole mounts using a diaminobenzidine-based chromogenic reaction (Wicklein and

Strausfeld, 2000). LFPs were always recorded in the MB calyx, using saline-filled patch

pipettes (DC R: 2-15 MΩ) or wire tetrodes (see Section 2.4.2).

2.4.7 Immunocytochemistry

Anti-GABA immunostaining (Figure 2-6 A) was carried out in whole locust brains using

the following protocol [modified from (Power, 1997)]. Partially desheathed locust brains

were fixed for 1 h in 5% formaldehyde, desheathed and washed for 20 h in phosphate

buffered saline (PBS). Brains were then dehydrated through an ethanol series, placed in

propylene oxide for 20 min, rehydrated and then agitated for 5 h in PBS containing 5%

Triton X-100 and 0.5% bovine serum albumin (PBS 5% T 0.5% BSA). They were then

washed for 30 min in PBS 0.5% T 0.5% BSA, and transferred to fresh PBS 0.5% T 0.5%

BSA containing anti-GABA at 1:100 dilution, or, for negative control, to PBS 0.5% T

0.5% BSA lacking primary antibody. After incubation at 4ºC for 6 days, brains were

washed for 2 h in PBS at room temperature and transferred to PBS 0.5% T 0.5% BSA

containing fluorescein isothiocyanate-conjugated goat anti-rabbit IgG at 1:20 dilution and

incubated at 4ºC for 4 days. They were then washed for 30 min in PBS, dehydrated

through ethanol series, cleared in methyl salicylate and examined by confocal laser

scanning microscopy. Figure 2-6 A is a projection along the z-axis of a stack of 30

optical slices each 2.7 μm thick, constructed using the public domain ImageJ program

(http://rsb.info.nih.gov/ij/). Negative control brains showed diffuse background staining.

2.4.8 Patch-clamp recordings

Whole-cell patch-clamp recordings from KCs (Figure 2-7 B to D) were obtained in a

semi-reduced preparation. After the brain was exposed, it was removed from the head

with antenna and eyes still attached, placed on a glass cover slip in a custom-built

chamber, and immobilized using insect pins placed in the eyes. The brain was then

desheathed as previously described (Laurent and Naraghi, 1994). Recordings were

obtained from KC somata under visual control using a microscope with IR-DIC imaging.

Patch pipettes (5 to 6 MΩ) were filled with a solution of (in mM): K gluconate 185,

HEPES 10, EGTA 1, MgATP 4, Na_3GTP 0.5 (335 mOsm, pH 7.2). Glucose (10 mM)

was substituted for an equimolar amount of sucrose in the external saline solution, and

the saline was bubbled continuously with O_2. Hyperpolarizing current injections (10 pA)

were used to continually measure intrinsic membrane properties, and the cell was

accepted for recording as long as $R_{input} > 1$ GΩ and $R_{access} < 40$ MΩ. Data was acquired

on an Axopatch 1D (Axon Instruments) amplifier at 10 kHz and lowpass filtered at 5

kHz. Note: In whole-cell current-clamp mode, typical EPSP duration in controls at -60

mV (Figure 2-7 B) was about twice that observed with sharp electrodes (Figure 2-7 A).

2.4.9 Picrotoxin injections

Patch pipettes were back-filled with a solution containing 1.67 mM PCT and 0.3% Fast Green. After the pipette was introduced into the MB calyx (dendritic region of the MB, see Figure 1-1), a pneumatic picopump (WPI) was used to apply a series of four to nine 100 ms, 10 psi pressure pulses. Each pulse injected approximately 1 pl of solution (as measured by previous injection into a drop of oil). Injected solution remained exclusively localized to calyx, as verified by dispersal of Fast Green.

2.5 Acknowledgments

(Figure 2-7 B to D). G. Laurent conducted the intracellular sharp electrode recordings of

KCs under olfactory stimulation (Figure 2-5).

3   Coincidence Detection and Oscillations in Kenyon Cells

3.1   Introduction

In many sensory systems the mean firing rate of neurons contains information about the stimulus (Adrian, 1926; Hubel and Wiesel, 1962; Britten et al., 1992; Parker and Newsome, 1998). For this information to be "read," downstream neurons must integrate their inputs over time, in effect averaging any temporal patterns occurring in time scales shorter than their integration window. Neurons however, could act as coincidence detectors integrating their inputs over much shorter time frames, therefore responding selectively to correlated input (Abeles, 1982; Carr and Konishi, 1990; Softky and Koch, 1993; Konig et al., 1996). In many different systems, selectivity for coincident inputs has been linked to different intrinsic and circuit neuronal properties, including active dendritic conductances (Margulis and Tang, 1998; Larkum et al., 1999; Galarreta and Hestrin, 2001; Schiller and Schiller, 2001; Williams and Stuart, 2002; Ariav et al., 2003), feedforward inhibition (Grothe and Sanes, 1994; Pouille and Scanziani, 2001; Brand et al., 2002), and oscillatory activity (Singer and Gray, 1995; Engel et al., 2001; Lucke and von der Malsburg, 2004). In the locust olfactory system all of these properties act together, conveying coincidence detection attributes to the decoders of olfactory information (Perez-Orive et al., 2002). To better understand how information is decoded in this system we further explore its intrinsic and circuit properties, both in control conditions and after oscillatory synchronization has been abolished.

Each locust antennal lobe (AL) has 830 excitatory projection neurons (PNs) which synapse onto the dendrites of the intrinsic cells of the ipsilateral mushroom body (MB), called Kenyon cells (KCs) (Laurent and Naraghi, 1994; Leitch and Laurent, 1996). Odor-evoked PN responses exhibit coherent 20-30 Hz oscillations and slow modulations of firing rate which are odor- and PN-specific (Laurent and Davidowitz, 1994; Laurent et al., 1996; Wehr and Laurent, 1996). Information contained in the oscillatory synchronization of PNs has been shown to be functionally and behaviorally relevant (Stopfer et al., 1997; MacLeod et al., 1998). This odor representation becomes drastically sparsened in the MB (Perez-Orive et al., 2002), a brain area involved in the formation, retrieval and extinction of olfactory memories (Heisenberg et al., 1985; McGuire et al., 2001; Schwaerzel et al., 2002; Heisenberg, 2003).

Previous intracellular recordings of KCs have indicated that these cells can generate sharp spikelets suggestive of active conductances which could summate coincident input supralinearly (Laurent and Naraghi, 1994; Perez-Orive et al., 2002). By using both intracellular recordings and computer simulations, we wished to further explore these subthreshold properties and their potential role in the detection of coincident inputs. To examine circuit behavior, we developed a network model which takes into account KC intrinsic and circuit properties, and is capable of reproducing the olfactory representation observed experimentally in the MB (Perez-Orive et al., 2002). We used this MB model to gain insight into the possible advantages of a decoding system based on coincidence detection. To test the role of oscillatory synchronization in the decoding of olfactory

information, we abolished AL oscillations pharmacologically [as in (MacLeod and Laurent, 1996)] and used experiments and models to understand the effect of disrupted AL temporal dynamics on KC odor tuning.

3.2 Results

3.2.1 KC subthreshold properties *in vivo*

We performed intracellular recordings on KC somata *in vivo* to study their subthreshold responses to PN input. Monosynaptic excitatory postsynaptic potentials (EPSPs) were evoked in the KCs by applying single pulse electrical stimulation to the AL, whose PNs send axons to the MB calyx, where they make direct excitatory connections with KC dendrites (Leitch and Laurent, 1996; Hansson and Anton, 2000). As more PNs were recruited by increasing the electrical stimulus amplitude (SA), the EPSPs recorded from a KC increased in amplitude indicating that several PNs converge on individual KCs. Eventually an action potential was evoked (not shown). Very often, particularly if the KC was held slightly hyperpolarized by DC current injection, we observed sharp "spikelets" with a SA threshold smaller than that required to evoke a full-blown action potential (Figure 3-1 A).
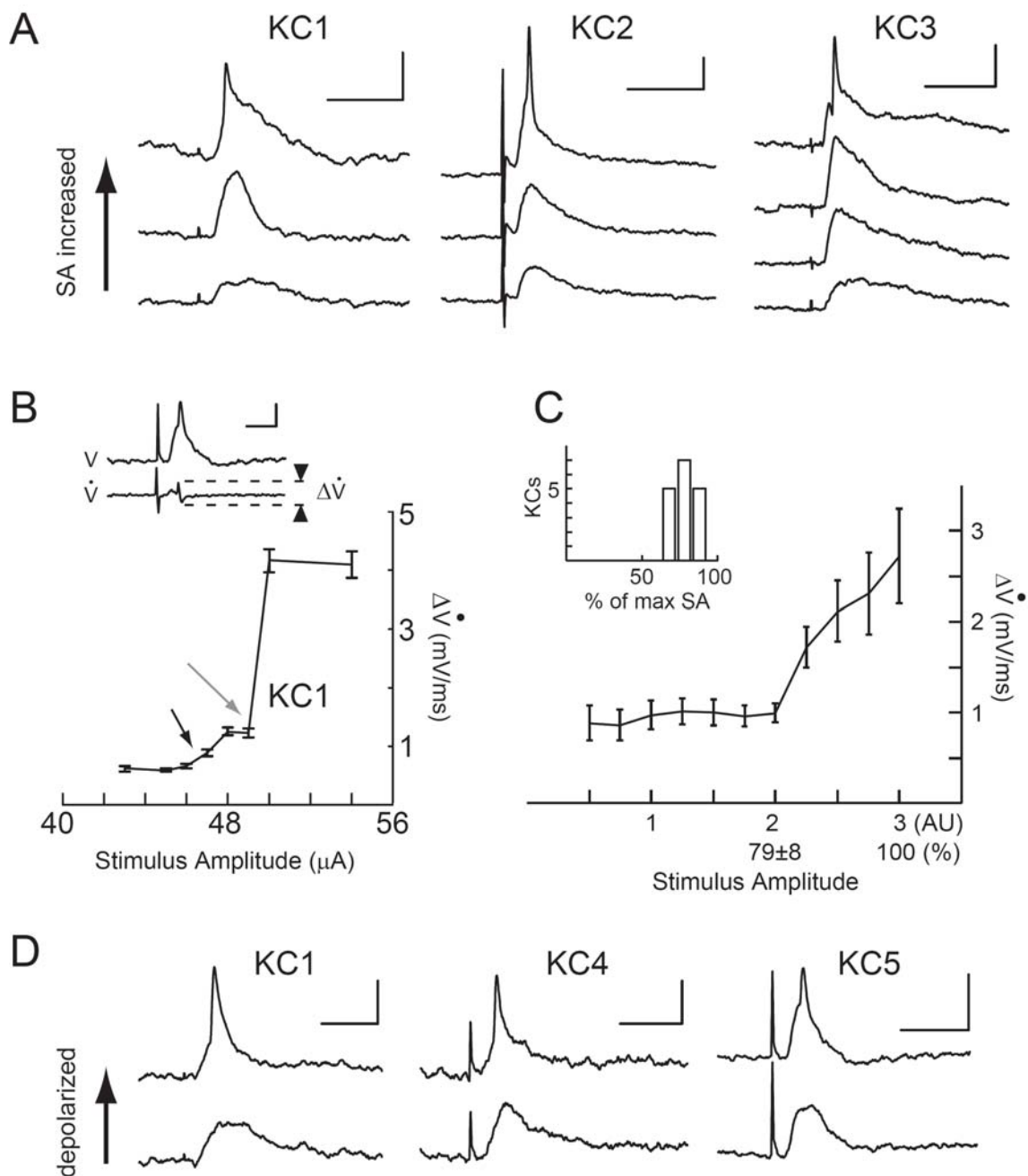
Figure 3-1. Subthreshold nonlinearities in KCs observed with intracellular recordings from KC somata *in vivo*. (A) Influence on KC EPSP shape of increasing SA to PNs. Examples for three different KCs. Increasing SA causes appearance of spikelet with distinct change in the waveform of the EPSPs (top traces). Calibrations: 50 ms, 5 mV. Stimulus artifacts of different sizes (caused by different SAs which varied across experiments because of slight differences in the placement of the stimulating electrode within the AL) can be observed before the EPSPs in all raw data traces. **(B)** Shape metric capturing transition in

EPSP waveform by measuring rate of voltage change. Inset: Voltage trace (upper) and its time derivative, Vdot (lower); calibrations: 30 ms, 3 mV, 3 mV/ms. The shape metric, ΔVdot, is defined as the maximal difference in Vdot. Main plot: ΔVdot as a function of SA (always below action potential threshold) for KC1 from (A). Gray arrow indicates abrupt nonlinear transition in shape metric as spikelet occurs. Smaller black arrow indicates smaller change in EPSP waveform that can be observed in the middle traces in (A). **(C)** Nonlinear behavior in KC EPSPs. Shape metric (mean ± SEM) measured for 17 KCs. Because each KC had a different SA sensitivity (due to positioning of PN stimulating electrode) SAs are normalized (arbitrary units, AU) at two points: SA = 3 is 100% of the SA before action potential threshold, and SA = 2 is 79±8% (mean ± SD) of this maximum, at which the largest stepwise increase in DVdot occurred in each series. Inset: histogram showing the point in which this largest stepwise increase occurred for all 17 KCs; the nonlinearity (SA = 2) occurs within a limited range of SA percentage values throughout the population of recorded KCs. **(D)** Influence of holding current on EPSP shape. Examples for three different KCs. EPSPs for each KC evoked by the same SA. Spikelets appear in a voltage dependent manner at more depolarized potentials (top traces). Calibrations: 50 ms, 5 mV.

To characterize this property across all recorded KCs we used a metric of postsynaptic potential shape, ΔVdot, that can be thought of as quantifying its "sharpness", taking into account both rising and falling phases of an EPSP (Figure 3-1 B). When EPSPs are slow, ΔVdot will be small, regardless of EPSP amplitude. ΔVdot increases as the EPSP rises or decays faster. ΔVdot for a KC recorded with a series of increasing SAs is shown in Figure 3-1 B. As the kinetics of the EPSP begin to change, ΔVdot increases slightly (middle traces in Figure 3-1 A; smaller black arrow, Figure 3-1 B), until an abrupt nonlinearity occurs (gray arrow). At this SA, the cell receives enough PN inputs to generate a spikelet. This nonlinear sub-spike-threshold behavior appears consistently across the population of intracellularly recorded KCs (Figure 3-1 C). The value of SA at which this nonlinearity occurs (expressed as a percentage of the maximum SA before action potential generation) lies within a relatively narrow range (Figure 3-1 C, inset). Spikelets could also be elicited by holding the KC at more depolarized potentials while

applying a constant SA, recruiting a fixed number of PNs (Figure 3-1 D). This supports

the idea that the nonlinear behavior is due to the recruitment of voltage-dependent

conductances by depolarization.

3.2.2 Single KC and network models

We explored the functional significance of this coincidence detection behavior in a

simplified model of a KC with realistic "active" conductances (see Methods Sections

3.4.5, 3.4.6) tuned to replicate the EPSP waveforms recorded *in vivo* (Figure 3-2 A). At

small stimulus amplitudes, EPSPs were not sufficient to depolarize the membrane

potential to potentials where the Ca^{2+} current could be activated; only passive responses

are exposed. When the EPSP amplitude was increased twofold, I_{Ca} activation, followed

by $I_{K,A}$ and $I_{K(Ca)}$, sharpened the EPSP (activation of the calcium current increasing the

speed of depolarization, the potassium currents ensuring fast repolarization). The sharp

"peak" riding on the otherwise smooth EPSP became more obvious at larger stimulus

amplitudes. At a stimulation amplitude just below Na^+ action potential threshold, the

EPSP contained a sharp spikelet whose return to baseline was accelerated, and whose

half-width was similar to those observed *in vivo* [Figure 3-1, see also (Perez-Orive et al.,

2002)]. Besides sharpening the EPSP, the interaction between active depolarizing and

hyperpolarizing conductances increased the firing threshold, and reduced the delay
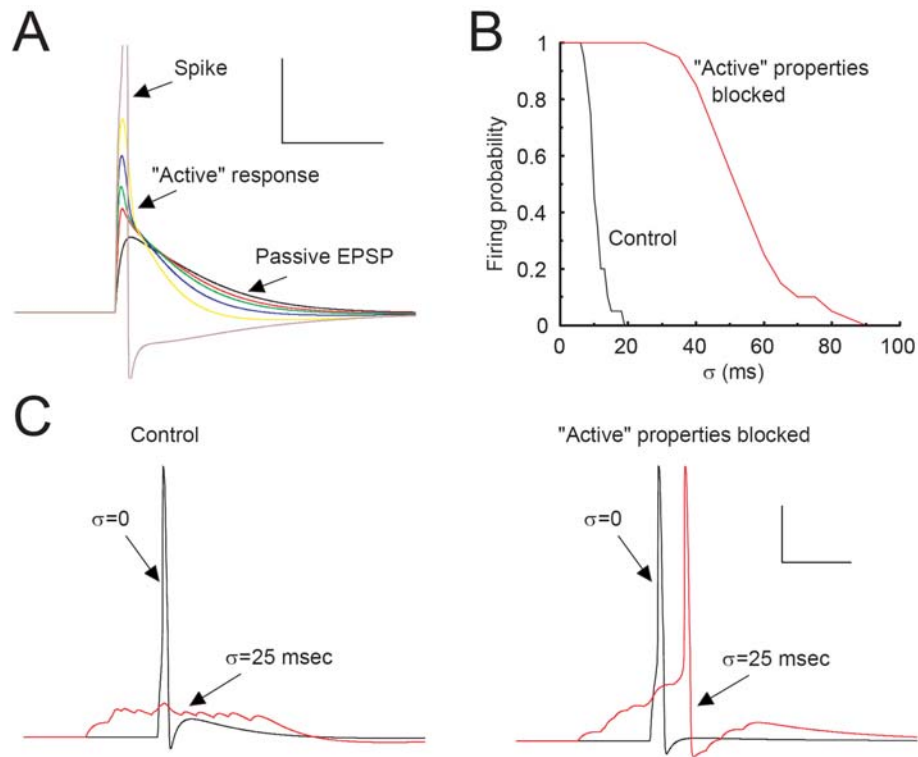
between EPSP onset and spike.

Figure 3-2. Effect of modeled intrinsic conductances on KC responsiveness. (A) Nonlinear response properties of the KC. The maximum synaptic conductivity, g^{syn}, was increased in integer multiples of the lowest value (black line), when only a passive response was found (black line), until a Na^+ spike was generated (brown line). Calibrations: 100 ms, 10 mV. **(B)** A train of 14 spikes was delivered through the cholinergic synapse to two different versions of a single KC model. To examine the effect of "active" intrinsic conductances on the temporal window of integration of the KC, different spike arrival times of the PN inputs were taken from Gaussian distributions with different standard deviations, σ. For the complete model, which included active conductances (see Methods Section 3.4.5), the firing probability falls rapidly as σ increases, whereas in the reduced model, including only I_{Na} and I_K, the firing probability remains high for much larger values of σ. **(C)** Responses of the complete (left) and reduced (right) KC models to similar inputs as described in (B). In the reduced model an input spike train with temporal jitter $\sigma = 25$ ms elicits a response from the KC, whereas in the complete model it does not. Calibrations: 50 ms, 25 mV.

If we assume that several EPSPs of similar amplitudes occur independently on the

dendrites of a KC, then jitter in the arrival times of the presynaptic spikes may critically

determine whether or not the KC will reach threshold. Figure 3-2 B and C illustrates the

responses of two different KC models: one with active properties as described above

(control), the other without any active conductances other than I_{Na} and I_K. A train of 14

spikes was delivered to each model with arrival times taken from a Gaussian distribution

with standard deviation σ. The synaptic weights from the PNs to the KCs were adjusted

so that the same minimal number of coincident EPSPs (with $\sigma = 0$ ms) was necessary to

trigger a KC spike (reducing them by 37% in the model without active conductances).

Thus, both models displayed a Na^+ spike when all input spikes were synchronized ($\sigma = 0$

ms). As the jitter of spike arrival times increased (Figure 3-2 B), the model with the

complete set of active conductances failed to generate a spike starting at $\sigma \sim 12$ ms, while

the reduced model showed reliable spiking up to $\sigma \sim 35$ ms. For the reduced model the

window of integration was determined solely by the membrane time constant and was

much larger than in the complete model, which was more sensitive to coincident inputs.

The KC units were used to construct a network model consisting of 20 KCs receiving

excitatory input from 210 PNs and feedforward inhibition from 20 lateral horn

interneurons (LHIs) (Figure 3-3 A). The PN activity of the model (Figure 3-3 B, see

Methods Section 3.4.7) includes dynamic ensembles of synchronized neurons replicating

the behavior of PNs recorded *in vivo* (Laurent et al., 1996; Wehr and Laurent, 1996;

Perez-Orive et al., 2002) as well as of PNs in a complete AL model (Bazhenov et al.,

2001a; Bazhenov et al., 2001b). Figure 3-3 C shows the responses of the KCs to four

different "odors", each represented by a unique input PN pattern. For each stimulus, one

to four KCs responded reliably with a Na^+ spike on most trials in spite of small variations

in the inputs (in spike number and timing) from one trial to the next. Different KCs

spiked at different times (e.g., compare responses of KC6 and KC10 to odor 1),

depending on the timing of transient correlations between their respective PN inputs [see

(Stopfer et al., 2003)]. In the majority of cases, KCs were silent or fired only very few

action potentials, which occurred when a few input spikes coincided. In this model, KC

responses depended both on their intrinsic properties (active conductances) and on a

feedforward inhibitory circuit (Perez-Orive et al., 2002) whose effect is to reduce the

integration window of KCs. When LHI-mediated feedforward inhibition was removed,

many KCs responded with 1-3 spikes for each odor (Figure 3-3 D), consistent with

experimental findings (Perez-Orive et al., 2002). These results indicate that a network of

KCs with a simple set of active conductances and realistic circuit connectivity can

respond with high specificity to different inputs, decoding the correlation structure

contained in the input spike trains.

Figure 3-3. Odor specificity of KC responses in network model. (A) Network model geometry. Each KC received 20 PN inputs from the AL; inputs were partially shared with neighboring KCs in the network

(input indexes are shown in the boxes). A network of 20 LHIs, each cell receiving all 210 inputs from the AL and contacting all 20 KCs, provided feedforward inhibition to the KCs (see Methods Section 3.4.7). **(B)** Firing patterns of 20 representative PNs are shown for 2 different odors. Each box represents activity for one PN. Each stimulus (1 s, horizontal bars) was presented 20 times and included small variations between trials. About half of the inputs were synchronized at each oscillation cycle and identities of the synchronized inputs changed slowly over the stimulus duration (see Methods Section 3.4.7). **(C)** KC responses to 4 different stimuli (1 s, horizontal bars). Each box represents one KC with 20 trials. Twenty cells are shown for each odor. Two to four KCs fired reliably in response to each stimulus. **(D)** Removing LHI mediated inhibitory input significantly reduced KC odor specificity. More than half of the KCs in the network responded reliably for each stimulus (20 trials; 1 s, horizontal bars).

3.2.3 Odor responses of KCs *in vivo* with disrupted AL dynamics

To test the effect of AL dynamics on KC tuning, we performed *in vivo* experiments in which picrotoxin (PCT), a $GABA_A$-like chloride channel blocker, was injected into the AL. Extracellular single unit tetrode recordings of KCs were made before and after PCT treatment. Blocking of fast GABA mediated inhibition in the AL has been shown to abolish PN oscillatory synchronization without significantly affecting mean PN firing rate or slow response patterning (on a time scale of hundreds of ms) (MacLeod and Laurent, 1996; MacLeod et al., 1998).

We tested KCs with a panel of odors (on average 12 odors per cell; range for each cell 5 to 17; 10 trials with 1 s odor pulses; 20 s inter-stimulus interval; $n = 16$ KCs) before and immediately after PCT injection into the AL. Figure 3-4 A shows representative examples of two cells and five odors. While neither cell showed a strong odor response in the control condition, both cells respond consistently to many odors after PCT treatment. Even though most KCs responded to zero or one odor in control conditions [as in (Perez-

Orive et al., 2002)], disrupting AL oscillatory dynamics with PCT in the AL increased

the probability of odor response of KCs (median probability of response: control, 0.00;

PCT, 0.42; Figure 3-4 B). Response intensity however (measured as the number of spikes

produced during an odor response), did not increase significantly with PCT treatment

(Figure 3-4 C). Because we observed few odor responses in control condition in the cells

recorded both before and after PCT (n = 16 KCs), this comparison includes additional

KCs that were each recorded in only one of the two conditions (control: n = 53 KCs with

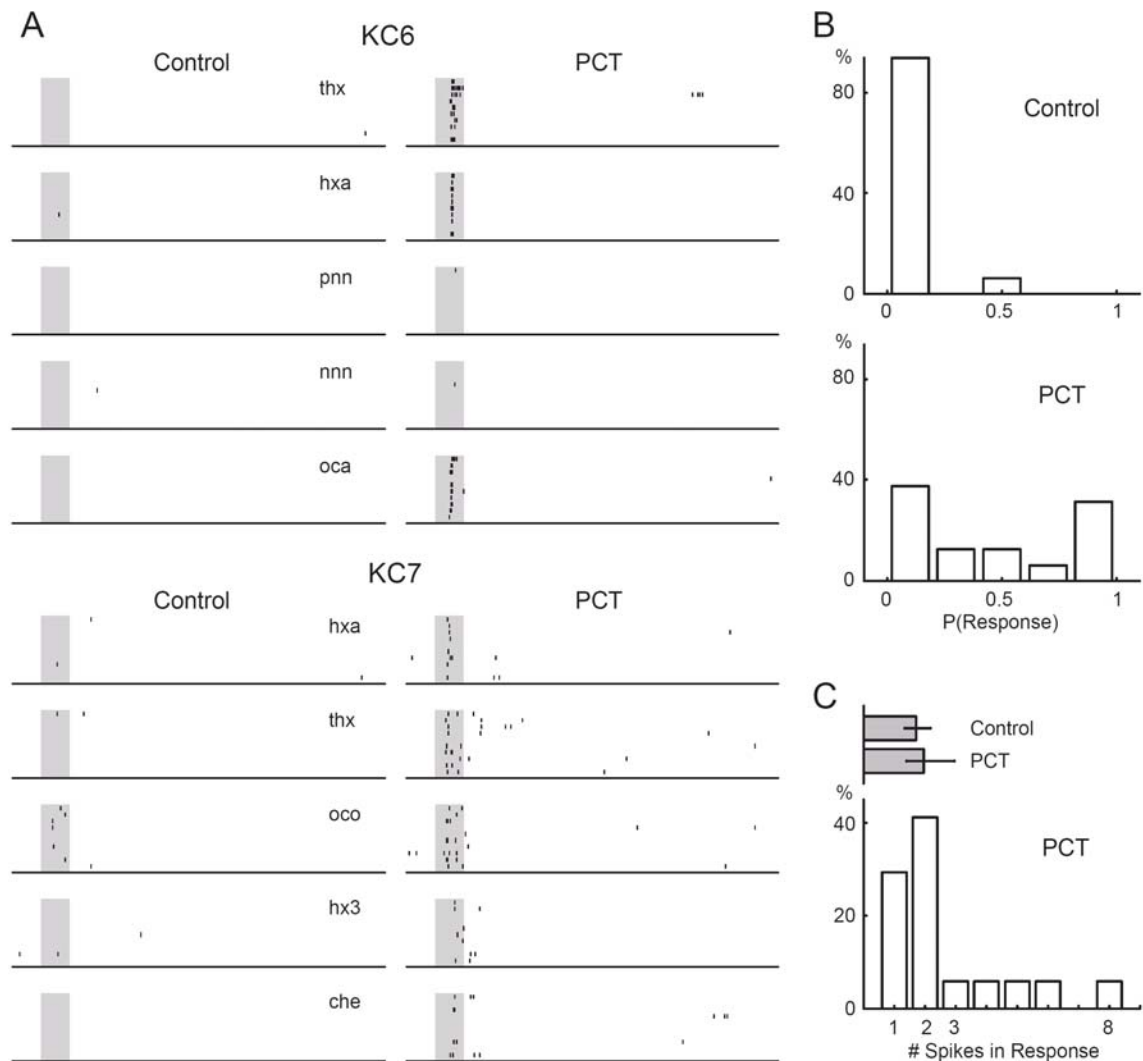responses; PCT: n = 17 KCs with responses).

Figure 3-4. Extracellular recordings of KC odor responses *in vivo* while blocking fast inhibition in the AL. (A) Responses of two different KCs to five different odors, recorded both before and after local PCT injection into the AL. Odor pulses (shaded area): 1 s; 10 trials per odor, top to bottom. Abbreviations are as follows: 1-hexen-3-ol (hx3), trans-2-hexen-1-ol (thx), 1-octanol (oco), hexanal (hxa), octanal (oca), 3-pentanone (pnn), 5-nonanone (nnn), cherry (che). **(B)** Frequency distribution of KC response probabilities (across all odors tested) before and after PCT injection into AL ($n = 16$ KCs recorded both before and after PCT treatment). Most KCs decrease their odor specificity after PCT injection. **(C)** Frequency distribution of KC response intensities, as measured by number of spikes in a 3 s window, after PCT treatment ($n = 17$ KCs). Spike counts were only computed for cell-odor pairs with a detected response. Top gray bars depict median, 25th and 75th percentiles for KC populations (control: $n = 53$ KCs with responses; PCT: $n = 17$ KCs with responses). Response intensity does not change significantly after PCT treatment.

Given that KCs appear to act as coincidence detectors, this result is counterintuitive, for it suggests that KCs fire more easily if their input is desynchronized. It can be explained, however, by considering the change in the instantaneous firing properties of PNs induced by PCT, and the contribution of LHIs to KC firing. The intrinsic and circuit properties of KCs confer upon them a preference for coincident input [Figure 3-1 - Figure 3-3; see also (Perez-Orive et al., 2002)]. Under control conditions this input arises in the form of periodic waves of excitation (from PNs) interspersed with periodic waves of inhibition (from LHIs). The local field potential (LFP) recorded in the MB reflects the overall influence of the PN population onto KCs. LFPs recorded during odor responses exhibit prominent 20-30 Hz oscillations reflecting the oscillatory synchronization of PN ensembles (Laurent and Davidowitz, 1994; Laurent and Naraghi, 1994; MacLeod and Laurent, 1996) (Figure 3-5 A). Disruption of AL dynamics with PCT abolishes this oscillatory synchronization (MacLeod and Laurent, 1996; Stopfer et al., 1997; MacLeod et al., 1998) and causes an increase, at odor onset, of LFP power in the 3-9 Hz frequency band (Figure 3-5 A and B). This increase in low frequency power at odor onset upon block of fast inhibition was also observed in an AL model (Bazhenov et al., 2001a) and reflects an excess of PN activity at odor onset but not later in the response (MacLeod and Laurent, 1996; Bazhenov et al., 2001a) which is explained by the loss of fast inhibition, but not slow inhibition, whose effect contributes to the sculpting of PN responses occurring in the presence of PCT (MacLeod and Laurent, 1996; MacLeod et al., 1998).
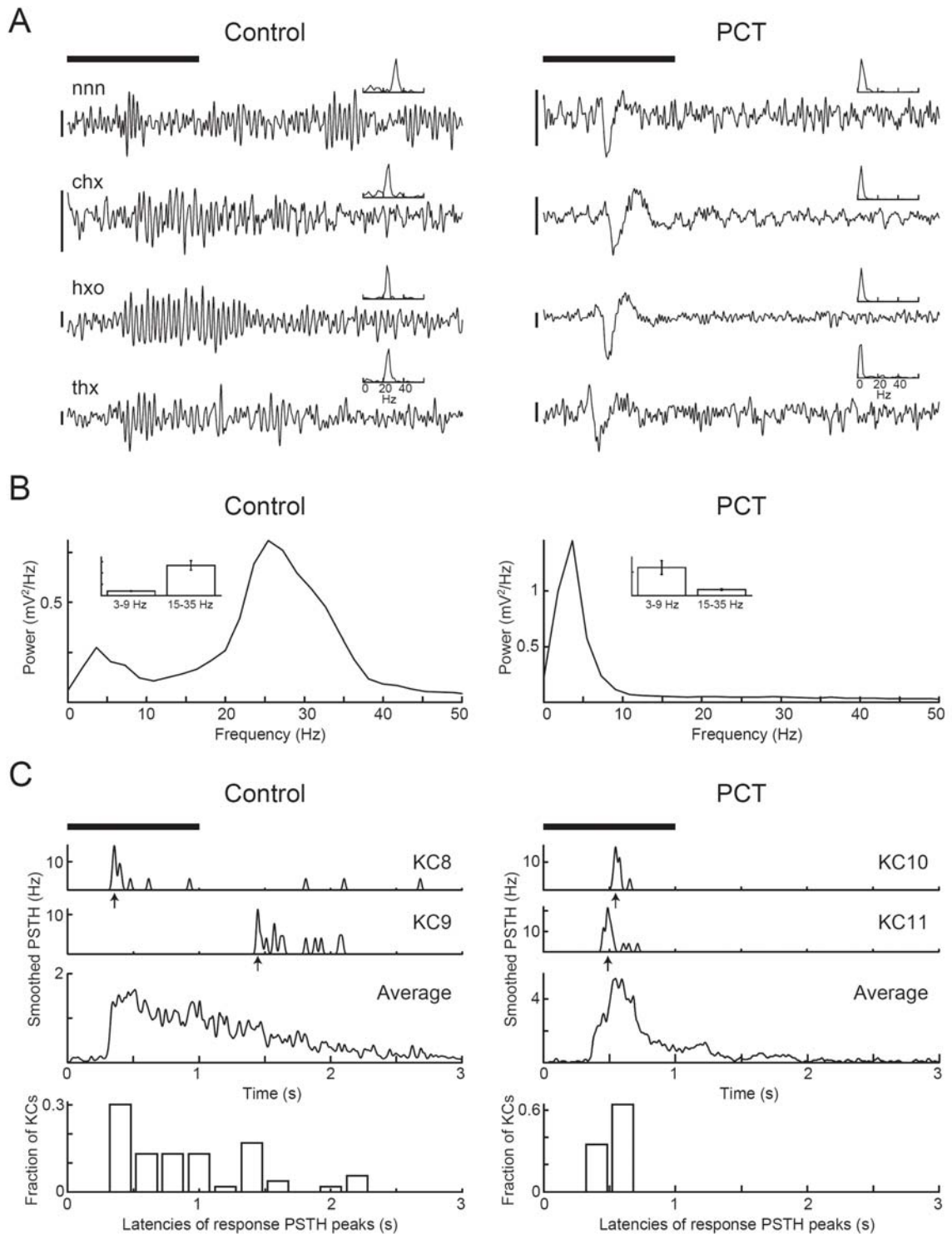
Figure 3-5. Changes to LFP and KC response latency *in vivo* while blocking fast inhibition in the AL.
(A) Examples of four pairs of LFP recordings (3-55 Hz bandpass filtered) from four different animals, each pair recorded with the same odor before and after PCT injection into the AL. Top bar indicates 1 s long

odor presentation; calibration bars 80 mV. Insets: power spectrum for each LFP recording, calculated from a 1 s window starting 300 ms after the odor stimulus trigger (300 ms is the approximate time it takes for the odor to reach the animal). Odor abbreviations: 5-nonanone (nnn), cis-3-hexen-1-ol (chx), 1-hexanol (hxo), trans-2-hexen-ol (thx). **(B)** Power spectrum averages for all recorded traces (same odors before and after PCT treatment; each condition: $n = 468$ trials, from 52 animal-odor pairs). Insets: mean $\pm$ SEM for 3-9 Hz and 15-35 Hz frequency bands in each condition. After PCT treatment power in the 15-35 Hz band is greatly reduced [due to abolishing of PN synchrony as described in (MacLeod and Laurent, 1996)] while power in the 3-9 Hz band increases ($p<0.02$, $n = 52$, two-sided paired t test). **(C)** KC odor response latencies. From top: PSTHs (smoothed with 10 ms Gaussian) of odor responses; examples of two KCs for each condition (arrows indicate latencies for each response measured at the time of PSTH maxima), population average, and frequency distribution of response latencies (control: $n = 53$ KCs with responses; PCT: $n = 17$ KCs with responses). In control condition response latencies are more widely distributed, while after PCT treatment all latencies occur close to odor onset, corresponding to the time of the low frequency LFP activity. All panels in (A) and (C) use the same temporal scale on abscissa.

We examined if this small change in PN response profile could explain the change in KC response probability induced by PCT. Our prediction was that the slight shift in PN activity towards the early phases of odor response might cause the excess KC responses seen in PCT conditions. If so, KC responses after PCT treatment would tend to occur at odor onset, while those in control conditions would be more widely distributed in time. This is indeed what we observed. The top three traces in Figure 3-5 C show smoothed PSTHs (two examples and group data) of KC odor responses before (left) and after (right) PCT treatment. The latencies of all recorded responses in both conditions (control: $n = 53$ KCs with responses out of 122 KCs recorded without treatment; PCT: $n = 17$ KCs with responses out of 22 KCs recorded after PCT treatment; different populations of KCs had to be used here given that among the population of 16 KCs recorded both before and after PCT treatment, there were too few responses in the control condition for a significant comparison to be made) are shown in the bottom panels of Figure 3-5 C.

While responses in the control condition occurred throughout the stimulus period and even beyond it, all responses under PCT conditions occurred at the time of the low frequency power increase in the LFP (compare Figure 3-5 A and C).

3.2.4 Model of KC responses with desynchronized AL input

We next used our network model to examine the possible contribution of different circuit effects on KC odor responses in PCT. To reproduce the effect of injecting PCT into the AL, odor-evoked PN firing activity was modified in two ways: a) oscillatory synchronization was eliminated, and b) the probability of PN firing at odor onset was increased (see Methods Section 3.4.7) so that the simulated LFP (obtained by summating all PN activity) displayed the early low frequency peak observed experimentally (Figure 3-5 A) and predicted by the full AL model when fast inhibition is blocked (Bazhenov et al., 2001a). The PNs maintained their overall slow temporal patterns (Figure 3-6 A) , as observed experimentally (MacLeod and Laurent, 1996; MacLeod et al., 1998) and the 20 Hz oscillations disappeared from the LFP (Figure 3-6 B).
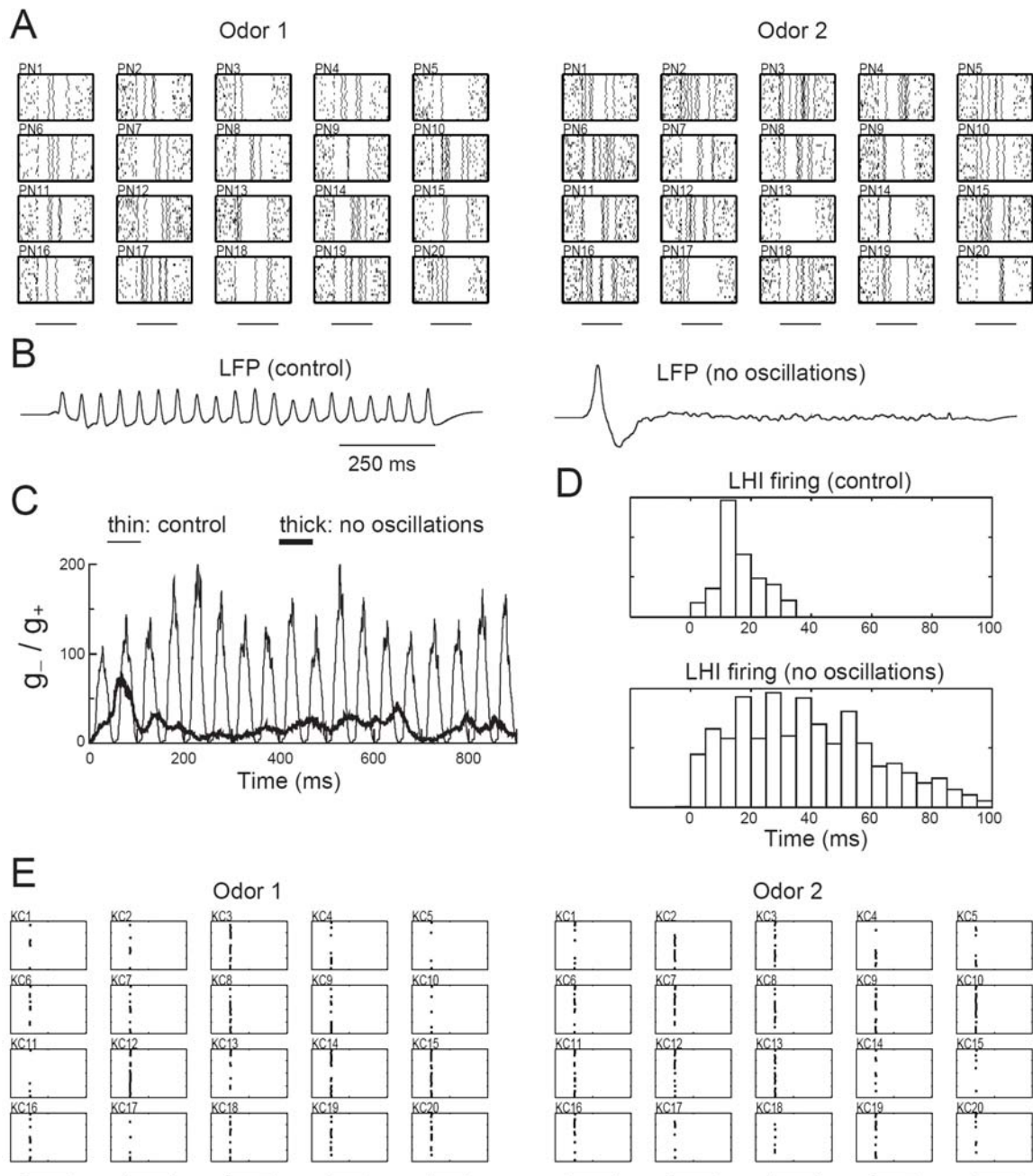
Figure 3-6. Effects of abolishing PN oscillatory synchronization in the network model. (**A**) Firing patterns of 20 representative PNs simulating PCT treatment of AL (20 trials for each PN). Horizontal bars: 1 s odor stimulus. Oscillatory synchronization has been abolished but slow temporal patterns remain. (**B**) LFP presents oscillations in the control condition (left), and a flatter pattern with a low frequency onset wave after blocking PN oscillatory synchrony (right). (**C**) Ratio of inhibitory (g_-) to excitatory (g_+) instantaneous synaptic conductances (g^{syn}[O], see Methods Section 3.4.6) of an average KC under control conditions (thin) and abolished oscillatory synchronization (thick). 1 s odor stimulus starts at time = 0 ms.

(D) PSTHs of all LHIs in the intact model (top; 0 ms, LFP maxima), and after abolishing PN oscillatory synchronization (bottom; 0 ms, odor onset). When synchronization is disrupted, LHI activity is more broadly distributed in time. **(E)** KCs exhibit a loss of odor specificity when AL oscillatory synchronization is abolished (20 trials for each KC). Horizontal bars: 1 s odor stimulus.

One effect of disrupting AL oscillatory dynamics is that the LHIs, which are driven by PNs, also lose their oscillatory synchronization. Figure 3-6 C shows the instantaneous ratio of inhibitory (LHI-mediated) to excitatory (PN-mediated) synaptic conductance on an average KC as a function of time during an odor stimulation. Given the observed phase-lag between feedforward inhibition and PN excitation in control conditions (Perez-Orive et al., 2002), this ratio directly reflected the 20 Hz periodicity of the excitatory PN drive. Most LHIs fired at a similar phase of the oscillation cycle, providing strong inhibitory input to their postsynaptic KCs (Figure 3-6 D) in antiphase with PN excitation. After blocking oscillatory synchronization in the AL, LHI firing times were broadly distributed (Figure 3-6 D) and the instantaneous contribution to KCs of inhibition relative to excitation was reduced (Figure 3-6 C, red). Because LHI inhibition normally limits the temporal window over which a KC can integrate its PN inputs (Perez-Orive et al., 2002), this relative reduction of feedforward inhibition will lengthen this integration window across oscillation cycles, reducing the preference of KCs for coincident input. Indeed, under these conditions, the model KCs lost much of their odor specificity (Figure 3-6 E). Furthermore, these responses occurred at odor onset (Figure 3-6 E), as observed experimentally (Figure 3-5 C). If, however, PNs were desynchronized without a slight increase in PN firing probability at odor onset (see Methods Section 3.4.7), KCs remained silent (not shown). This suggests that the active properties of KCs alone could

limit the duration of the integration window and that an increase in random correlated PN spikes is required. When KC active conductances were also blocked under these conditions (and EPSP size properly adjusted as described above), no other mechanisms remained in the model to select for coincident input and odor specificity was further reduced (not shown).

3.2.5 Coincidence detection vs. temporal integration (modeling)

Theoretically, the high specificity of KCs to odors (Perez-Orive et al., 2002) might result not from their ability to detect coincident input, but from appropriately tuned integrative properties. We wished to test whether there is an intrinsic advantage to using coincidence detection instead of classical integration over longer time windows to generate sparse response patterns. Past behavioral work indicated that disrupting oscillatory synchronization of PNs impairs the discrimination of molecularly similar odors (Stopfer et al., 1997). A set of similar input vectors (simulated odors), which differed only in the fast temporal structure of evoked PN activity (see Methods Section 3.4.7), was tested on two versions of our network model: a complete "coincidence detector" model, as in Figure 3-3 A, and an "integrator" model, in which the KCs' active conductances (other than those for Na$^+$ spike generation) and feedforward inhibition were removed. The synaptic weights from the PNs to the KCs were adjusted so that the same minimal number of EPSPs was necessary to trigger a KC spike in both models. The coincidence detector model responded to these odors in a highly specific way, with distinct KCs responding to different odors (Figure 3-7 A, top). Conversely, in the integrator model, the

same set of KCs responded to all similar odors, losing their ability to discriminate between them (Figure 3-7 A, bottom).

In another set of tests we used very dissimilar input vectors, differing by the identities of the PNs that fired at different epochs of the odor responses. That is, not only the fast temporal structure (as in Figure 3-7 A), but also the slower temporal structure varied among odors. In our model this corresponds to molecularly diverse odors, belonging to distinct chemical groups. In this case we observed that different KCs responded to different odors in both the coincidence detector and the integrator models (not shown). The fact that "integrator" KCs retain their specificity for these odors is a reflection of their long time windows of integration, which are able to distinguish between input vectors that differed in these longer time scales. Conversely, when the differences between the input vectors consist only in changes in their fast temporal structure (i.e., whether they synchronize with each other at certain oscillation cycles or not), only the coincidence detector models (with short temporal windows of integration) will be able to discriminate between them.
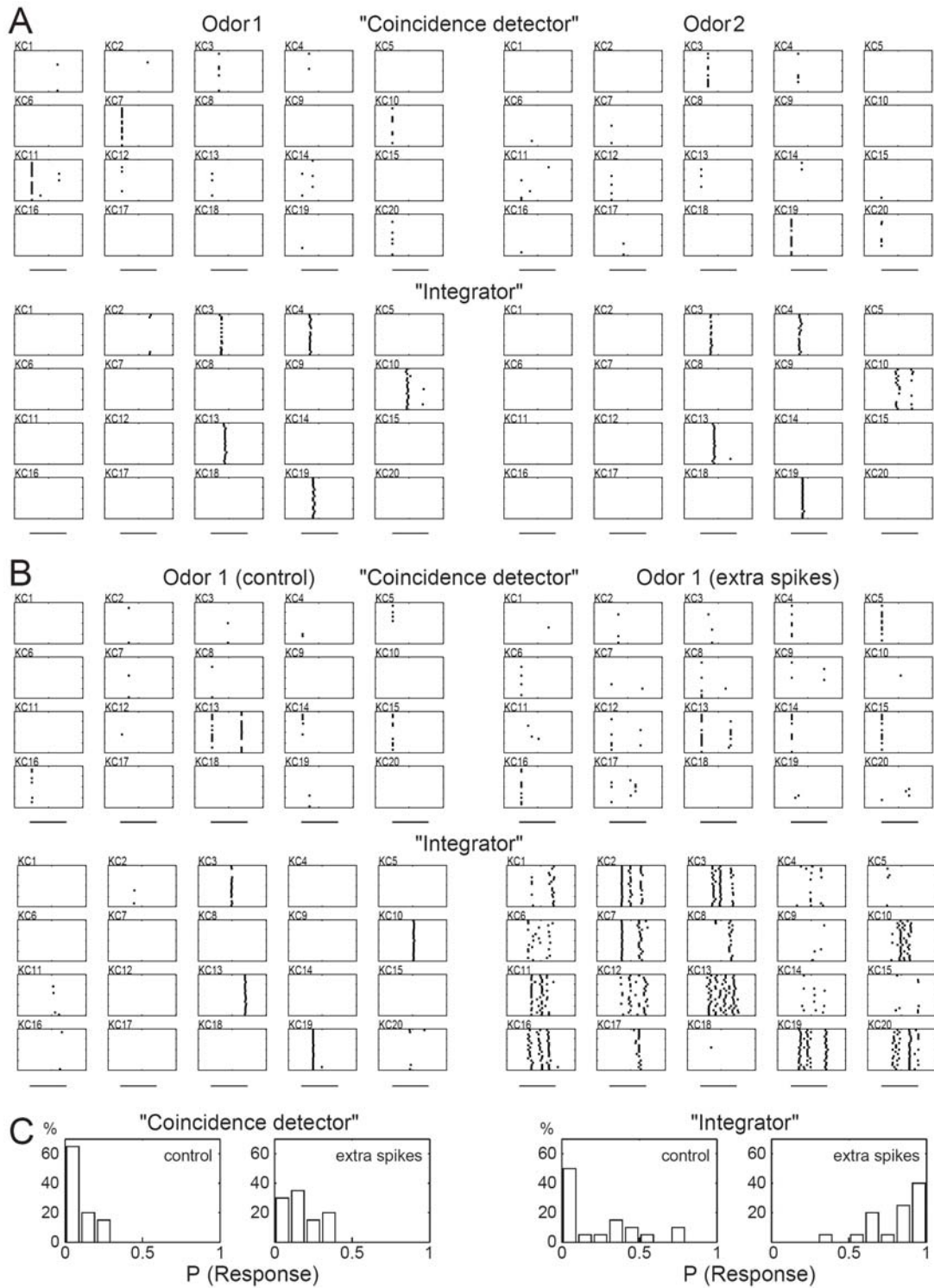
Figure 3-7. Effects of coincidence detection vs. temporal integration in the network model. (A) Sets of "similar" inputs (differing only in the fine temporal structure of PN firing) were presented to the models.

The control network ("coincidence detector", top) responded with specific response patterns for each of these odors (2 representative examples are shown). The model network with neither active conductances nor feedforward inhibition ("integrator", bottom) responded with the same pattern of active KCs for each of these odors (same 2 odors as in top panels are shown). **(B)** Effect of additional PN "noise" spikes on KC responses. Left, control input. Right, 25% extra spikes were added randomly to the input spike trains. Coincidence detection model (top) responded with minor changes in firing patterns after adding the extra spikes. In contrast, the response of the integrator model (bottom) changed dramatically and odor specificity was lost. **(C)** Frequency distribution of KC response probabilities in both models after adding the extra spikes. The coincidence detector model shows only a slight increase in response probabilities, while the integrator model exhibits a drastic reduction in response specificity.

To explore the sensitivity to noise of these two types of models, we used two modeled stimuli: a pure one and a "noisy" one, presented them with normal PN inputs representing odor responses, and "noisy" inputs in which 25% extra PN action potentials were added randomly. The coincidence detector model responded with minor differences to the control and noisy inputs, while the integrator model was drastically affected by the extra spikes, losing most of its odor specificity (Figure 3-7 B). Figure 3-7 C shows the distribution of the probabilities of odor responses for KCs from the two models. After adding extra spikes to the input, KCs from the coincidence detector model retained their odor specificity, while those from the integrator model responded to most odors tested. In the coincidence detector model an additional PN spike can potentially impact the KC response only if it is placed within a small time window, which is a rare event if the extra spikes come from uncorrelated noise. Conversely, in the integrator model, additional spikes occurring in much larger time windows can contribute to the KC responses. These modeling results suggest that the preference of KCs for coincident input confers upon

them the ability to discriminate between similar odors, as well as an increased robustness
to input noise.

3.2.6 KC tuning specificity and phase-locking (experiments)

Some of the mechanisms conferring coincidence detection properties to KCs (oscillatory
drive, subthreshold active properties, phase-delayed feedforward inhibition) also
contribute to the phase-locking of their action potentials to the cycles of LFP oscillations
(Perez-Orive et al., 2002). However, the precision of phase-locking varies among KCs, as
does their degree of odor specificity. We analyzed the relationship between odor
responsiveness and phase-locking in individual KCs, and found that the more odor
specific KCs display tighter phase-locking than the more promiscuous KCs. Figure 3-8
illustrates the degree of phase-locking for the 10 most specific KCs (having
P(Response)<0.06, which is typical for KCs), compared to 10 promiscuous KCs (having
0.35<P(Response)<0.48, which was less common). These KCs were the 10 most
promiscuous KCs with the exception of a few KCs with P(Response)≥0.7; these had
similarly poor phase-locking, but might be considered outliers because they were very
rare. Even though the average phase of KC spikes was the same in both groups, the
degree of phase-locking, as reflected by the polar histograms and vector magnitudes, was
stronger in the specific than in the promiscuous KCs (Figure 3-8). Throughout the
population of recorded responses in KCs, we found a significant negative correlation
between the probability of odor response and the phase vector magnitude of individual

KCs (r = -0.43, p<0.005, n = 42 KCs with responses and simultaneously recorded LFPs,
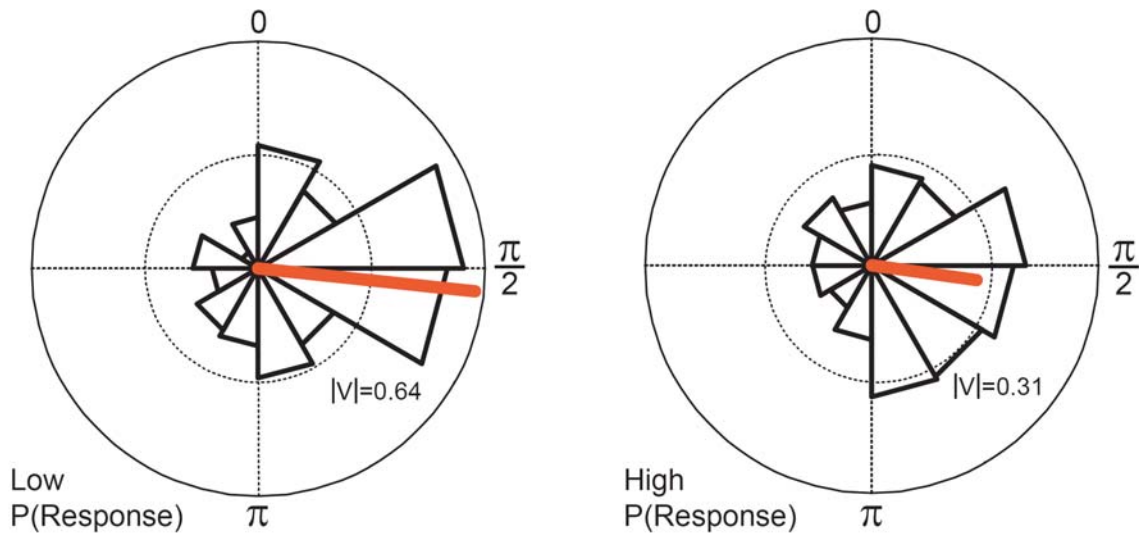
two-sided correlation t test).

Figure 3-8. Relationship between degree of KC phase-locking and odor specificity. Polar phase plots of
10 specific and 10 promiscuous KCs. LFP cycle maxima defined as 0 rad, minima as π rad. Red bar
indicates average phase and vector magnitude for each group. While average phases are similar, vector
magnitude for the promiscuous cells is 48% of that for the specific cells. Gridlines represent 0.10
(probability per bin).

3.3 Discussion

Active dendritic conductances have been shown, in culture and slices, to contribute to

coincidence detection by nonlinear summation of synchronized input in hippocampal and

neocortical pyramidal cells (Margulis and Tang, 1998; Williams and Stuart, 2002; Ariav

et al., 2003). Our *in vivo* experiments show that KCs in the locust exhibit highly

nonlinear subthreshold properties. In particular, they indicate that coincident EPSPs can

summate supralinearly, favoring coincidence detection. Many of these observed

subthreshold nonlinearities are likely due to the active conductances observed in KCs in

culture (Schafer et al., 1994; Grunewald, 2003). These nonlinearities can amplify

coincident EPSPs (as in the case of spikelets). Other nonlinear properties appear to be

caused by feedforward inhibition (e.g., middle traces in Figure 3-1 A and smaller black

arrow in Figure 3-1 B), as suggested by whole-cell patch-clamp recordings in which

inhibition to KCs was blocked (Perez-Orive et al., 2002). In this sense, both intrinsic and

inhibitory mechanisms appear to act together at the subthreshold level to confer KCs with

a preference for coincident input.

The active conductances which have been observed in cultured KCs (Schafer et al., 1994;

Grunewald, 2003) were included in a Hodgkin-Huxley type KC model (see Methods

Section 3.4.5). This simple model of a KC with realistic active conductances can produce

EPSP waveforms similar to those observed *in vivo* and demonstrates the important effect

that these active properties have on the temporal window in which a neuron integrates its

input. In particular, the active repolarizing currents decrease the width of postsynaptic

potentials, narrowing the temporal window in which the active depolarizing currents can

summate inputs supralinearly (Johnston et al., 1996; Fricker and Miles, 2000; Galarreta

and Hestrin, 2001). In agreement with these results, theoretical studies have found that

the temporal duration of EPSPs is a critical factor determining whether neurons

selectively detect coincident input (Abeles, 1982; Gerstner et al., 1996; Kempter et al.,

1998). When realistic PN activity is injected into a network model that includes these

active KC conductances and feedforward inhibition, KCs are silent most of the time and

their responses are highly specific and brief, indicating that these mechanisms are

sufficient to explain the sparsening of the odor representation observed *in vivo* (Perez-Orive et al., 2002).

Disruption of PN oscillatory synchronization has been shown to decrease odor discriminability behaviorally (Stopfer et al., 1997) and physiologically at the output neurons of the MB (β-lobe neurons, directly downstream of KCs), but interestingly, not at the level of PNs themselves (MacLeod et al., 1998). The present results shed light on the location and possible mechanisms involved in this loss of discriminability. Our *in vivo* recordings indicate that the loss of specificity exists first at the level of KCs. A loss of information under these conditions must therefore occur in the decoding of PN output by KCs. The increase in LFP low frequency power at odor onset, together with the fact that all KC responses occur at this time, suggest that an increase in instantaneous PN firing at odor onset contributes to the loss of specificity. A complete AL model in which fast inhibition is blocked without disrupting slow inhibition, predicted similar changes in the LFP as those observed here *in vivo* (Bazhenov et al., 2001a). In the AL model these LFP changes reflect a small increase in PN activity exclusively at odor onset, before slow inhibition has been activated (Bazhenov et al., 2001a).

Our network model supports the idea that a slight increase in PN activity that is time-locked to odor onset is important for generating the observed KC loss of specificity. Furthermore, the model predicts that a disruption of LHI feedforward inhibition contributes as well to the observed increase in KC responsiveness: this inhibition is driven by PN activity and when PN oscillatory synchronization disappears, the net

inhibitory drive on KCs is reduced (Figure 3-6 C), disrupting the periodic resetting of KC postsynaptic potentials. Under control conditions KCs respond selectively to coincident PN input that is synchronized within an oscillation cycle (Perez-Orive et al., 2002). When oscillatory synchronization is abolished by blocking fast inhibition in the AL, this coincident input can arise from spurious correlations caused by a small (and non odor-specific) increase in PN activity which is time-locked to odor onset. Furthermore, if the net effect of feedforward inhibition is weakened as suggested by the model, the selectivity for coincident input is reduced, allowing KCs to integrate over larger temporal windows. Experimental findings in the hippocampus (Pouille and Scanziani, 2001) and auditory systems (Grothe and Sanes, 1994; Brand et al., 2002; Wehr and Zador, 2003) support the idea that feedforward inhibition can be critical for allowing a neuron to detect temporal differences in its inputs.

We found a significant correlation between the degree of phase-locking of individual KCs and their odor specificity: the more odor-specific a KC is, the tighter its phase-locking tends to be. Given that in this system phase-locking and coincidence detection share common mechanisms —PN oscillatory drive, KC active properties, feedforward inhibition— (Perez-Orive et al., 2002) and are therefore likely to be correlated, our current results suggest a possible link between the sensitivity of individual KCs to coincidence detection and their odor specificity.

The sparsening of the olfactory representation in the MB arises as a result of the selectivity of KCs for input that is coincident within an oscillation cycle (Perez-Orive et

al., 2002). Given that theoretically the sparsening could have resulted from different mechanisms relying on integration of inputs over longer time windows, it is important to consider what are the possible computational advantages that can arise from coincidence detection over classical integration strategies [e.g., (Sherrington, 1906; Adrian, 1926; Eccles, 1957; Shadlen and Newsome, 1998)]. Two difficult problems an olfactory system must solve are the discrimination between similar odors and robustness of odor classification in a highly noisy environment (Cain and Potts, 1996; Laurent, 2002); other sensory modalities need to solve analogous problems [e.g., (Dusenbery, 1992)], and to the extent that they face comparable constraints, it is possible that they use similar strategies. Our modeling results indicate that a coincidence detector strategy presents important advantages in both of these problems over a classical integrator model. By being sensitive to the timing of incoming action potentials on a fine time scale, a coincidence detector allows for an extra coding dimension with which to solve these complex problems (Laurent, 1999). Our modeling results show that this extra dimension can allow an olfactory system to discriminate between similar odors, which only differ in the fine temporal structure of the AL input, in a manner beyond the capabilities of a decoding system integrating over longer time scales. Moreover, our current experimental results indicate that oscillatory synchronization is required for the sparsening of the olfactory representation that occurs in the MB. Abolishing these oscillations has been shown to affect behavioral odor discriminability (Stopfer et al., 1997) supporting the idea that a decrease in sparseness implies a reduced capacity of the system to represent distinct odors (Marr, 1969; Kanerva, 1988; Laurent, 2002). In addition to this, by focusing on specific time windows within an oscillation cycle, the coincidence detector model is less

sensitive to uncorrelated noise in its input, in agreement with theoretical studies in other systems (Konig et al., 1996; Salinas and Sejnowski, 2000). In the locust, these coincidence detection mechanisms provide a powerful strategy with which to solve complex problems every olfactory system encounters.

3.4 Methods

3.4.1 Experimental preparation and stimuli

Electrophysiological experiments were conducted on locusts (*Schistocerca americana*) from an established, crowded colony. Young adults of either sex were immobilized, with one antenna left intact for olfactory stimulation. The brain was exposed, desheathed and superfused with locust saline, as previously described (Laurent and Naraghi, 1994). Odors were delivered by injection of a controlled volume of odorized air within a constant stream of desiccated air. Teflon tubing was used at and downstream from the mixing point to prevent odor lingering and cross-contamination. Several compounds commonly associated in nature with green plants were used as odor stimuli. The complete set of odors that were used are: 1-hexen-3-ol, trans-2-hexen-1-ol, cis-3-hexen-1-ol, 1-hexanol, 1-heptanol, 1-octanol, hexanal, octanal, nonanal, 3,7-dimethyl-2,6-octadiene-nitrile, 3-pentanone, 2-heptanone, 3-heptanone, 5-nonanone, 6-undecanone (Sigma Chemical, St. Louis, MO), cherry, mint and geraniol (LorAnn Oils, Lansing, MI). Odors were used at 10% vapor pressure (90% of KCs) or 100% vapor pressure (10% of KCs), further diluted (approximately 1:10) in the desiccated air stream. Electrical stimulation of PN axons was performed in the AL using 25 μm tungsten wire bipolar electrodes and a

WPI A360 stimulus isolator (World Precision Instruments, Sarasota, FL): 300 μs pulses; typical stimulus amplitudes 20-100 μA.

3.4.2 Electrophysiology

Intracellular sharp electrode recordings of KCs (Figure 3-1) were made with borosilicate glass micropipettes (World Precision Instruments, Sarasota, FL) filled with 0.2 M K-acetate (DC R>200 MΩ). KC input resistance at the soma was usually around 1 GΩ. Signals were recorded with an Axoclamp–2B (Axon Instruments, Union City, CA) and acquired (10 kHz, 12 bits) with a PCI-MIO-16E-4 data acquisition board and LabVIEW software (National Instruments, Austin, TX). For extracellular recordings (Figure 3-4, Figure 3-5 and Figure 3-8), wire tetrodes were constructed with 0.0005" and 0.0004" (12.7 and 10.2 μm, respectively) insulated nichrome wire (REDIOHM wire with PAC insulation; Kanthal Palm Coast, Palm Coast, FL). Four strands of wire were twisted together and heated to partially melt the insulation. The tip was cut with fine scissors and each channel tip was electroplated with gold solution (SIFCO, Cleveland, OH) to reduce the impedance to between 200 and 350 kΩ at 1 kHz. Tetrode recordings were made with a custom-built 16-channel preamplifiers (unitary gain) and amplifiers (10,000X). Data from each tetrode were filtered (in custom-built amplifiers, bandpass 300-6000 Hz) acquired continuously (15 kHz/channel, 12 bits) and stored. Electrodes (either sharp glass or one to three simultaneous tetrodes) were placed within the MB cell body layer, dorsal to the neuropils, at depths less than 200 μm. Cell identification was unambiguous because all the somata located in the layer above the MB calyx belong to KCs. Local field

potentials (LFPs) were recorded in the MB calyx, using wire tetrodes (bandpass filtered 1-6000 or 3-6000 Hz).

3.4.3 Picrotoxin microinjections

Patch pipettes were backfilled with a solution containing 5 mM (PCT) and 0.3% Fast Green (Sigma Chemical, St. Louis, MO). The pipette was introduced into the AL and a pneumatic picopump (World Precision Instruments, Sarasota, FL) was used to apply a series of three or four 100 ms, 10 psi pressure pulses. Each pulse injected *ca.* 1 pl of solution (as measured by previous injection into a drop of oil). Injected solution remained exclusively localized to the AL, as verified by dispersal of Fast Green.

3.4.4 Analysis of experimental data

Data were analyzed using Matlab (The Mathworks, Natick, MA) and Igor Pro (WaveMetrics, Lake Oswego, OR). Single unit activity was obtained from extracellular data by using a modified expectation maximization algorithm and an empirically characterized noise model (Pouzat et al., 2002), which allowed us to perform several statistical tests so as to select only well isolated units meeting rigorous quantitative criteria (Pouzat et al., 2002). A KC was classified as responding (e.g., in Figure 3-4) if its firing behavior during a 3 s window starting at odor onset met two independent criteria of response amplitude and reliability (Perez-Orive et al., 2002). The amplitude criterion was satisfied in a given trial if at least one 200 ms bin had a firing rate which exceeded by 3 SDs the mean baseline rate. Baseline rate was measured for each cell-odor pair over a

period of 3 s preceding stimulus onset over all trials with that odor. To ensure that

detected responses were reliable even at low firing rates, the reliability criterion required

that the amplitude criterion be satisfied in more than half of all trials with each odor.

Several variations of this response definition were tested and yielded nearly identical

results (Perez-Orive et al., 2002). Phases of KC spikes with respect to LFP oscillations

were measured by linearly interpolating the time between the maximum (0° or 360°) and

minimum (180°) of the bandpass filtered (15-45 Hz) LFP.

3.4.5 Computational model; intrinsic currents

KCs and lateral horn interneurons [LHIs, (Perez-Orive et al., 2002)] were modeled as a

single compartment with channels governed by Hodgkin-Huxley kinetics: $C_m dV/dt = -g_L(V - E_L) - I^{int} - I^{syn}$, where C_m is the membrane capacitance, g_L is the leakage

conductance, E_L is the leak reversal potential, V is the membrane potential, I^{int} is the sum

of active intrinsic currents and I^{syn} is the sum of synaptic currents. The KC model

included a transient Ca^{2+} current, I_{Ca} (Laurent et al., 1993), a Ca^{2+} dependent K^+ current,

$I_{K(Ca)}$ (Sloper and Powell, 1979), a transient (A-type) K^+ current, $I_{K,A}$ (Grunewald, 2003);

fast Na^+, I_{Na}, and delayed rectified K^+, I_K, currents were included to account for spike

generation (Traub, 1982). Current kinetics were adjusted to 23°C. The LHI model

included only I_{Na} and I_K. The intrinsic currents were described as follows: $I^{int}_j = g_j$

$m^M h^N(V-E_j)$, where g_j is the maximal conductance for current 'j', E_j is its reversal

potential, m(t) and h(t) are activation and inactivation variables. In most of the

simulations, the maximal conductances and passive properties were $C_m = 2.9 \cdot 10^{-4}$ μF, g_L

= 2.9·10^{-3} µS, E$_L$ = -65 mV, g$_{KL}$ = 1.16·10^{-3} µS (K$^+$ component of the leak current), g$_{Na}$ =

26.1 µS, g$_K$ = 2.9 µS, g$_{Ca}$ = 0.029 µS, g$_{K(Ca)}$ = 0.29 µS, g$_{K,A}$ = 0.0145 µS for KCs; and C$_m$

= 1.43·10^{-4} µF, g$_L$ = 7.15·10^{-3} µS, g$_{KL}$ = 7.15·10^{-4} µS, g$_{Na}$ = 14.3 µS, g$_K$ = 1.43 µS for

LHIs. E$_L$ values for LHIs were taken from a random distribution with 10 mV variability

(E$_L$ = -70 ± 5 mV) which led to variability in resting membrane potential across them.

Many of the maximal conductances indicated above were systematically varied in our

study to find the limits of observed phenomena.

The I$_{Ca}$ current used for KCs had M = 2, N = 1, m$_\infty$ = 1/(1+exp(-(v+40)/10.0)), τ$_m$ = 0, h$_\infty$

= 1/(1+exp((v+50)/4)), τ$_h$ = (30.8+(211.4+exp((v+115.2)/5))/(1+exp((v+86)/3.2)))/18.

The I$_{K,A}$ current used for KCs had M = 1, N = 0, m$_\infty$ = 1/(1+exp(-(v+60)/1)), τ$_m$ =

(1/(exp((v+35.82)/19.69)+exp(-(v+79.69)/12.7))+0.37)/3.74. The I$_{K(Ca)}$ current used for

KCs had M = 2, N = 0, m$_\infty$ = 3333[Ca]^2/(3333[Ca]^2+1), τ$_m$ = 0. I$_{Na}$ and I$_K$ were modeled

as in (Traub, 1982). For all cells E$_{Na}$ = 50 mV, E$_K$ = -95 mV, E$_{Ca}$ = 12.8 log([Ca]$_O$/[Ca]),

[Ca]$_O$ = 2 mM. For KCs, intracellular Ca^{2+} dynamics were described by a simple first-

order model: d[Ca]/dt = - A I$_{Ca}$ - ([Ca]-[Ca]$_\infty$)/τ, where [Ca]$_\infty$ = 2.4 ·10^{-4} mM is the

equilibrium intracellular Ca^{2+} concentration, A = 1.7862 mM/(ms·µA) and τ = 100 ms.

3.4.6 Computational model; synaptic currents

All synaptic currents were calculated according to I^{syn} = g^{syn} [O] (V - E^{syn}), where g^{syn} is

the maximal conductivity, [O](t) is the fraction of open channels and E^{syn} is the reversal

potential. E$^{syn}_{nACh}$ = 0 mV for cholinergic receptors, E$^{syn}_{GABA-A}$ = -74 mV for GABA$_A$

receptors. Synaptic currents were modeled by first-order activation schemes (Destexhe et al., 1994): $d[O]/dt = \alpha(1-[O])[T] - \beta[O]$, where $[T]$ represents the concentration of transmitter (Bazhenov et al., 2001b). The rate constants, α and β, were $\alpha = 10$ ms^{-1} and $\beta = 0.12$ ms^{-1} for GABA$_A$ synapses and $\alpha = 0.94$ ms^{-1} and $\beta = 0.18$ ms^{-1} for cholinergic synapses. The maximal conductances were $g_{nACh(KC)} = 0.044$ μS for AL afferents into KCs, $g_{nACh(LHI)} = 0.0044$ μS for AL afferents into LHIs, $g_{GABA\text{-}A} = 0.05$ μS for synapses from LHIs to KCs.

3.4.7 Network geometry and stimulation

The MB model consisted of populations of 20 KCs and 20 LHIs. Each KC received 20 inputs from the AL, with an overlap of 10 inputs between neighboring KCs (Figure 3-3 A). Thus a total of 210 afferents from the AL (PNs) were modeled. Each LHI received the sum of all AL afferents. Random time delays (mean = 15 ms; S.D. = 7 ms) were introduced to the LHI inputs to provide a response delay and some variability across LHI firing (Perez-Orive et al., 2002). GABAergic synapses from all 20 LHIs projected then to each KC. Each "odor" stimulus was represented by an input vector characterized by a unique spatio-temporal pattern of activity across the 210 PNs. Typically about half of the PNs were active at each instant of a given odor presentation. Additionally, about 50% of the active PNs were synchronized with each other, producing 20 Hz oscillations in the population average (representing the LFP). The identities of the active PNs changed slowly over the stimulus duration to model the slow temporal structure of PN responses. Similarly, the identities of the PNs that were synchronized at each oscillation cycle varied

to model transient spike synchronization. More specifically, we assumed that about 50%
of all PNs are active at the first cycle of odor-induced oscillations. Any active PN could
then become silent at the next cycle and vice versa. However, to maintain a realistic
correlation between PN activity patterns in successive cycles (Stopfer et al., 2003), a
higher probability (p = 0.6) was assigned for PNs to stay in their current activation state.
This created a temporal structure with excitatory and inhibitory epochs lasting on average
150 – 200 ms, consistent with experimental findings (Laurent et al., 1996; Stopfer et al.,
2003) and our previous results of AL modeling (Bazhenov et al., 2001a). The specific
spike timing of active PNs at different trials was calculated from Gaussian distributions
whose standard deviations, σ, were a function of PN and cycle numbers. Narrow
distributions (small σ) characterized PN spikes locked to the same phase of the LFP
oscillation across trials. Wide distributions characterized non-synchronized spikes (for a
given PN and time during the response). For a given neuron σ changed from one
oscillation cycle to the next to model transient patterns of spike synchronization (Wehr
and Laurent, 1996). To avoid abrupt transitions between synchronous and asynchronous
states, we gave higher probabilities for PN spikes to maintain their assigned σ from one
cycle to the next. In this way, approximately 50% of all active neurons were
synchronized at each oscillation cycle. Finally, to simulate multiple trials with the same
odor, small variations (from one trial to another) were included in the identities and
synchronization patterns of active PNs. Random low frequency spiking (4 ± 2 Hz) was
modeled to simulate baseline AL activity between odor presentations. "Different" odors
were modeled by completely different spatio-temporal patterns of PN activation, while
"similar" odors were represented by inputs having the same slow temporal structure (the

same PNs were active at each cycle of oscillations) but different patterns of synchronization (i.e., even though the same PNs were activated at a given cycle, the identities of those that were synchronized to the LFP was different). This choice of "similar" versus "different" odors was motivated by experiments showing that PCT application to the locust AL eliminated PN oscillatory synchronization, while preserving the slow temporal structure of PN firing (MacLeod and Laurent, 1996; MacLeod et al., 1998), and that this intervention disrupts the behavioral ability of the animal to discriminate between odors belonging to the same chemical group ("similar" odors), but preserves the ability to discriminate between chemically different odors (Stopfer et al., 1997). To model the effect of PCT application to the AL, oscillatory synchrony across PNs was eliminated and the probability of PN firing at odor onset was increased so that the simulated LFP displayed the early low-frequency peak observed experimentally and predicted by a full AL model when fast inhibition is blocked (Bazhenov et al., 2001a). To accomplish this we assumed that within the first 50 ms of odor presentation each PN can produce up to 4 spikes (vs. 1 spike in control conditions) with a probability $P = P_0 + 0.6(1 - P_0)$, where P_0 is the probability of spiking in control conditions. In order to maintain a similar number of total PN spikes during the complete odor presentation, the probability of spiking during the rest of the stimulus (after the first 50 ms) was reduced to $P = 0.5P_0$.

3.5 Acknowledgments

Biological Studies. J. Perez-Orive performed the intracellular (Figure 3-1) and extracellular (Figure 3-4, Figure 3-5 and Figure 3-8) electrophysiological experiments. M. Bazhenov performed the KC (Figure 3-2) and network (Figure 3-3, Figure 3-6 and Figure 3-7) modeling work.

4   Kenyon Cell Electrophysiology: Additional Properties

4.1 Introduction

As described in Section 1.2 of this dissertation, the mushroom bodies (MBs) are important model systems which offer valuable advantages for the study of several critical neuroscientific issues, such as learning and memory (Hammer and Menzel, 1995; McGuire et al., 2001; Pascual and Preat, 2001; Heisenberg, 2003), olfactory and other sensory physiology (Strausfeld et al., 1998; Gronenberg and Holldobler, 1999; Laurent et al., 2001; Laurent, 2002; Marin et al., 2002), and neural coding (Laurent, 1996; Grunewald, 1999a; Laurent, 1999; Strausfeld and Li, 1999b; Perez-Orive et al., 2002). A significant amount of genetic and anatomical work has been conducted on the intrinsic cells of the MB, the Kenyon cells (KCs). However, there are very limited electrophysiological descriptions of these important neurons (Laurent and Naraghi, 1994).

This chapter will provide further descriptions of electrophysiological properties of KCs, and how these may be related to some important neural coding issues. It is comprised of three parts which characterize different aspects of KC physiology, odor responses and relationship to local field potential (LFP) oscillations. Specifically, in Section 4.2 the conduction velocity of their axons is measured; in Section 4.3 I will study whether their olfactory responses are clustered by chemical structure of odorants (within a given KC), or by spatial location of their cell bodies (for a given odor); finally, in Section 4.4 the

temporal evolution of LFP power will be characterized, and the relationship between this

population phenomenon and KC activity will be analyzed.

4.2 Conduction Velocity of Kenyon Cell Axons

4.2.1 Methods

In vivo electrophysiological experiments were conducted in locusts (*Schistocerca*

americana) ($n = 6$ locusts) from an established, crowded colony, as described in Section

3.4.1 and (Laurent and Naraghi, 1994). *In vitro* experiments were also carried out in

which the MB was dissected out of the head capsule ($n = 2$ locusts). Similar results were

obtained in both conditions.

A 25 μm tungsten wire bipolar electrode was used for electrical stimulation, applied with

a WPI A360 stimulus isolator (World Precision Instruments). Typical stimulation

parameters were 500 μs pulse width and 30-400 μA stimulus amplitudes. Extracellular

compound action potentials (CAPs) were recorded using saline-filled patch pipettes (DC

R: 1-3 MΩ). Recording electrodes were often covered with Sylgard (Dow Corning) in

order to reduce the transmural capacitance of the electrode, and therefore minimize the

effects of the preparation saline level on the recording (Purves, 1981). Signals were

recorded with an Axoclamp–2B (Axon Instruments). For projection neuron (PN)

conduction velocity measurements, the stimulating electrode was placed in the center of

the AL, and the recording electrode was placed in the MB calyx, where the PN axons

contact KC dendrites. For KC conduction velocity measurements, the stimulating

electrode was placed in the KC cell body layer of the MB, and the recording electrode

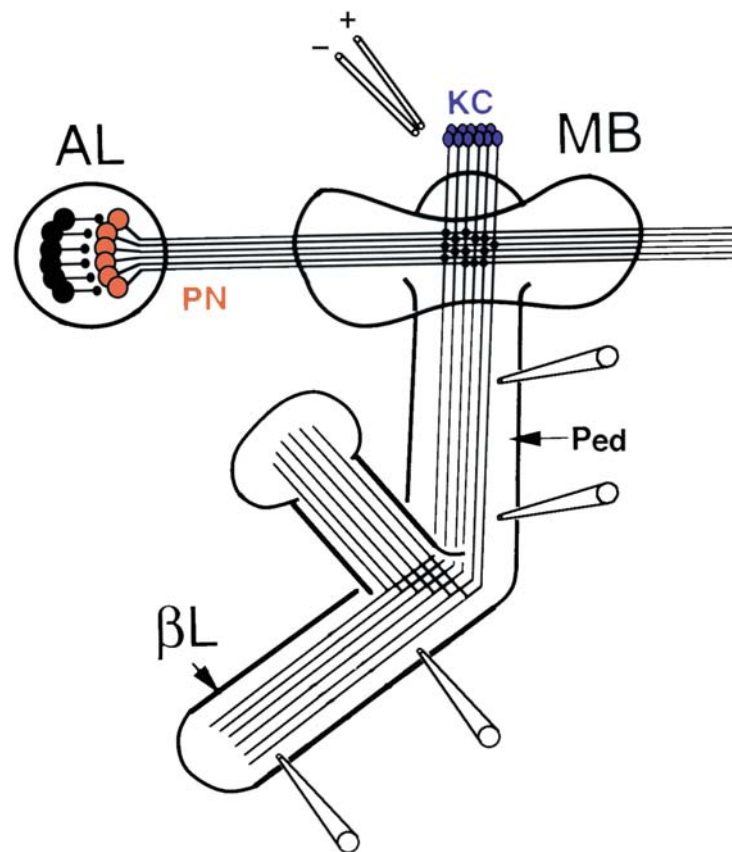was placed at different points along the MB pedunculus and β-lobe (Figure 4-1; see also

Figure 1-1).

Figure 4-1. Schematic of experimental setup for KC conduction velocity measurements. Bipolar stimulating electrodes were placed in the KC cell body layer. Field electrodes were placed at different sites along the MB pedunculus and β-lobe in order to record CAPs from KC axons [figure adapted from (MacLeod et al., 1998)].

Data were analyzed using Matlab (The Mathworks). The distances from the stimulating to the recording electrodes were obtained using a measurement grid on the microscope eyepiece, which was calibrated with a stage micrometer standard (AO Scientific Instruments). The calibrated eyepiece grid was found to have a resolution of 41 ± 1 μm. In order to estimate the actual distance traversed by the axons which are not rectilinear (as in the case of KC axons recorded in the β-lobe and PN axons), the measured distances were adjusted using a normalizing coefficient, *K* (Figure 4-2). The values for the *K* coefficient were obtained by taking measurements from locust Bodian-stained whole brains in which the straight line distance ("measured distance" in the electrophysiological experiments) was compared to the actual distances traversed by the axons (broken down into three segments). Two different values of *K* were obtained in this way, one for PN axons going from the AL to the MB calyx, and another for KC axons from the MB calyx to the β-lobe. In KC recordings obtained from the pedunculus, this adjustment was not performed because the path of KC axons at this stage does not include significant deviations from a straight line.
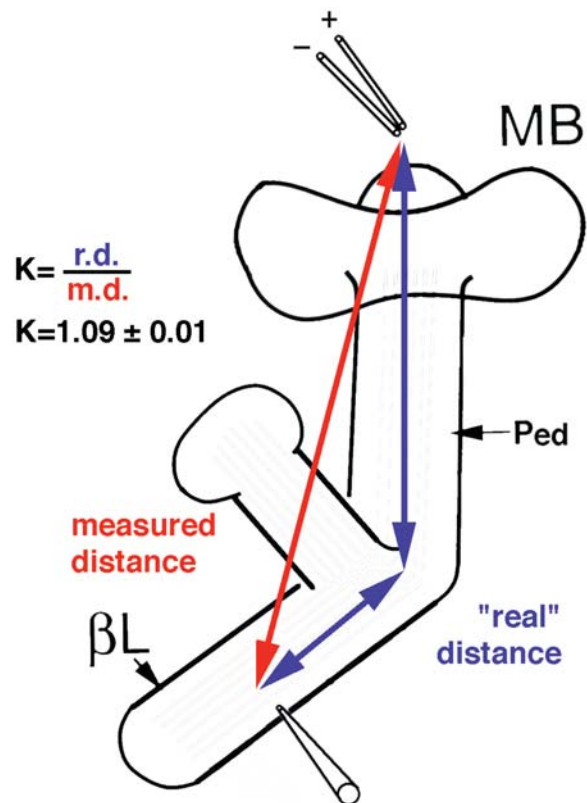
Figure 4-2. Schematic illustrating the correction for distance measurements conducted in the β-lobe. The measured distance corresponds to the straight line measurement between stimulating and recording electrodes. A more accurate value of the "real" distance was estimated by adjusting the measured distance with a normalizing coefficient, *K* (see Methods Section 4.2.1). A similar correction was applied to PN axon measurements.

4.2.2 Results

The conduction velocity, *v*, of action potentials propagating along an axon can be

obtained by measuring the time of propagation, *t*, along a given distance, *d*, and

calculating $v = d/t$. I conducted electrophysiological experiments in which CAPs were

evoked by stimulating extracellularly a population of KCs or PNs and measuring the time

it took the CAP to reach a recording electrode placed a known distance away along the axon (see Methods Section 4.2.1).

The distance was measured during the experiment along a straight line from the stimulating to the recording electrode. In order to estimate the actual distance traversed by the axon, a normalizing coefficient was used (see Methods Section 4.2.1 and Figure 4-2). The values obtained for these coefficients were: $K_{KC} = 1.09 \pm 0.01$, $K_{PN} = 1.23 \pm 0.05$ (mean $\pm$ S.E.M.; $n = 4$ Bodian stain measurements). Measured distances were multiplied by K in order to obtain a more accurate estimate of the actual distance traveled by the CAPs (Figure 4-2).

CAPs were elicited in order to measure their time of propagation along the axon. Examples of recorded waveforms are shown in Figure 4-3. Previous work studied the components of the PN-evoked waveform recorded in the calyx and determined that the initial downward deflection corresponds to PN action potentials, the positive peak succeeding it to KC EPSPs and the large negative deflection to synaptically evoked KC action potentials (Oleskevich et al., 1997). Given that the KC-evoked waveform shown in Figure 4-3 was recorded in the pedunculus, an area with fewer axodendritic synaptic connections (Leitch and Laurent, 1996), the postsynaptic potential component is much smaller and the larger biphasic deflections dominating the waveform are assumed to be caused by the electrical stimulus-evoked KC action potentials.
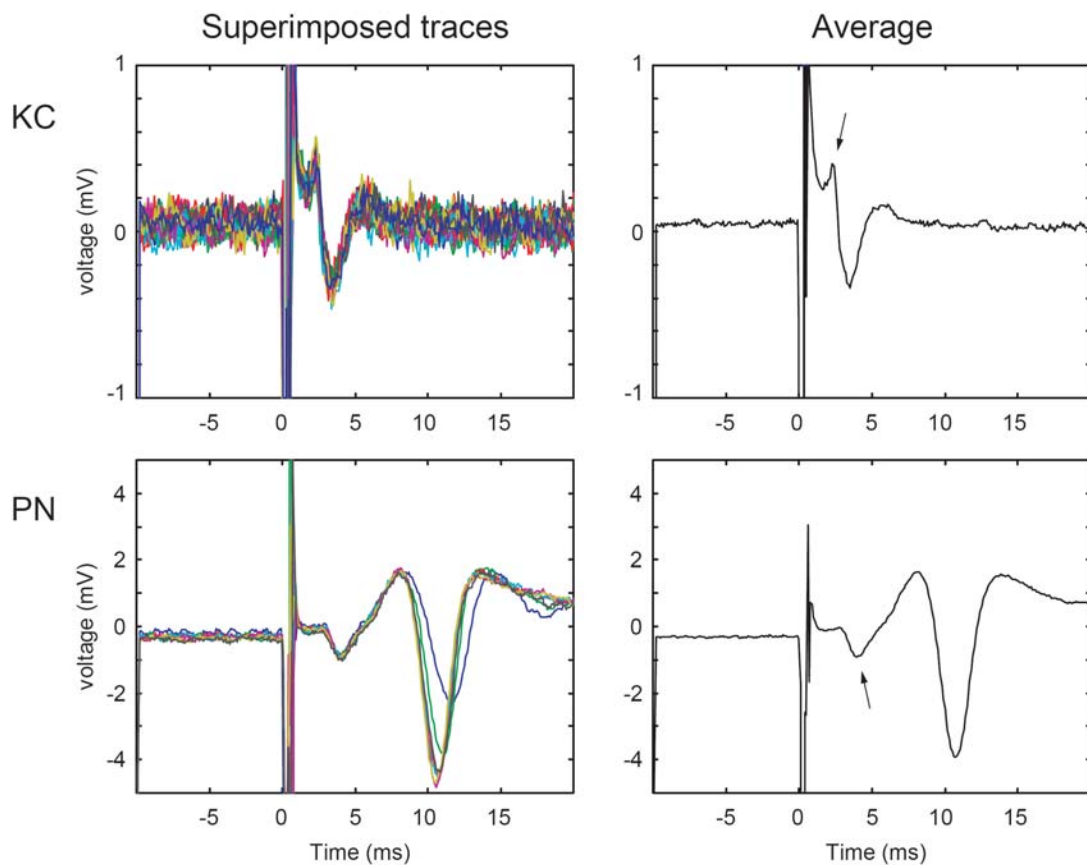
Figure 4-3. CAPs evoked by KC and PN electrical stimulations (top and bottom, respectively). Individual traces are superimposed on the left column ($n = 29$, for KCs; $n = 7$ for PNs) and the same traces are averaged on the right column. Arrows indicate the phases of the waveforms at which time measurements were taken.

Figure 4-4 shows the grouped results for KC and PN conduction velocities. When conduction velocity is measured as the average of the individual measurements (Figure 4-4 B) we obtain $v_{KC} = 0.19 \pm 0.01$ m/s and $v_{PN} = 0.22 \pm 0.02$ m/s. The conduction velocity of KCs is slightly slower than that of PNs, but it is not significantly different (Figure 4-4 B). Since KC CAPs were recorded at different distances along the pedunculus and β-lobe, we can also estimate their conduction velocity from the inverse of the slope

of the linear regression line (Figure 4-4 A): slope^{-1} = 0.23 m/s. The results obtained in
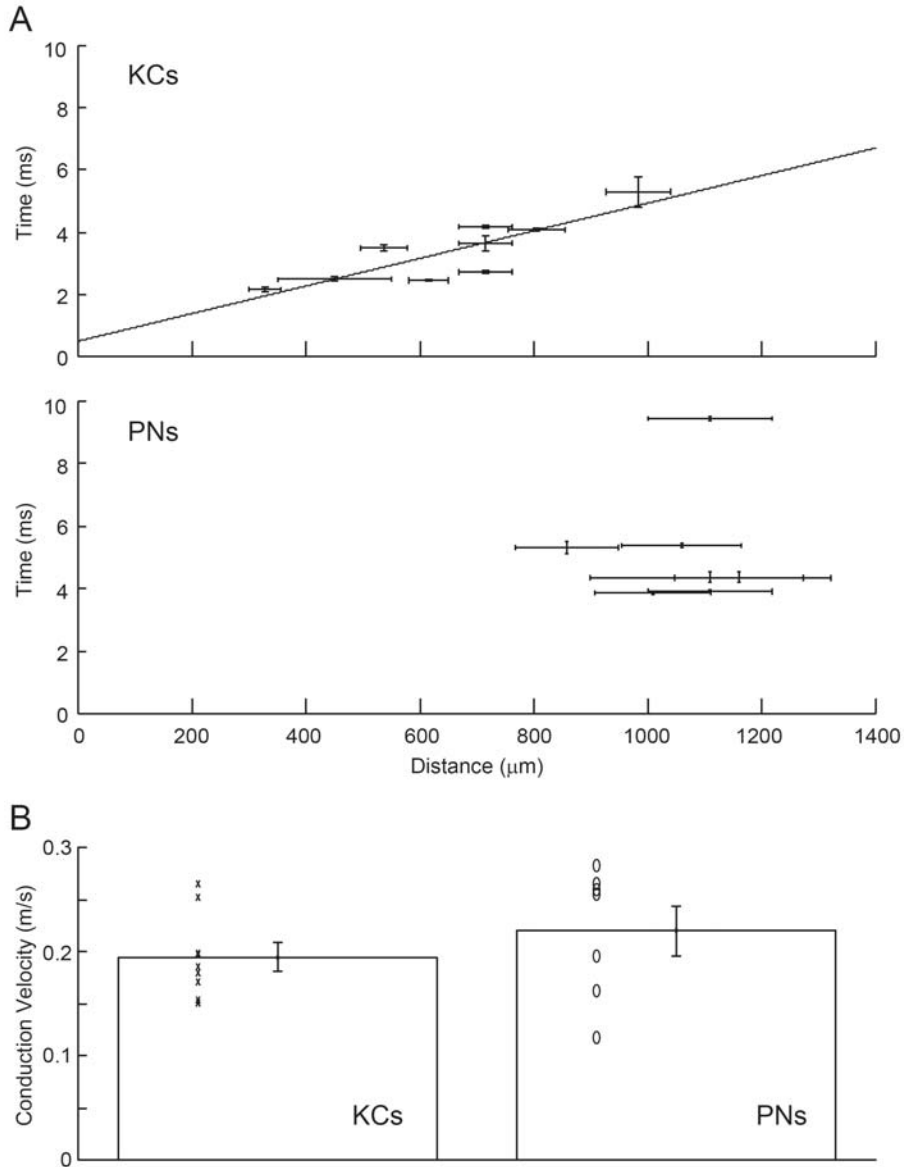these two ways are similar.

Figure 4-4. Conduction velocity results for KCs and PNs. **(A)** Distance vs. time measurements for KC-
evoked CAPs, recorded at different locations along the KC axon path in the pedunculus and β-lobe (top)
and PN-evoked CAPs recorded at the MB calyx (bottom). Time error bars correspond to S.E.M. Distance
error bars were calculated by considering the error introduced by changes in microscope focusing distance

(± 1 μm), the grid resolution (± 20 μm) and the scaling effects of the multiplicative coefficients ($K_{KC} = 1.09 \pm 0.01$, $K_{PN} = 1.23 \pm 0.05$; F2) (Pentz and Shott, 1988). The linear regression line is shown for the KCs (correlation coefficient, $r = 0.84$). **(B)** Average conduction velocity ($\pm$ S.E.M.) for KC ($n = 9$) and PN ($n = 7$) $v = d/t$ measurements. Symbols represent individual measurements.

4.2.3 Discussion

The work presented here measures the conduction velocity of KC and PN axons. The result obtained here for locust PN conduction velocity, 0.22 ± 0.02 m/s is similar to that previously found for honey bee PNs, 0.25 m/s (Oleskevich et al., 1997). The result for KC conduction velocity, 0.23 m/s (from the slope of the linear regression), is new to the best of our knowledge.

Measurements of conduction velocity in unmyelinated axons have suggested a relationship with the axon diameter of the form: $v = d^{n}$ [where v is measured in m/s and d in μm; (Ritchie, 1995)]. Previous estimates of n have yielded, $n = 0.61 \pm 0.03$ in squid and cuttlefish (Pumphrey and Young, 1938), $0.5 < n < 1.0$ in crab (Abbott et al., 1958) and $n = 1$ in mammalian dorsal root ganglion C fibers (Gasser, 1950). Given that KC axons are about 200-300 nm in diameter (Leitch and Laurent, 1996), our current conduction velocity result yields a value for KCs of $0.91 < n < 1.22$, which is consistent with the previously reported findings.

The conduction velocity observed here for KCs does not support the hypothesis that the MBs play a role in sequence detection of PN inputs. This idea stems from the fact that PN

axons continue into the lateral protocerebrum (Ernst et al., 1977; Hansson and Anton, 2000) after contacting KC dendrites (see Figure 1-1). In the lateral protocerebrum they can contact MB efferent neurons which also receive inputs from the KC axons in the MB lobes (Li and Strausfeld, 1997, 1999) (Figure 4-5). Thus, MB efferent neurons could receive PN olfactory input via two different pathways: one through a direct monosynaptic connection from PNs in the lateral protocerebrum, and a longer pathway through the KCs (Figure 4-5). In this idea, KC axons could be acting as delay lines which would cause signals occurring in sequential LFP oscillation cycles to coincide in the efferent neurons. In this way, efferent neurons could selectively respond to specific sequences of PN activation. For this hypothesis to work, the conduction velocity of KC axons should be such that they delay the signals from one cycle long enough to coincide with the signals from the next. Considering LFP oscillation cycles of 30-50 ms, 5-10 ms synaptic delays and a distance of 800 μm from the calyx to the β-lobe, KC conduction velocity should be about 0.02-0.04 m/s for this hypothesis to work. Our KC conduction velocity measurements result in values approximately an order of magnitude greater than these, and therefore rule out this possibility.
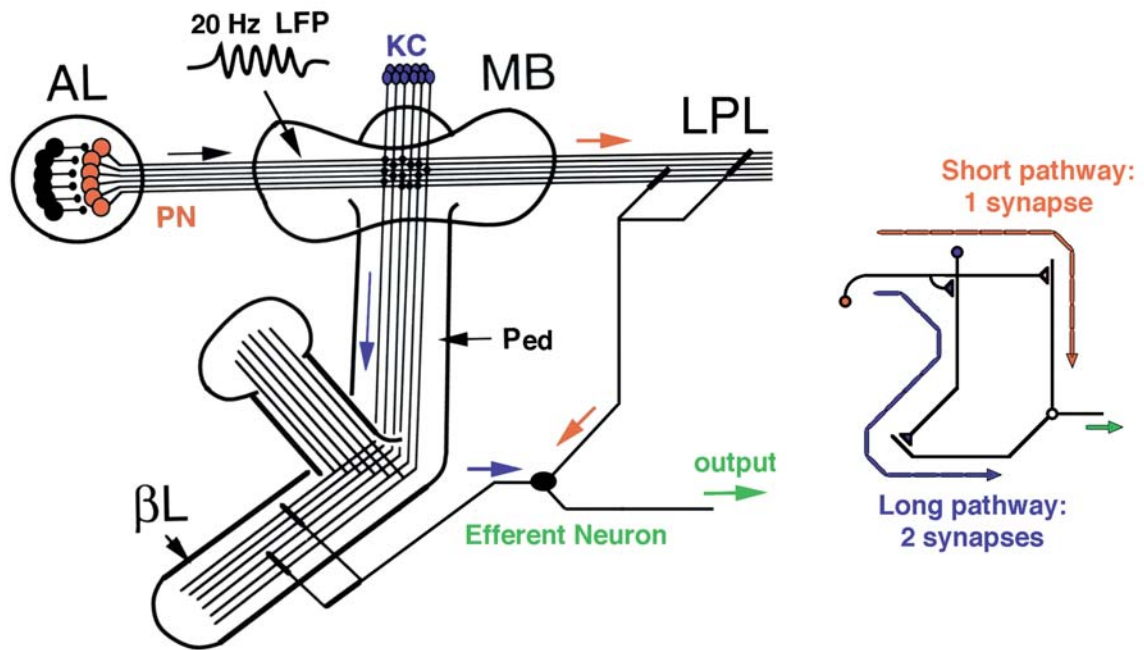
Figure 4-5. Schematic circuit of two convergent pathways of olfactory information onto MB efferent neurons: a short monosynaptic pathway via PNs (orange), and a long disynaptic pathway via PNs and KCs (blue).

4.3 Chemical or Spatial Clustering of Kenyon Cell Responses

4.3.1 Methods

In vivo electrophysiological experiments were conducted on locusts. Extracellular KC and LFP recordings were made with wire tetrode electrodes placed in the MB cell body layer, while presenting a panel of odors. Details of these electrophysiological experiments are the same as those described in Sections 3.4.1 and 3.4.2.

Responses were defined with separate amplitude and reliability criteria, as described in Section 3.4.4. Given the very low baseline firing rate of KCs, the amplitude criterion was

satisfied in the majority of cases with a single action potential per trial. The reliability

criterion is satisfied if this amplitude is exceeded in more than half of the trials (black

squares in Figure 4-6). In Figure 4-6 B, a "weak" response (gray squares) is defined with

the same amplitude criterion but with a relaxed reliability criterion, in which only a

response in more than a quarter of the trials is required. For calculating Hamming

distances (Figure 4-8), binary vectors are formed by taking all the odors that a KC is

presented with (i.e., each column in Figure 4-6 A will be a vector) and assigning ones to

responses and zeros to non-responses. The Hamming distance between two such vectors

provides a measure of their similarity making no assumptions about odor groupings.

4.3.2 Results

In this section I will explore whether KC responses can be grouped by either chemical

similarities of odors or by spatial location of KC somas. That is, will KCs that respond to

a given odor tend to respond as well to odors of similar chemical composition? and, do

KCs whose cell bodies are in spatial proximity to each other share similar odor response

profiles? Figure 4-6 presents an initial approach to these issues. It shows in matrix format

all cell-odor pairs for 64 KCs (out of a total of 122 KCs recorded with odor presentations)

that were presented with a complete panel of the same 17 odors. There does not seem to

be any obvious clustering of responses by either chemical group (rows within horizontal

arrows separating chemical families) or spatial location (columns within vertical arrows

separating tetrodes). Similarly, there are no obvious clusters that emerge by including

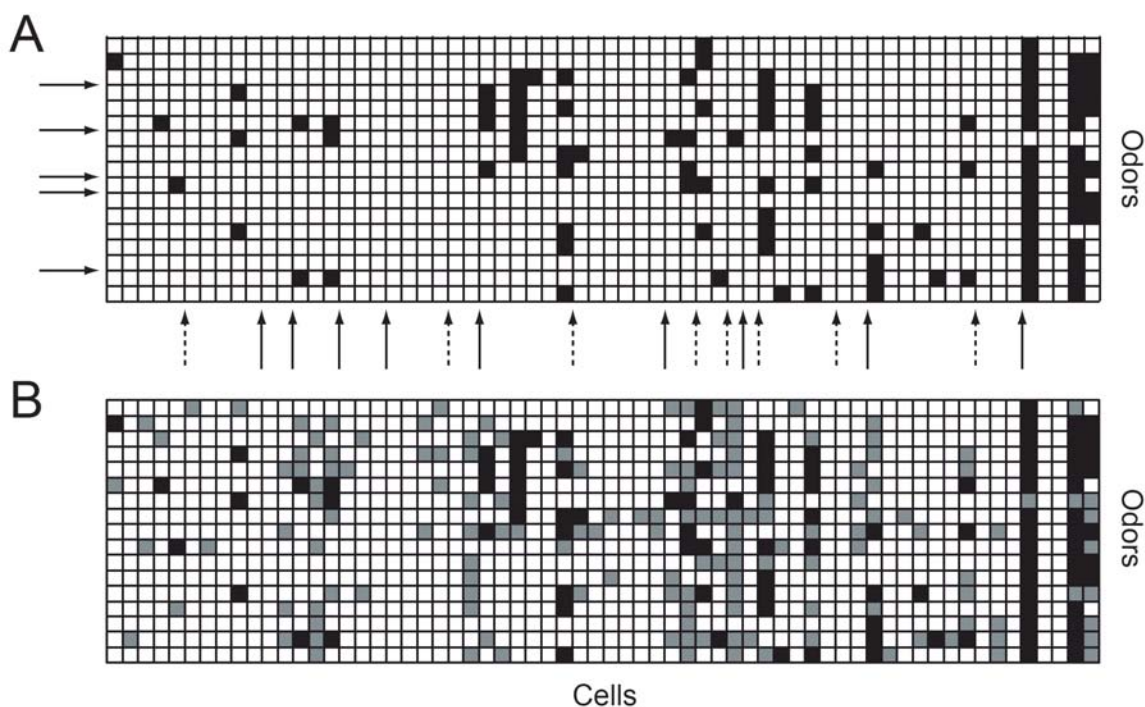"weak" responses (gray squares in Figure 4-6 B).

Figure 4-6. Response matrices for 64 KCs (columns) which were all presented with the same 17 odors (rows). **(A)** Black and white squares denote odor response or lack thereof, respectively. Vertical arrows (both solid and dashed) separate cells recorded with different tetrodes; dashed arrows separate simultaneous tetrode recordings. Horizontal arrows separate chemical families of odors (Solomons, 1988), from top to bottom: alkene alcohols (1-hexen-3-ol, *trans*-2-hexen-1-ol, *cis*-3-hexen-1-ol), alkane alcohols (1-hexanol, 1-heptanol, 1-octanol), aldehydes (hexanal, octanal, nonanal), dimethyl-2,6-octadiene-nitrile (this odor does not belong to any of the chemical groups used here), ketones (3-pentanone, 2-heptanone, 3-heptanone, 5-nonanone, 6-undecanone) and mixtures (cherry, mint). **(B)** Same as (A), except that "weak" responses (see Methods Section 4.3.1) are also included (gray squares). No clusters are clearly apparent, either by odor or by tetrode.

In order to address whether KCs respond to odors with similar chemical properties, odors are grouped into four standard organic chemistry families: alkene alcohols, alkane alcohols, aldehydes and ketones (Solomons, 1988). In addition to these four groups, I used a fifth one which included odors composed of a mixture of several different

molecules (cherry, mint). Figure 4-7 addresses whether the odor responses of a given KC tend to be clustered by chemical family. Strictly speaking, once a KC has responded to an odor, X_i, I tested whether the conditional probability to respond to odors from the same chemical group $P(X_j|X_i)$ is greater than to odors from different chemical groups $P(Y|X_i)$. Out of the five groups studied, only one, alkane alcohols, showed a significant grouping of responses (Figure 4-7).
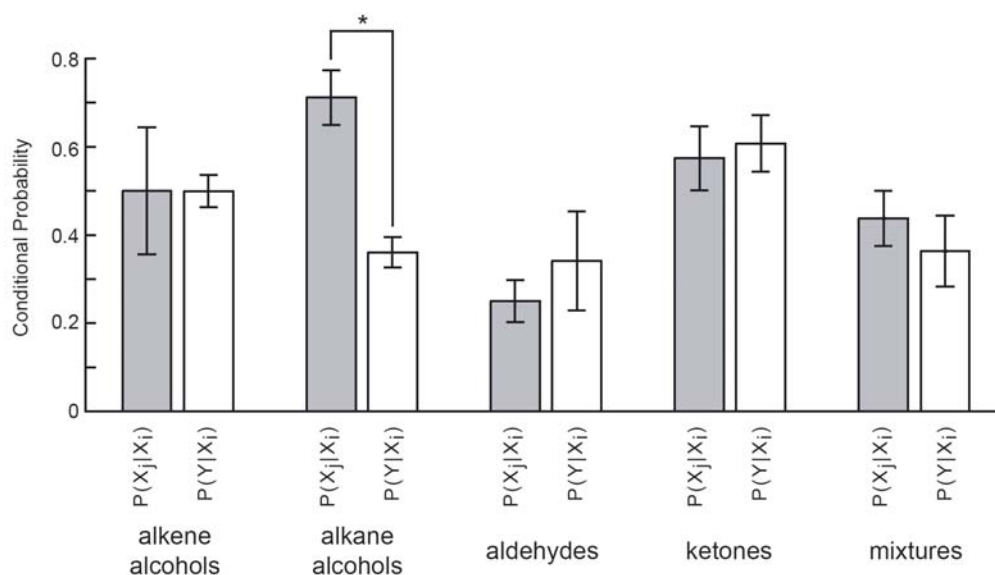

Figure 4-7. Clustering of KC responses by chemical family of odorant. Odors are grouped into one of five groups: four distinct chemical families (Solomons, 1988) plus a group of odor mixtures (individual odors used are those listed for Figure 4-6). The conditional probabilities of KCs responding to odors within the same group (gray bars), $P(X_j|X_i)$, or across different groups (white bars), $P(Y|X_i)$, are compared (mean $\pm$ S.E.M.). KCs that respond to an alkane alcohol are more likely to respond to other odors from this chemical family than to odors from other groups ($p = 0.01$, two-sided paired t test). However, no significant preference for a specific chemical family appears in the four other groups studied here ($p > 0.05$ for all of them, two-sided paired t test).

Assuming that KCs recorded in the same tetrode have their somas in spatial proximity, one can test whether nearby KCs respond to the same odors. Figure 4-8 compares the conditional probabilities that given a KC recorded from a specific tetrode responds to an odor, T_i, other KCs recorded from the same tetrode, $P(T_j/T_i)$, versus different tetrodes, $P(U/T_i)$, will respond to that odor. The probabilities that a KC recorded in another tetrode responds to a given odor (white bars), are all about 0.1, which agrees with the overall probability of response of KCs to odors (Perez-Orive et al., 2002). The probabilities that KCs in the same tetrode respond to the same odor (gray bars) vary greatly from one tetrode to another (from 0.0 to 0.6), with no clear pattern becoming apparent. Thus, there does not seem to be a strong clustering of similar responses throughout tetrode recordings (six tetrodes showed $P(T_j/T_i) > P(U/T_i)$, while 4 showed the opposite relationship). Measuring the Hamming distances between response profiles recorded from KCs within the same tetrode and across tetrodes does not show a significant difference based on the spatial location of KCs (Figure 4-8, inset), supporting the result obtained from the conditional probabilities.
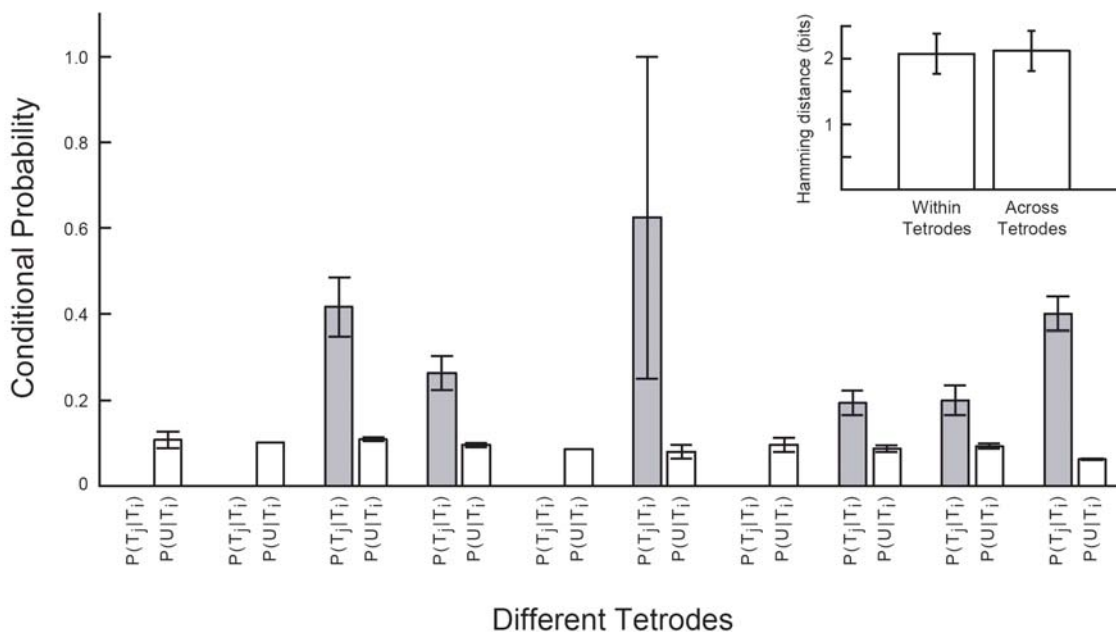
Figure 4-8. Clustering of similar odor responses by KCs recorded from the same tetrode. The conditional probabilities of responses to the same odors by KCs recorded simultaneously from the same tetrode (gray bars), $P(T_j/T_i)$, or from different tetrodes (white bars), $P(U/T_i)$, are compared (mean ± S.E.M.). In these experiments, between 2 and 7 KCs were recorded simultaneously from each tetrode. Of the 18 different tetrode recordings presented with the panel of 17 odors, 10 satisfy the criteria necessary for this analysis: having at least two KCs and at least one odor response (Figure 4-6). Inset: Hamming distances (i.e., the number of bits that are different among two binary numbers) for odor response profiles from KCs recorded in the same tetrode, compared to KCs from a simultaneous recording with another tetrode (see Methods Section 4.3.1 for details). Response profiles measured in this way are not significantly more similar for KCs within the same tetrode.

4.3.3 Discussion

The present results do not support a view for either chemical or spatial grouping of KC odor responses. With respect to chemical grouping, the data only show evidence of grouping for one chemical family (alkane alcohols) out of the five included. It could be that this reflects a difference in the way alkane alcohols are represented in the MB,

however it is not possible to conclude this from the presents results. The other four families show no significant grouping of responses. Of course, odors might be grouped along a different dimension that does not correspond to the conventional chemical families used here. It is not clear what this alternative dimension might be, so most previous studies have looked at broad chemical categories (Amoore, 1967; Amoore et al., 1969; Friedrich and Korsching, 1997; Uchida et al., 2000).

The current approach to the question of whether spatially grouped KCs have similar response profiles rests on the assumption that KCs recorded in the same tetrode have their somas in spatial proximity to each other, and to the tetrode. All KC somas have similar sizes (Leitch and Laurent, 1996) and it is likely that their action potentials will elicit currents of similar amplitudes in the extracellular medium. Thus, there is no reason to believe that for similar firing rates, KCs from distant locations will evoke larger signals in a tetrode than KCs proximal to it.

The present results support the idea that there is no strong spatial ordering at the level of KC somas, but do not address the question of spatial ordering in the calyx or lobes. However, studies of the relationship between the locations of KC somas and those of their dendrites and axons [in honey bees (Mobbs, 1982; Strausfeld, 2002) and cockroaches (Strausfeld and Li, 1999b)] have found that somas with specific locations in the cell body layer have dendrites with distinct projection patterns in the calyx, and that their axons maintain their relative positions to each other as they travel down the pedunculus and lobes. The results presented here do not show a clear grouping of odor

profiles by KC location, and therefore argue against a topographical ordering [e.g., (Belluscio and Katz, 2001; Marin et al., 2002; Wong et al., 2002)] of odor representation in the MB, in agreement with results in mammals studying projections from the olfactory bulb into the piriform cortex (Haberly, 1997; Zou et al., 2001).

4.4 Local Field Potential Spectrograms and Kenyon Cell Activity

4.4.1 Methods

In vivo electrophysiological experiments were conducted on locusts. Extracellular KC and LFP recordings were made with wire tetrode electrodes placed in the MB cell body layer, while presenting a panel of odors. Details of these electrophysiological experiments are the same as those described in Sections 3.4.1 and 3.4.2. Data analysis and response definitions were carried out as described in 3.4.4.

The spectrograms were calculated using the 'specgram.m' function from the Signal Processing Toolbox in Matlab (The Mathworks). This function calculates the fast Fourier transform (FFT) for overlapping windows across the signal. For the higher temporal resolution analysis (Figure 4-9, Figure 4-10), the LFP signal was split into windows of size 2^{13} data points (i.e., 8,192 points / 14,881 Hz sampling frequency = 551 ms window), with 2^{13}-2^9 data point overlaps between windows (i.e., 7,680 / 14,881 Hz = 516 ms overlap). The temporal resolution of the spectrogram will be the difference between the window size and the overlap between windows, $2^9/14,881 = 34$ ms.

In order to analyze the lower frequency components of the LFP (e.g., 3 Hz) in Figure 4-12, larger windows need to be used for computing the FFT, which causes a loss of temporal resolution in the spectrogram. For Figure 4-12, window size is 2^{15} (i.e., 32,768 points / 14,881 Hz = 2,202 ms window), with 2^{15}-2^{11} overlaps between windows (i.e., 30,720 points / 14,881 Hz = 2,064 ms overlap). This yields a temporal resolution of 2^{11}/14,881 = 137 ms. However, given that power spectra are calculated on the overall window (2.2 s in this case), individual time bins are not independent of each other, and therefore this temporal resolution is only approximate. This explains the reason why the LFP power is observed to increase before stimulus onset in Figure 4-12.

4.4.2 Results

Odor presentations elicit oscillatory synchronization of AL neurons reflected in LFP oscillations (Laurent and Naraghi, 1994; MacLeod and Laurent, 1996). A useful way to look at how the power at different frequencies evolves over time is by plotting a spectrogram of the signal. Figure 4-9 shows the average spectrogram of the LFP evoked by 18 different odors. The odor delivery system has about 300 ms of delay from the moment the trigger occurs until the odor reaches the locust, and physiological responses in the AL or MB are never observed before this time. Thus, the first 300 ms after odor onset display baseline activity (both in terms of LFP and single cell responses). The spectrogram shows that, on average, a slightly higher frequency (centered between 30-35 Hz) predominates during approximately the first 400-500 ms of the response.

Subsequently the predominant LFP frequency is 20-30 Hz, on average, and an increase in power in this band over baseline can still be observed more than 1 s after odor offset.
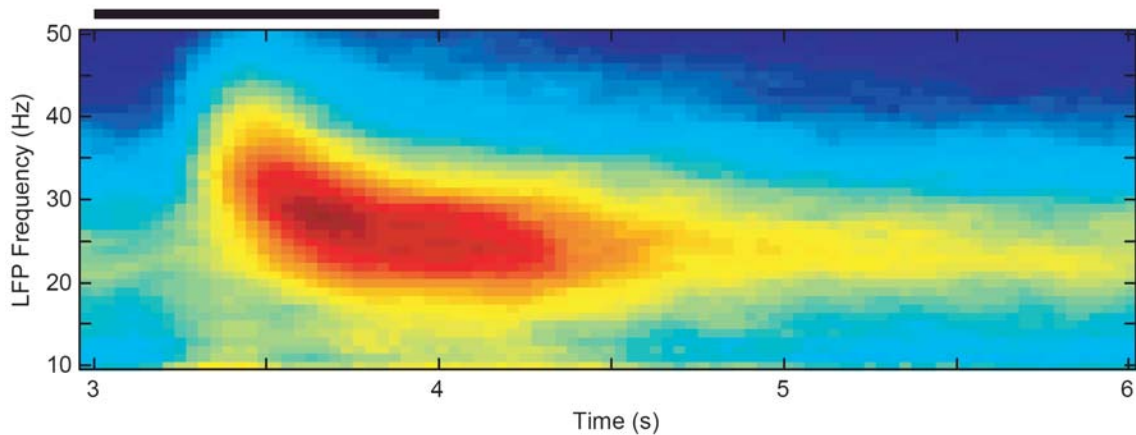

Figure 4-9. Average spectrogram of LFP over 1,300 odor presentations (using 18 different odors on 14 locusts). Frequency resolution, 1 Hz. Temporal resolution, 34 ms (see Methods Section 4.4.1). Horizontal bar, 1 s odor delivery (odor presentation is delayed by about 300 ms, see text Section 4.4.2). Warm/red colors: high power; cold/blue colors: low power.

The oscillations evoked by different odors are found to vary to some extent in frequency and temporal structure (Figure 4-10 A). Similarly, KC responses can vary somewhat in latency, duration and intensity (Perez-Orive et al., 2002; Perez-Orive et al., 2004). In the particular KC shown in Figure 4-10 C, the responses have similar temporal structure than the LFP power of the specific odor evoking the response. Occurrences of LFPs with such large latencies were not common, and so examples with such clear latency covariability as this are infrequent. To study the relationship between LFP oscillatory power and KC odor responses in a systematic way, smoothed PSTHs from KCs were compared to the

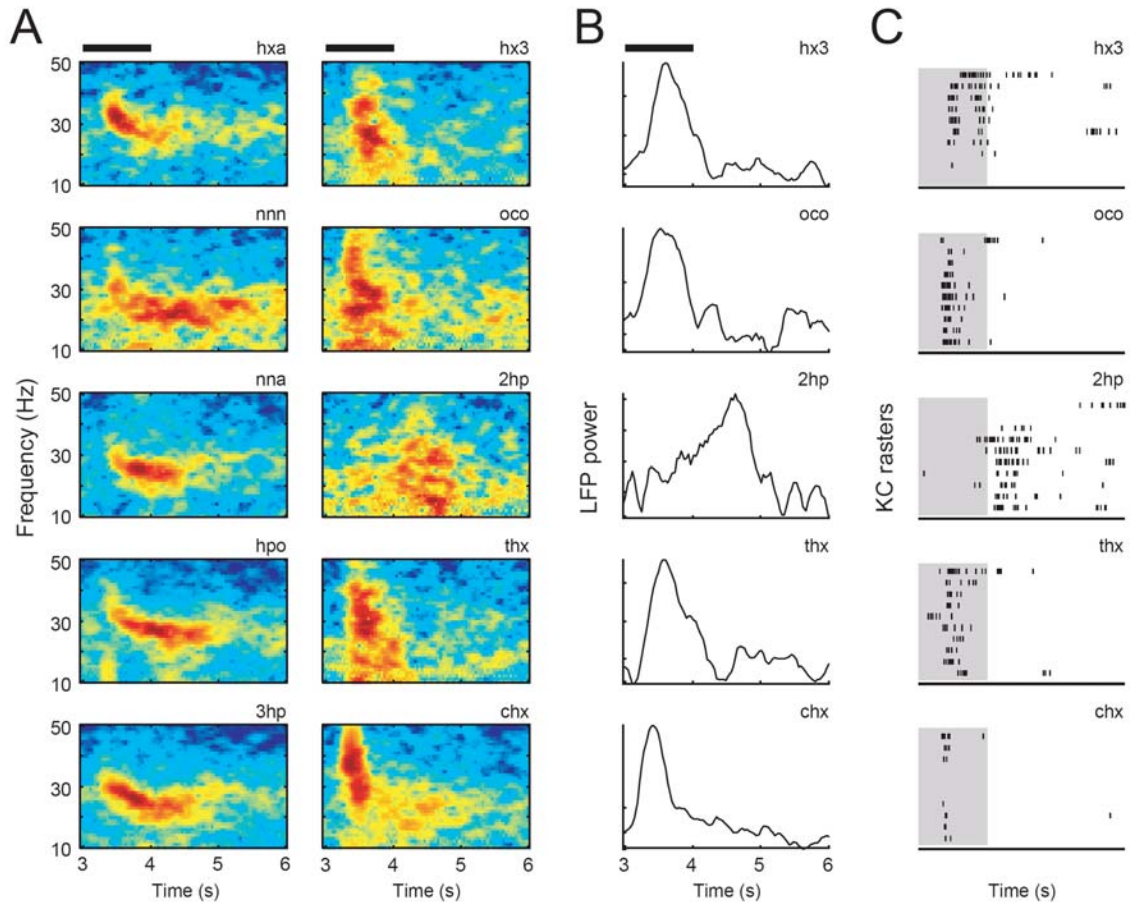LFP power evolving over time (Figure 4-10 B), and the correlations between both waveforms were calculated.

Figure 4-10. Examples of LFP spectrograms and KC responses for different odors. **(A)** Spectrograms for 10 different odors recorded from two locusts (10 trials for each odor). Spectrogram parameters and resolution as in Figure 4-9. Horizontal bars: 1 s odor stimulus. Odor abbreviations are: hexanal (hxa), 5-nonanone (nnn), nonanal (nna), 1-heptanol (hpo), 3-heptanone (3hp), 1-hexen-3-ol (hx3), 1-octanol (oco), 2-heptanone (2hp), *trans*-2-hexen-1-ol (thx), *cis*-3-hexen-1-ol (chx). **(B)** LFP oscillatory power (summated across the 19-31 Hz frequency band) plotted as a function of time for the five odors in the right-hand column of (A). **(C)** Responses from a single KC recorded simultaneously as the five odors in the right-hand column of (A). Shaded area: 1 s odor stimulus. 10 trials for each stimulus displayed top to bottom [this particular KC had a larger than average number of spikes per response, which is related to the fact that it responds to many odors (Perez-Orive et al., 2002)]. Note similar delays of KC responses and LFP power increase, specially noticeable for '2hp'.

Figure 4-11 A shows the distribution of correlation values calculated for all cell-odor response pairs (mean correlation coefficient of the distribution, $r = 0.42$; $n = 130$ cell-odor pairs with responses). The null hypothesis that the two waveforms are not correlated was rejected ($p<0.05$, two-sided t test) in 60% of these cell-odor pairs. However, it should be remembered that the LFP reflects the degree of synchrony of the total PN population, while KC firing only requires a relatively small subset of PNs to become synchronized (Perez-Orive et al., 2002), and this subset may or may not be reflected in the overall LFP power. Therefore, it is to be expected that some cell-odor pairs do not show significant correlations between KC firing and LFP power, as shown in Figure 4-11 A. A useful way of assessing the significance of these correlations is to calculate the likelihood that the experimentally observed degree of correlation is due to global similarities between KC responses and LFP power (i.e., that they are caused by global, as opposed to cell- and odor-specific, correlations). This was assessed as follows: a) the members of the 130 cell-odor pairs were randomly shuffled so that new pairs were formed in which the KC responses did not correspond to the LFP for the odor evoking the response, b) the correlation coefficients of the shuffled pairs were computed, c) the mean correlation of the new distribution is calculated. This procedure was repeated 1,000 times (Figure 4-11 B). The results indicate that the probability that the average correlation found experimentally could be generated with random pairings is $p = 0.01$. This suggests that there is a cell-odor pair specific correlation between LFP power and KC firing.
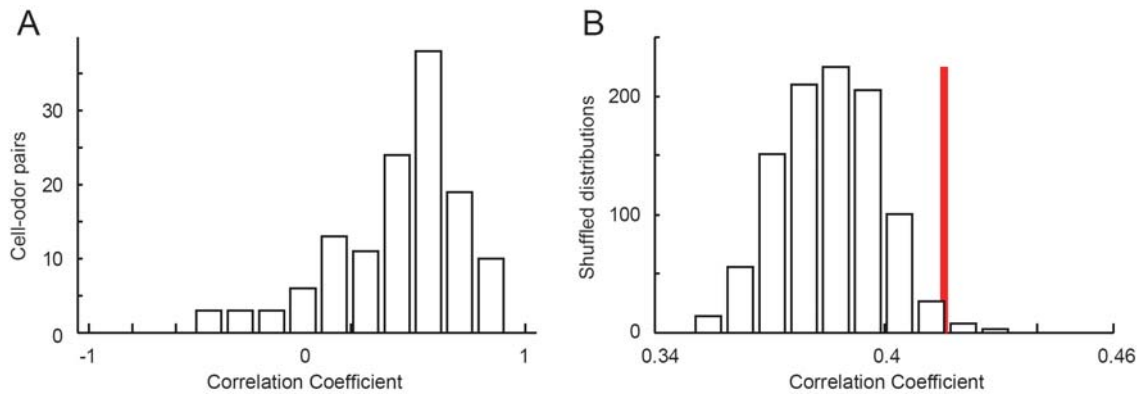
Figure 4-11. Correlation coefficients (*r*) between LFP power in the 19-31 Hz frequency band (as in Figure 4-10 B) and KC response PSTH (smoothed by convolving rasters with a 50 ms S.D. Gaussian). **(A)** Distribution of correlations for 130 cell-odor pairs (mean *r* = 0.42). **(B)** KC responses and LFP power were randomly shuffled into 130 new pairs, correlation coefficients were calculated for each pair and the mean *r* of the distribution was calculated (see text Section 4.4.2). Distribution of 1,000 mean *r*'s calculated in this way is shown here. Red vertical bar shows mean *r* = 0.42 of the experimentally observed distribution. The randomly shuffled distributions yielded mean *r* values as large as the experimental one with *p* = 0.01.

An interesting question would be to examine the degree of correlation between the response of a given KC and the overall PN firing rate, and then compare these correlations to those between KC firing and LFP power described above (Figure 4-11). Addressing this directly would require experiments with simultaneous PN and KC recordings, which currently present important technical challenges. An alternative possibility is to use information contained in the LFP as an indirect measure of average PN activity. LFP power in a lower frequency band (3-6 Hz) is a possible candidate to reflect overall PN activity (Perez-Orive et al., 2004). I therefore compared the degrees of correlations between PN and KC firing with LFP power at two different frequency bands: a higher band (19-31 Hz) reflecting oscillatory synchronization (Laurent and Davidowitz, 1994; MacLeod and Laurent, 1996), and a lower band (3-6 Hz), which would putatively

reveal overall PN activity. If the lower frequency band indeed reflects average PN activity, PNs should have stronger correlations with the lower than with the higher frequency band. Assuming KCs respond preferentially to synchronized PN input (Perez-Orive et al., 2002), one would then expect their responses to correlate more strongly with the higher than the lower frequency bands. The average odor-evoked spectrograms for these two frequency bands and the time course of the LFP power are shown in Figure 4-12 A and B. KC response activity is indeed more strongly correlated with the higher than the lower frequency band (Figure 4-12 C, left panel; $p<0.01$, two-sided t test). Conversely, PN activity is more strongly correlated with the lower than the higher frequency band (Figure 4-12 C, right panel; $p<0.01$, two-sided t test). Despite this significance however, the correlation between the PN PSTHs and the lower frequency band is relatively small (Figure 4-12 C, right panel), which casts doubt on whether LFP power at this band can be used as an appropriate measure of PN overall activity.
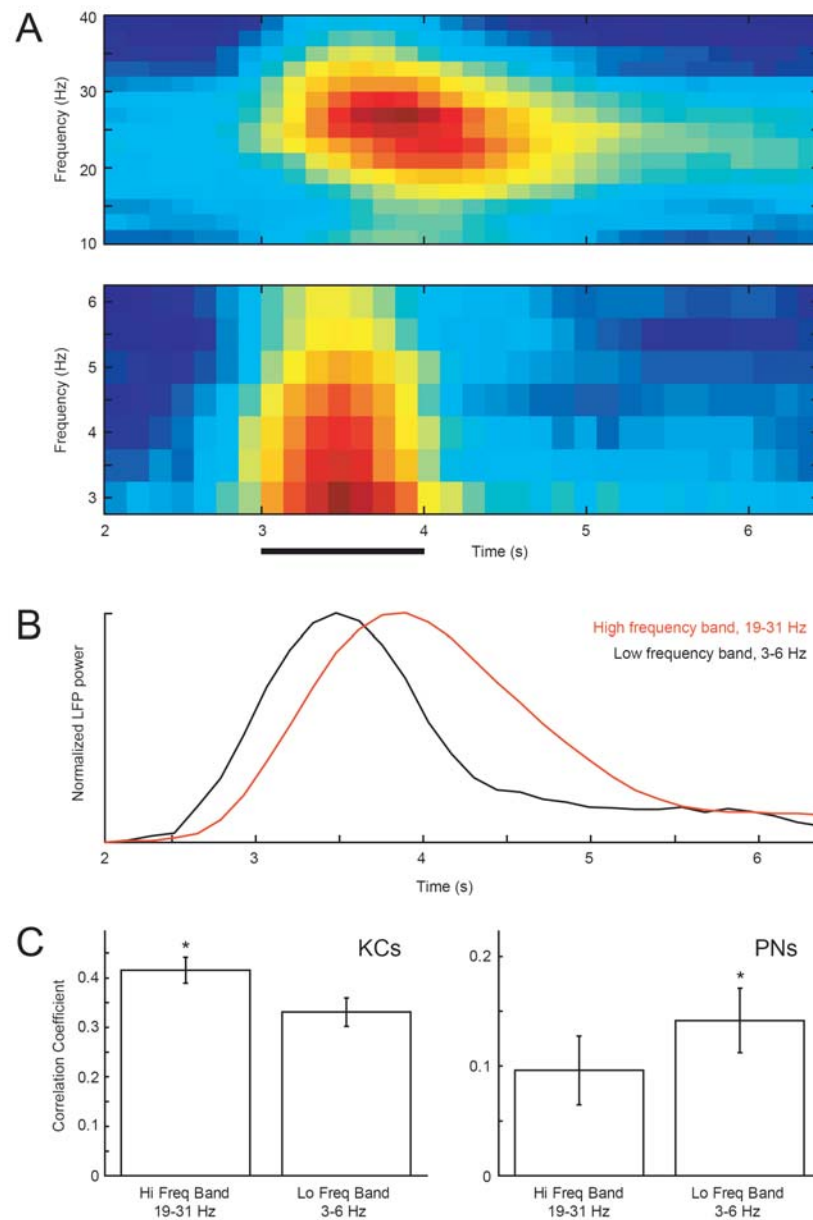
Figure 4-12. Comparison of high (19-31 Hz) and low (3-6 Hz) frequency bands of the LFP. **(A)** Average spectrograms of LFP over 1,300 odor presentations for both frequency bands (using 18 different odors on 14 locusts). Frequency resolution: 2 Hz, high band; 0.5 Hz, low band. Temporal resolution (the same for both frequency bands), 137 ms (see Methods Section 4.4.1). Horizontal band, 1 s odor stimulus. **(B)** LFP power summated over high (red) and low (black) frequency bands and plotted as a function of time. In order to compare time courses, amplitudes are normalized to maximum for each band. Note later onset and longer duration of power increase for higher band. **(C)** Comparison of correlations between KC / PN response PSTHs and LFP power for high and low frequency bands. Bars show mean ± S.E.M. of

correlations calculated for 130 responsive cell-odor pairs (KCs; left panel) and 249 cell-odor pairs (PNs; right panel), as described in Figure 4-11. KC responses are more strongly correlated with the high than the low frequency band ($p<0.01$, two-sided t test), whereas PN responses are more correlated with the low frequency band ($p<0.01$, two-sided t test). [PN tetrode recordings used for the right panel in (C) generously provided by S. Cassenaer and O. Mazor.]

4.4.3 Discussion

The work in this section describes the temporal evolution of odor-evoked LFP oscillatory power, and how it correlates to KC firing. The evidence presented here supports the idea that KCs respond preferentially when there is strong PN synchrony (Perez-Orive et al., 2002), as reflected by LFP power in the 20-30 Hz band.

However there are several reasons why these correlations are not stronger, and therefore this measure is suboptimal. On the one hand, as mentioned above, the LFP reflects the activity of the PN population, while KC firing does not depend explicitly on this measure, but rather on whether the specific subset of PNs converging onto it synchronize or not (Perez-Orive et al., 2002; Stopfer et al., 2003). Very often the synchronization of this PN subset will be reflected in the LFP, which is manifested in the statistically significant degree of correlation found here (Figure 4-11). Additionally, LFP power and KC PSTHs follow very different temporal dynamics: whereas the increase in LFP power lasts from several hundred milliseconds up to a few seconds (Figure 4-9, Figure 4-10), KC responses are typically brief and transient (Perez-Orive et al., 2002). Therefore, several different KCs might respond at different times within an epoch of sustained LFP power increase.

Taking these caveats into account, it is interesting that KC odor-evoked activity is more strongly correlated with LFP power in the 20-30 Hz band than with the lower, 3-6 Hz band, with which PN activity is more correlated. In spite of this, the correlation between the lower frequency band and overall PN activity is small, and the mechanistic explanation of LFP power at this band remains to be determined. Additionally, direct experimental comparison between the activity of a KC and the degree of synchrony among its converging PNs remains to be done, and could provide important supporting evidence for these ideas.

4.4.4 Acknowledgments

5 Concluding Remarks

I will now conclude by briefly recapitulating the main results of my Ph.D. work, discussing their overall significance and some open questions that remain to be answered.

5.1 Summary of Main Results

Kenyon cells (KCs) were found to have extremely low baseline activity, firing typically only one action potential every 10-40 seconds. They have highly specific odor responses and when they do respond, they tend to do so with a small number of action potentials (one or two, typically) which are phase-locked to local field potential (LFP) oscillations. This leads to a dramatic sparsening of the olfactory representation in the mushroom body (MB) [as assessed with binary response definitions, population sparseness and lifetime sparseness measures (Willmore and Tolhurst, 2001)][8].

---

[8] Given that these results are obtained with extracellular recordings, the only neurons that are counted are those that fire action potentials. Thus, it is possible that this misses KCs that do not spike at all during the recording period, or spike only such a small number of action potentials that they cannot be isolated with the spike-sorting procedure (Pouzat et al., 2002). This implies that the results presented here with respect to baseline activity, odor specificity and sparseness are conservative. It would be interesting to calculate precisely the volume that the tetrodes can record from. However, this depends on the properties of a complicated anisotropic, non-uniform volume conductor, which are not trivial to calculate (Perez-Orive and Durand, 2000). In any case, the fact that our measure is conservative only reinforces the main results, namely, that KCs have a low baseline firing rate, high specificity and that their odor representation in the MB is sparse.

Feedforward inhibition contributes to odor specificity and the sparse representation found in the MB. Blocking inhibitory input specifically to the KC dendrites was found to broaden KC odor tuning. Furthermore, KCs become desynchronized, as indicated by the fact that they lose their phase-locking to the LFP oscillations. This loss of phase-locking when lateral horn interneuron (LHI) inhibition is blocked strongly supports the idea that feedforward inhibition limits, on a cycle by cycle basis, the temporal window during which KCs can integrate their inputs (Pouille and Scanziani, 2001).

Together with feedforward inhibition, the intrinsic properties of KCs favor coincident input detection. Coincident EPSPs were found to summate supralinearly. In addition, both coincident EPSPs and superimposed DC depolarizations can lead to the production of active EPSPs and sharp spikelets (below action potential threshold), signifying the contribution of intrinsic voltage-dependent conductances to this nonlinear behavior. Compared to "passive" EPSPs, the half-width of these spikelets is significantly reduced, partly due to active repolarizing conductances [e.g., (Fricker and Miles, 2000)], which further contribute to the selectivity of KCs for coincident input (Kempter et al., 1998).

Taken together, these results indicate that oscillations serve as a framework on which KCs act as coincidence detectors: not all projection neuron (PN) spikes will be equally relevant to KCs, their specific relevance depending on whether they are correlated, within a specific phase of an oscillation cycle, with other PN spikes. Abolishing oscillations by blocking fast Cl⁻-mediated inhibition in the antennal lobe (AL) (MacLeod and Laurent, 1996) disrupts KC odor responses, decreasing their specificity and the sparseness of the

olfactory representation in the MB. This disruption appears to be caused by a shift of PN

activity towards odor onset and by a weakening of the net effect on KCs of feedforward

inhibition.

5.2 Open Questions for Future Work

These results have advanced our understanding of the processing of information in the

insect olfactory system, and specifically in the MBs. However, several open questions

remain to be answered by future work.

More information on the specific roles played by the MBs —and by the transformation of

the olfactory representation that takes place in them— would be important. The work

presented in this dissertation has shown that odor representations are transformed as they

progress from the AL to the MB, where there is a sparse and highly synthesized

representation available to downstream neurons. Thus, for elucidating the possible roles

the MBs might perform, it can be useful to consider what might be the potential

advantages of having such a representation.

The energy consumption of the brain constitutes a large percentage of the total resting

metabolic energy of various organisms (Howard et al., 1987; Nilsson, 1996; Clarke and

Sokoloff, 1999) and presents an important evolutionary constraint (Aiello and Wheeler,

1995; Martin, 1996; Allman, 1999). This constraint is likely to influence the anatomical

and physiological properties of nervous systems, favoring energy efficient codes in which

the information contained in a given number of spikes is maximized (Laughlin, 2001; Laughlin and Sejnowski, 2003). In this sense, an important advantage of the very brief and specific KC responses —as well as their extremely low baseline firing rate— could be a high metabolic efficiency for representing olfactory information.

However, there are also significant metabolic costs associated with maintaining a large number of silent neurons. Levy and Baxter (1996) calculated the optimal proportion of active neurons as a function of the ratio, r_e, of the energy costs of firing action potentials compared to the costs of maintaining the resting potential of a silent neuron. Assuming r_e values close to 10, they determined that a code that minimizes energy expenditure, while maximizing representational capacity, would activate approximately 16% of the total number of neurons for any given stimulus (Levy and Baxter, 1996). Our current results, indicating that approximately 10% of KCs respond to a given odor, are close to this prediction and thus consistent with this optimization. A comprehensive breakdown of metabolic energy costs has been computed for rat neocortical gray matter (Attwell and Laughlin, 2001). This method uses biophysical and biochemical measurements of neuronal properties such as ionic conductances and neurotransmitter release to calculate the numbers of ions and molecules involved in firing spikes and maintaining the resting potential. The amount of ATP required to restore the required gradients is then calculated. In this way, the metabolic costs of signaling through action potentials were calculated to be 84% of the total energy consumed by neurons, whereas the maintenance of resting potential was found to be only 13% (Attwell and Laughlin, 2001). These results predict that a sparse code, in which fewer than 15% of neurons are simultaneously active,

will optimize energy efficiency, in agreement with the predictions of (Levy and Baxter, 1996) and our current results for KCs. Similar calculations adjusted to account for differences between human and rat neocortex found that about 1% of neurons in human cortex should be "substantially" active (i.e., firing at about 50 Hz for a short time) at any given time (Lennie, 2003). It would be interesting to calculate r_e for KCs in order to evaluate whether the sparse representation discovered in the MB is actually optimal in terms of energy efficiency. But in any case, the previously cited work indicates that metabolic constraints are likely to favor sparse representations, similar to those described here for the MB, in other neural systems including neocortex.

Other possible advantages of a sparse code involve increasing the capacity and discriminability of odor representations. Theoretical works focusing on cerebellar circuits —with similar convergence and divergence properties as those that exist in the insect olfactory system— (Marr, 1969), the insect AL (Holub et al., 2002), and artificial neural networks (Okada, 1996; Dominguez and Bolle, 1998) suggest possible advantages of a sparse and distributed representation, such as reducing overlap between input patterns, improving memory capacity and decreasing spurious memories [(see also Discussions on Sections 2.3 and 3.3 and (Laurent, 2002)]. Having odor patterns be more separated in coding space could facilitate the discrimination between similar odors in the MB, and the matching of noisy stimuli to patterns stored in memory. Furthermore, modeling work performed by Maxim Bazhenov indicates that coincidence detection —the mechanism producing the sparse representation in the MB—has important advantages over temporal

integration with respect to improving the discriminability of similar odors and making the representation more robust to uncorrelated noise (Perez-Orive et al., 2004).

As described in Section 1.2.3, the role of the MB in learning and memory has received ample attention, particularly in the fruit fly [e.g., (Zars et al., 2000; McGuire et al., 2001); see (Heisenberg, 2003) for review]. These investigations routinely mention that MB interventions do not affect spontaneous (usually aversive) odor responses [e.g., (Heisenberg et al., 1985; de Belle and Heisenberg, 1994; Dubnau et al., 2001; McGuire et al., 2001)]. Thus, the claim has been made that MBs are not involved in olfactory discrimination. However, this claim does not seem well grounded given that those tests are admittedly "very crude" (Heisenberg et al., 1985) and only address whether the MBs are required to detect the presence or absence of an odor, not whether they are involved in discriminating between two, potentially similar, odors. Results obtained in the locust suggest that in fact odor discrimination is likely to involve the MBs (Stopfer et al., 1997; MacLeod et al., 1998; Perez-Orive et al., 2002; Perez-Orive et al., 2004). In agreement with this, preliminary experiments in flies indicate that the spontaneous discrimination of complex odors requires the MBs (Heisenberg, 2003).

The simpler representation available in the MB might also make possible further processing of the olfactory information (in addition to olfactory discrimination and memory), such as that required for deciding between different behaviors based on contradictory cues (Tang and Guo, 2001), controlling motor output (Heisenberg, 1998; Mizunami et al., 1998b), or integrating olfactory information with other sensory

modalities. Work in several insect species has shown that, in addition to olfactory input,

the MB calyces receive visual (Honegger and Schurmann, 1975; Mobbs, 1982;

Gronenberg, 1999), mechanosensory and auditory afferents (Strausfeld and Li, 1999a).

There is also evidence of multimodal responses in the MB efferent neurons that have

dendritic processes in the lobes (Li and Strausfeld, 1999), suggesting that at least some

KCs respond to different sensory modalities. Furthermore, morphometric analysis of

different ant species has revealed a correlation between the sizes of the antennal and optic

lobes, and the calycal zones where they project, the lip and the collar, respectively

(Gronenberg and Holldobler, 1999). The fact that the MBs are an area of convergence for

several different modalities, has led researchers to hypothesize that one of their functions

might be to carry out multimodal sensory integration [for a review, see (Strausfeld et al.,

1998)]. It will be interesting to determine whether all of these sensory modalities

converge on the same KCs, perhaps modulating olfactory information, or if different

subsets of KCs process different modalities in parallel, with multimodal integration

occurring downstream. Future experimental and theoretical work to determine the

specific advantages that the sparse representation provides to this system (e.g., in terms of

metabolic energy, coding capacity, readout by MB efferents) will help clarify the

potential role of the MBs in learning and memory, odor discrimination, multimodal

integration and motor responses.

Another important issue that remains to be conclusively established is the quantitative

pattern of connectivity between PNs and KCs (see Section 1.2.3 for current estimates of

PN-KC convergence/divergence ratios). This could be addressed with anatomical and

electrophysiological techniques. For instance, simultaneous intracellular KC and

extracellular PN recordings could potentially uncover directly connected PN-KC pairs

(although recent developments in tetrode recording techniques are important for this, it

still remains a highly challenging experiment). Analyzing correlations between PN spikes

and KC EPSPs and spikes could provide valuable information for estimating the number

of PNs converging onto a KC, and the number of coincident PNs needed for a KC to

respond.

An additional important area for future investigations concerns the understanding of how

signals from KCs are decoded by their downstream targets. Extrinsic MB neurons which

send dense dendritic projections to the α- and β-lobes (often perpendicularly to KC

axons, thus making cross-sections of the lobes) are generally considered to be the output

of the MB [e.g., (MacLeod et al., 1998; Li and Strausfeld, 1999); see also Section 1.2.1].

Some of these neurons can be uniquely identified between individuals, often respond to

stimuli from multiple sensory modalities and seem to receive convergent input from a

large number of KCs (Rybak and Menzel, 1998; Li and Strausfeld, 1999; Strausfeld,

2002). Some extrinsic MB neurons send feedback projections back into the MB calyx

[many of these feedback neurons are GABAergic (Leitch and Laurent, 1996; Grunewald,

1999a, b)] and others project to the lateral protocerebrum, a brain area about which very

little is known and which also receives olfactory information through direct PN

projections from the AL (Ernst et al., 1977; Hansson and Anton, 2000). Establishing the

roles that different extrinsic MB neurons play, how they decode KC activity, and how

this information —coming from the MB— might be integrated in the lateral

protocerebrum with olfactory information coming directly from the AL, are challenging but important problems that need to be tackled in the future.

5.3 Relevance of Dissertation

The work described in this dissertation has significantly expanded our knowledge of the decoding of neural information by the MB. Gaining a better comprehension of how information is decoded by downstream neurons provides useful knowledge which supports and enhances our previous understanding of the neural code used by the insect olfactory system (Laurent et al., 1996; Wehr and Laurent, 1996; Stopfer et al., 1997; MacLeod et al., 1998; Laurent, 1999). Furthermore, the work presented here provides a mechanism for decoding precise timing information and indicates that not all spikes are equally relevant for downstream neurons.

These general principles need not apply only to the insect olfactory system, but might also provide useful insights into neural coding and decoding in other, more complex, neural systems.

The different phenomena whose interactions have been studied here have been observed in many other systems. For instance: sparse codes have been described in primate temporal (Rolls and Tovee, 1995) and primary (Olshausen and Field, 1996; Vinje and Gallant, 2000) visual cortices; furthermore, recordings from monkey prefrontal and premotor cortices reveal highly reliable neuronal firing events —consisting of only one or

two action potentials— correlated with behavior (Abeles et al., 1993; Prut et al., 1998),

likewise, complex natural sounds can elicit reliable responses consisting of a single spike

in rat auditory cortex (DeWeese et al., 2003) [similarly brief and specific responses have

been observed in olfactory cortex, as will be discussed below]; oscillations are ubiquitous

across different systems and animal groups [e.g., (Ottoson, 1959; Gelperin and Tank,

1990; Rodriguez et al., 1999; Buzsaki, 2002; van Swinderen and Greenspan, 2003)] and

have been linked to a wide range of sensory and cognitive processes, such as olfaction

(Adrian, 1942; Lam et al., 2000; Neville and Haberly, 2003; Martin et al., 2004), binding

of perceptual objects (Gray et al., 1989; Engel et al., 1991; Csibra et al., 2000), attention

(Fries et al., 2001) and memory formation (Howard et al., 2003; Sederberg et al., 2003),

to name a few; coincidence detection plays an important role in the auditory system (Carr

and Konishi, 1990; Joris et al., 1998) and spike-timing dependent plasticity (Markram et

al., 1997); feedforward inhibition has been described *in vitro* in the hippocampus (Pouille

and Scanziani, 2001) and medial superior olive (Grothe and Sanes, 1994).

Different active dendritic conductances have also been observed *in vitro* in various

contexts in mammalian hippocampus and neocortex: action potentials can backpropagate

into dendrites (Stuart and Sakmann, 1994), voltage-dependent conductances can reduce

the time course of EPSPs (Fricker and Miles, 2000; Galarreta and Hestrin, 2001; Ariav et

al., 2003), and coincident EPSPs can elicit dendritic spike generation (Williams and

Stuart, 2002; Ariav et al., 2003). In a particularly relevant experiment, temporal

summation was studied in cultured rat hippocampal neurons, in which photolysis of

caged glutamate was used to simulate dendritic excitation and evoke miniature EPSPs

(Margulis and Tang, 1998). Under these conditions, temporal summation was studied as a function of interpulse interval. With intervals of 10 ms or less, the summation of EPSPs was observed to be supralinear, an effect partly caused by tetrodotoxin-sensitive Na^+ channels.

The previous examples illustrate that the mechanisms involved in the decoding of olfactory information by the KCs are ubiquitous throughout different nervous systems. However, they have been typically studied in isolation, with a limited understanding of the functional interactions between all of them. A great advantage of the model system used in this dissertation is that its relative simplicity has allowed a more thorough understanding of how all of these features can interact *in vivo*.

For example, one of the most common functional roles attributed to synchronized neuronal firing states that synchrony can be used to group distributed responses in order to bind perceptual objects [(von der Malsburg and Schneider, 1986), for reviews see (Singer and Gray, 1995; Singer, 1999)]. Evidence in support of this idea has come from recordings in cat visual cortex from sites with overlapping orientation preferences, finding that the synchronization between cell assemblies is modulated by whether the stimulus consists of one continuous bar or two separate bars [(Engel et al., 1991), see also (Gray et al., 1989)]. Coincidence detection has been suggested as the mechanism that could distinguish synchronous events (Singer and Gray, 1995). However, it has not been determined in this system how specific components of cortical circuits might bring about

this selectivity, and thus important insights can be gained from the work in this dissertation.

Theoretical studies have established the relationship between the time constant of EPSPs —modified by active dendritic conductances— and coincidence detection, and determined that the briefer the EPSP half-width is, the stronger the preference for coincidence detection will be [(Kempter et al., 1998); see also (Abeles, 1982; Konig et al., 1996)]. Research in rat hippocampus (Pouille and Scanziani, 2001) and auditory cortex (Wehr and Zador, 2003) has found that precisely timed inhibition limits the temporal window in which these neurons integrate their inputs, favoring their detection of coincident input. Additionally, theoretical models of cortical macrocolumns (Lucke and von der Malsburg, 2004) have found that oscillatory inhibition can define phases within an oscillatory cycle at which the activity of individual minicolumns is evaluated, lending theoretical insights into how the results obtained for the MBs may apply in more complex systems.

Particularly in the vertebrate olfactory cortex, an area downstream of the olfactory bulb (OB) and analogous to the arthropod MB, several features similar to those studied here have been described. Work conducted in frog olfactory cortex (Duchamp-Viret et al., 1996), as well as in rat (McCollum et al., 1991) and monkey (Tanabe et al., 1975) piriform cortices, has found very sparse odor representations in these areas, with neurons responding specifically to very few odors. Furthermore, some of these responses reliably consist of only one or two action potentials (Nemitz and Goldberg, 1983; Duchamp-Viret

et al., 1996) over extremely low baseline firing rates (Biedenbach and Stevens, 1969). It has been hypothesized that these specific and brief responses may result from detection of coincident input (Duchamp-Viret et al., 1998). Additionally, several of the mechanisms involved in the sparsening of the representation in the MB are known to exist in mammalian piriform cortex: there is evidence for feedforward inhibition (Tseng and Haberly, 1988; Ekstrand et al., 2001); spatially distributed and overlapping projections of mitral cells onto pyramidal cells with no apparent topographical ordering, as described in Section 4.3 (Haberly, 1997; Zou et al., 2001), and OB-generated oscillatory activity (Ketchum and Haberly, 1993; Neville and Haberly, 2003). Specifically, it has been hypothesized that phase-locked inhibition limits the window in which piriform cortex pyramidal cells integrate their input (Ketchum and Haberly, 1993), in agreement with our results. Our current work, combining all of these features, provides information and insights that can be highly relevant for enhancing our understanding of these cortical olfactory areas.

The work described in this dissertation shows that in the insect olfactory system all of these features (oscillatory population activity, coincidence detection, feedforward inhibition, active dendritic properties, sparse coding) occur together, and illustrates mechanisms through which they can interact to bring about a drastic transformation of sensory representations, increasing our understanding of how nervous systems can process information.

References

Abbott BC, Hill AV, Howarth JV (1958) The positive and negative heat production associated with a nerve impulse. Proc R Soc Lond Ser B-Biol Sci 148:149-187.

Abbott LF, Dayan P (1999) The effect of correlated variability on the accuracy of a population code. Neural Comput 11:91-101.

Abeles M (1982) Role of the cortical neuron: Integrator or coincidence detector? Isr J Med Sci 18:83-92.

Abeles M, Bergman H, Margalit E, Vaadia E (1993) Spatiotemporal firing patterns in the frontal-cortex of behaving monkeys. J Neurophysiol 70:1629-1638.

Adrian E (1926) The impulses produced by sensory nerve endings. J Physiol (Lond) 61:49-72.

Adrian E (1942) Olfactory reactions in the brain of a hedgehog. J Physiol (Lond) 100:459-473.

Aiello LC, Wheeler P (1995) The expensive tissue hypothesis: The brain and the digestive system in human and primate evolution. Curr Anthropol 36:199-221.

Allman JM (1999) Evolving brains. New York: Scientific American Library.

Amoore JE (1967) Specific anosmia - a clue to olfactory code. Nature 214:1095-&.

Amoore JE, Palmieri G, Wanke E, Blum MS (1969) Ant alarm pheromone activity - correlation with molecular shape by scanning computer. Science 165:1266-&.

Anton S, Hansson BS (1994) Central processing of sex-pheromone, host odor, and oviposition deterrent information by interneurons in the antennal lobe of female Spodoptera-littoralis (Lepidoptera, Noctuidae). J Comp Neurol 350:199-214.

Anton S, Hansson BS (1995) Sex-pheromone and plant-associated odor processing in antennal lobe interneurons of male Spodoptera-littoralis (Lepidoptera, Noctuidae). J Comp Physiol A-Sens Neural Behav Physiol 176:773-789.

Ariav G, Polsky A, Schiller J (2003) Submillisecond precision of the input-output transformation function mediated by fast sodium dendritic spikes in basal dendrites of CA1 pyramidal neurons. J Neurosci 23:7750-7758.

Attwell D, Laughlin SB (2001) An energy budget for signaling in the grey matter of the brain. J Cereb Blood Flow Metab 21:1133-1145.

Barlow H (1969) Pattern recognition and the responses of sensory neurones. Ann NY Acad Sci 156:872-881.

Bazhenov M, Stopfer M, Rabinovich M, Abarbanel HD, Sejnowski TJ, Laurent G (2001a) Model of cellular and network mechanisms for odor-evoked temporal patterning in the locust antennal lobe. Neuron 30:569-581.

Bazhenov M, Stopfer M, Rabinovich M, Huerta R, Abarbanel HD, Sejnowski TJ, Laurent G (2001b) Model of transient oscillatory synchronization in the locust antennal lobe. Neuron 30:553-567.

Belluscio L, Katz LC (2001) Symmetry, stereotypy, and topography of odorant representations in mouse olfactory bulbs. J Neurosci 21:2113-2122.

Biedenbach MA, Stevens CF (1969) Electrical activity in cat olfactory cortex produced by synchronous orthodromic volleys. J Neurophysiol 32:193-203.

Bragin A, Jando G, Nadasdy Z, Hetke J, Wise K, Buzsaki G (1995) Gamma (40-100 Hz) oscillation in the hippocampus of the behaving rat. J Neurosci 15:47-60.

Brand A, Behrend O, Marquardt T, McAlpine D, Grothe B (2002) Precise inhibition is essential for microsecond interaural time difference coding. Nature 417:543-547.

Britten KH, Shadlen MN, Newsome WT, Movshon JA (1992) The analysis of visual motion: A comparison of neuronal and psychophysical performance. J Neurosci 12:4745-4765.

Brody CD, Hopfield JJ (2003) Simple networks for spike-timing-based computation, with application to olfactory processing. Neuron 37:843-852.

Buzsaki G (2002) Theta oscillations in the hippocampus. Neuron 33:325-340.

Cain WS, Potts BC (1996) Switch and bait: Probing the discriminative basis of odor identification via recognition memory. Chem Senses 21:35-44.

Carr CE, Konishi M (1990) A circuit for detection of interaural time differences in the brain-stem of the barn owl. J Neurosci 10:3227-3246.

Clarke DD, Sokoloff L (1999) Circulation and energy metabolism of the brain. In: Basic neurochemistry: Molecular, cellular and medical aspects (Siegel GJ, Agranoff BW, Albers RW, Fisher SK, Uhler MD, eds), pp 637-669. Philadelphia: Lippincott-Raven.

Clyne PJ, Warr CG, Freeman MR, Lessing D, Kim JH, Carlson JR (1999) A novel family of divergent seven-transmembrane proteins: Candidate odorant receptors in Drosophila. Neuron 22:327-338.

Connolly JB, Roberts IJ, Armstrong JD, Kaiser K, Forte M, Tully T, O'Kane CJ (1996) Associative learning disrupted by impaired Gs signaling in Drosophila mushroom bodies. Science 274:2104-2107.

Contreras D, Destexhe A, Steriade M (1997) Intracellular and computational characterization of the intracortical inhibitory control of synchronized thalamic inputs in vivo. J Neurophysiol 78:335-350.

Csibra G, Davis G, Spratling MW, Johnson MH (2000) Gamma oscillations and object processing in the infant brain. Science 290:1582-1585.

de Belle JS, Heisenberg M (1994) Associative odor learning in Drosophila abolished by chemical ablation of mushroom bodies. Science 263:692-695.

Destexhe A, Mainen ZF, Sejnowski TJ (1994) Synthesis of models for excitable membranes, synaptic transmission and neuromodulation using a common kinetic formalism. J Comput Neurosci 1:195-230.

DeWeese MR, Wehr M, Zador AM (2003) Binary spiking in auditory cortex. J Neurosci 23:7940-7949.

Diesmann M, Gewaltig MO, Aertsen A (1999) Stable propagation of synchronous spiking in cortical neural networks. Nature 402:529-533.

Distler P (1989) Histochemical-demonstration of GABA-like immunoreactivity in cobalt labeled neuron individuals in the insect olfactory pathway. Histochemistry 91:245-249.

Dobritsa AA, van der Goes van Naters W, Warr CG, Steinbrecht RA, Carlson JR (2003) Integrating the molecular and cellular basis of odor coding in the Drosophila antenna. Neuron 37:827-841.

Dominguez DRC, Bolle D (1998) Self-control in sparsely coded networks. Phys Rev Lett 80:2961-2964.

Dubnau J, Grady L, Kitamoto T, Tully T (2001) Disruption of neurotransmission in Drosophila mushroom body blocks retrieval but not acquisition of memory. Nature 411:476-480.

Duchamp-Viret P, Palouzier-Paulignan B, Duchamp A (1996) Odor coding properties of frog olfactory cortical neurons. Neuroscience 74:885-895.

Duchamp-Viret P, Palouzier-Paulignan B, Duchamp A (1998) Sensory information processing in the frog olfactory pathways. Experimental basis for modeling studies. Biosystems 48:37-45.

Dujardin F (1850) Memoire sur le systeme nerveux des insectes. Annales des Sciences Naturelles-Zoologie et biologie animale 14:195-206.

Dusenbery DB (1992) Sensory ecology. New York: W. H. Freeman and Company.

Eccles JC (1957) The physiology of nerve cells. Baltimore, MD: Johns Hopkins Press.

Eckhorn R, Bauer R, Jordan W, Brosch M, Kruse W, Munk M, Reitboeck HJ (1988) Coherent oscillations - a mechanism of feature linking in the visual-cortex - multiple electrode and correlation analyses in the cat. Biol Cybern 60:121-130.

Ehmer B, Hoy R (2000) Mushroom bodies of vespid wasps. J Comp Neurol 416:93-100.

Ekstrand JJ, Domroese ME, Feig SL, Illig KR, Haberly LB (2001) Immunocytochemical analysis of basket cells in rat piriform cortex. J Comp Neurol 434:308-328.

Engel AK, Konig P, Singer W (1991) Direct physiological evidence for scene segmentation by temporal coding. Proc Natl Acad Sci U S A 88:9136-9140.

Engel AK, Fries P, Singer W (2001) Dynamic predictions: Oscillations and synchrony in top-down processing. Nat Rev Neurosci 2:704-716.

Ernst KD, Boeckh J (1983) A neuroanatomical study on the organization of the central antennal pathways in insects .3. Neuroanatomical characterization of physiologically defined response types of deutocerebral neurons in Periplaneta-americana. Cell Tissue Res 229:1-22.

Ernst KD, Boeckh J, Boeckh V (1977) Neuroanatomical study on organization of central antennal pathways in insects .2. Deutocerebral connections in Locusta-migratoria and Periplaneta-americana. Cell Tissue Res 176:285-308.

Flanagan D, Mercer AR (1989) Morphology and response characteristics of neurons in the deutocerebrum of the brain in the honeybee Apis-mellifera. J Comp Physiol A-Sens Neural Behav Physiol 164:483-494.

Fonta C, Sun XJ, Masson C (1993) Morphology and spatial-distribution of bee antennal lobe interneurons responsive to odors. Chem Senses 18:101-119.

Fricker D, Miles R (2000) EPSP amplification and the precision of spike timing in hippocampal neurons. Neuron 28:559-569.

Fricker D, Miles R (2001) Interneurons, spike timing, and perception. Neuron 32:771-774.

Friedrich RW, Korsching SI (1997) Combinatorial and chemotopic odorant coding in the zebrafish olfactory bulb visualized by optical imaging. Neuron 18:737-752.

Fries P, Reynolds JH, Rorie AE, Desimone R (2001) Modulation of oscillatory neuronal synchronization by selective visual attention. Science 291:1560-1563.

Fujita I, Konishi M (1991) The role of GABAergic inhibition in processing of interaural time difference in the owls auditory-system. J Neurosci 11:722-739.

Galarreta M, Hestrin S (2001) Spike transmission and synchrony detection in networks of GABAergic interneurons. Science 292:2295-2299.

Gao Q, Yuan BB, Chess A (2000) Convergent projections of Drosophila olfactory neurons to specific glomeruli in the antennal lobe. Nat Neurosci 3:780-785.

Gasser HS (1950) Unmedullated fibers originating in dorsal root ganglia. J Gen Physiol 33:651-690.

Gelperin A (1999) Oscillatory dynamics and information processing in olfactory systems. J Exp Biol 202 (Pt 14):1855-1864.

Gelperin A, Tank DW (1990) Odor-modulated collective network oscillations of olfactory interneurons in a terrestrial mollusk. Nature 345:437-440.

Gerstner W, Kempter R, van Hemmen JL, Wagner H (1996) A neuronal learning rule for sub-millisecond temporal coding. Nature 383:76-81.

Gray CM, Konig P, Engel AK, Singer W (1989) Oscillatory responses in cat visual cortex exhibit inter-columnar synchronization which reflects global stimulus properties. Nature 338:334-337.

Gronenberg W (1999) Modality-specific segregation of input to ant mushroom bodies. Brain Behav Evol 54:85-95.

Gronenberg W, Holldobler B (1999) Morphologic representation of visual and antennal information in the ant brain. J Comp Neurol 412:229-240.

Grothe B, Sanes DH (1994) Synaptic inhibition influences the temporal coding properties of medial superior olivary neurons: An in vitro study. J Neurosci 14:1701-1709.

Grunewald B (1999a) Morphology of feedback neurons in the mushroom body of the honeybee, Apis mellifera. J Comp Neurol 404:114-126.

Grunewald B (1999b) Physiological properties and response modulations of mushroom body feedback neurons during olfactory learning in the honeybee, Apis mellifera. J Comp Physiol 185:565-576.

Grunewald B (2003) Differential expression of voltage-sensitive K(+) and Ca(2+) currents in neurons of the honeybee olfactory pathway. J Exp Biol 206:117-129.

Haberly LB (1997) Olfactory cortex. In: The synaptic organization of the brain, 4th Edition (Shepherd GM, ed). New York: Oxford University Press.

Hammer M, Menzel R (1995) Learning and memory in the honeybee. J Neurosci 15:1617-1630.

Hansson BS, Anton S (2000) Function and morphology of the antennal lobe: New developments. Annu Rev Entomol 45:203-231.

Heisenberg M (1998) What do the mushroom bodies do for the insect brain? An introduction. Learn Mem 5:1-10.

Heisenberg M (2003) Mushroom body memoir: From maps to models. Nat Rev Neurosci 4:266-275.

Heisenberg M, Borst A, Wagner S, Byers D (1985) Drosophila mushroom body mutants are deficient in olfactory learning. J Neurogenet 2:1-30.

Hildebrand JG, Shepherd GM (1997) Mechanisms of olfactory discrimination: Converging evidence for common principles across phyla. Annu Rev Neurosci 20:595-631.

Holub A, Laurent G, Perona P (2002) A digital antennal lobe for pattern equalization: Analysis and design. In: Advances in Neural Information Processing Systems 15. Vancouver, Canada.

Homberg U, Montague RA, Hildebrand JG (1988) Anatomy of antenno-cerebral pathways in the brain of the sphinx moth Manduca-sexta. Cell Tissue Res 254:255-281.

Honegger HW, Schurmann FW (1975) Cobalt sulfide staining of optic fibers in brain of cricket, Gryllus-campestris. Cell Tissue Res 159:213-225.

Howard J, Blakeslee B, Laughlin SB (1987) The intracellular pupil mechanism and photoreceptor signal - noise ratios in the fly Lucilia-cuprina. Proc R Soc Lond Ser B-Biol Sci 231:415-435.

Howard MW, Rizzuto DS, Caplan JB, Madsen JR, Lisman J, Aschenbrenner-Scheibe R, Schulze-Bonhage A, Kahana MJ (2003) Gamma oscillations correlate with working memory load in humans. Cereb Cortex 13:1369-1374.

Hubel DH, Wiesel TN (1962) Receptive fields, binocular interaction and functional architecture in the cat's visual cortex. J Physiol 160:106-154.

Hughes JR, Mazurowski JA (1962) Studies on supracallosal mesial cortex of unanesthetized, conscious mammals .2. Monkey B responses from olfactory bulb. Electroencephalogr Clin Neurophysiol 14:635-645.

Jefferis G, Marin EC, Stocker RF, Luo LQ (2001) Target neuron prespecification in the olfactory map of Drosophila. Nature 414:204-208.

Johnston D, Magee JC, Colbert CM, Christie BR (1996) Active properties of neuronal dendrites. Annu Rev Neurosci 19:165-186.

Joris PX, Smith PH, Yin TCT (1998) Coincidence detection in the auditory system: 50 years after Jeffress. Neuron 21:1235-1238.

Kanerva P (1988) Sparse distributed memory. Cambridge, MA: MIT Press.

Keil TA (1982) Contacts of pore tubules and sensory dendrites in antennal chemosensilla of a silkmoth - demonstration of a possible pathway for olfactory molecules. Tissue Cell 14:451-462.

Keil TA (1989) Fine-structure of the pheromone-sensitive sensilla on the antenna of the hawkmoth, Manduca-sexta. Tissue Cell 21:139-151.

Kempter R, Gerstner W, van Hemmen JL, Wagner H (1998) Extracting oscillations. Neuronal coincidence detection with noisy periodic spike input. Neural Comput 10:1987-2017.

Kenyon FC (1896) The brain of the bee. J Comp Neurol 6:133-210.

Ketchum KL, Haberly LB (1993) Synaptic events that generate fast oscillations in piriform cortex. J Neurosci 13:3980-3985.

Konig P, Engel AK, Singer W (1996) Integrator or coincidence detector? The role of the cortical neuron revisited. Trends Neurosci 19:130-137.

Lam YW, Cohen LB, Wachowiak M, Zochowski MR (2000) Odors elicit three different oscillations in the turtle olfactory bulb. J Neurosci 20:749-762.

Larkum ME, Zhu JJ, Sakmann B (1999) A new cellular mechanism for coupling inputs arriving at different cortical layers. Nature 398:338-341.

Laughlin SB (2001) Energy as a constraint on the coding and processing of sensory information. Curr Opin Neurobiol 11:475-480.

Laughlin SB, Sejnowski TJ (2003) Communication in neuronal networks. Science 301:1870-1874.

Laurent G (1990) Voltage-dependent nonlinearities in the membrane of locust nonspiking local interneurons, and their significance for synaptic integration. J Neurosci 10:2268-2280.

Laurent G (1996) Dynamical representation of odors by oscillating and evolving neural assemblies. Trends Neurosci 19:489-496.

Laurent G (1999) A systems perspective on early olfactory coding. Science 286:723-728.

Laurent G (2002) Olfactory network dynamics and the coding of multidimensional signals. Nat Rev Neurosci 3:884-895.

Laurent G, Naraghi M (1994) Odorant-induced oscillations in the mushroom bodies of the locust. J Neurosci 14:2993-3004.

Laurent G, Davidowitz H (1994) Encoding of olfactory information with oscillating neural assemblies. Science 265:1872-1875.

Laurent G, Seymour-Laurent KJ, Johnson K (1993) Dendritic excitability and a voltage-gated calcium current in locust nonspiking local interneurons. J Neurophysiol 69:1484-1498.

Laurent G, Wehr M, Davidowitz H (1996) Temporal representations of odors in an olfactory network. J Neurosci 16:3837-3847.

Laurent G, Stopfer M, Friedrich RW, Rabinovich MI, Volkovskii A, Abarbanel HD (2001) Odor encoding as an active, dynamical process: Experiments, computation, and theory. Annu Rev Neurosci 24:263-297.

Lee JK, Strausfeld NJ (1990) Structure, distribution and number of surface sensilla and their receptor-cells on the olfactory appendage of the male moth Manduca-sexta. J Neurocytol 19:519-538.

Leitch B, Laurent G (1996) GABAergic synapses in the antennal lobe and mushroom body of the locust olfactory system. J Comp Neurol 372:487-514.

Lennie P (2003) The cost of cortical computation. Curr Biol 13:493-497.

Levy WB, Baxter RA (1996) Energy efficient neural codes. Neural Comput 8:531-543.

Li Y, Strausfeld NJ (1997) Morphology and sensory modality of mushroom body extrinsic neurons in the brain of the cockroach, Periplaneta americana. J Comp Neurol 387:631-650.

Li Y, Strausfeld NJ (1999) Multimodal efferent and recurrent neurons in the medial lobes of cockroach mushroom bodies. J Comp Neurol 409:647-663.

Linster C, Smith BH (1999) Generalization between binary odor mixtures and their components in the rat. Physiol Behav 66:701-707.

Livermore A, Laing DG (1996) Influence of training and experience on the perception of multicomponent odor mixtures. J Exp Psychol-Hum Percept Perform 22:267-277.

Lucke J, von der Malsburg C (2004) Rapid processing and unsupervised learning in a model of the cortical macrocolumn. Neural Comput 16:501-533.

MacLeod K, Laurent G (1996) Distinct mechanisms for synchronization and temporal patterning of odor-encoding neural assemblies. Science 274:976-979.

MacLeod K, Backer A, Laurent G (1998) Who reads temporal information contained across synchronized and oscillatory spike trains? Nature 395:693-698.

Margulis M, Tang CM (1998) Temporal integration can readily switch between sublinear and supralinear summation. J Neurophysiol 79:2809-2813.

Marin EC, Jefferis GS, Komiyama T, Zhu H, Luo L (2002) Representation of the glomerular olfactory map in the Drosophila brain. Cell 109:243-255.

Markram H, Lubke J, Frotscher M, Sakmann B (1997) Regulation of synaptic efficacy by coincidence of postsynaptic APs and EPSPs. Science 275:213-215.

Marr D (1969) A theory of cerebellar cortex. J Physiol-London 202:437-470.

Martin C, Gervais R, Hugues E, Messaoudi B, Ravel N (2004) Learning modulation of odor-induced oscillatory responses in the rat olfactory bulb: A correlate of odor recognition? J Neurosci 24:389-397.

Martin RD (1996) Scaling of the mammalian brain: The maternal energy hypothesis. News Physiol Sci 11:149-156.

Masson C, Mustaparta H (1990) Chemical information-processing in the olfactory system of insects. Physiol Rev 70:199-245.

McCollum J, Larson J, Otto T, Schottler F, Granger R, Lynch G (1991) Short-latency single unit processing in olfactory cortex. J Cogn Neurosci 3:293-299.

McGuire SE, Le PT, Davis RL (2001) The role of Drosophila mushroom body signaling in olfactory memory. Science 293:1330-1333.

McGuire SE, Le PT, Osborn AJ, Matsumoto K, Davis RL (2003) Spatiotemporal rescue of memory dysfunction in Drosophila. Science 302:1765-1768.

Mizunami M, Weibrecht JM, Strausfeld NJ (1998a) Mushroom bodies of the cockroach: Their participation in place memory. J Comp Neurol 402:520-537.

Mizunami M, Okada R, Li Y, Strausfeld NJ (1998b) Mushroom bodies of the cockroach: Activity and identities of neurons recorded in freely moving animals. J Comp Neurol 402:501-519.

Mobbs PG (1982) The brain of the honeybee Apis mellifera. 1. The connections and spatial organization of the mushroom bodies. Phil Trans R Soc Lond B 298:309-354.

Mombaerts P, Wang F, Dulac C, Chao SK, Nemes A, Mendelsohn M, Edmondson J, Axel R (1996) Visualizing an olfactory sensory map. Cell 87:675-686.

Nemitz JW, Goldberg SJ (1983) Neuronal responses of rat pyriform cortex to odor stimulation: An extracellular and intracellular study. J Neurophysiol 49:188-203.

Neville KR, Haberly LB (2003) Beta and gamma oscillations in the olfactory system of the urethane-anesthetized rat. J Neurophysiol 90:3921-3930.

Nilsson GE (1996) Brain and body oxygen requirements of Gnathonemus petersii, a fish with an exceptionally large brain. J Exp Biol 199:603-607.

Okada M (1996) Notions of associative memory and sparse coding. Neural Netw 9:1429-1458.

O'Keefe J, Recce ML (1993) Phase relationship between hippocampal place units and the EEG theta-rhythm. Hippocampus 3:317-330.

Oleskevich S (1999) Cholinergic synaptic transmission in insect mushroom bodies in vitro. J Neurophysiol 82:1091-1096.

Oleskevich S, Clements JD, Srinivasan MV (1997) Long-term synaptic plasticity in the honeybee. J Neurophysiol 78:528-532.

Olshausen BA, Field DJ (1996) Emergence of simple-cell receptive field properties by learning a sparse code for natural images. Nature 381:607-609.

Ottoson D (1959) Comparison of slow potentials evoked in the frogs nasal mucosa and olfactory bulb by natural stimulation. Acta Physiol Scand 47:149-159.

Parker AJ, Newsome WT (1998) Sense and the single neuron: Probing the physiology of perception. Annu Rev Neurosci 21:227-277.

Pascual A, Preat T (2001) Localization of long-term memory within the Drosophila mushroom body. Science 294:1115-1117.

Patel AD, Balaban E (2000) Temporal patterns of human cortical activity reflect tone sequence structure. Nature 404:80-84.

Pentz M, Shott M (1988) Handling experimental data. Philadelphia: Open University Press.

Perez-Orive J, Durand DM (2000) Modeling study of peripheral nerve recording selectivity. IEEE Trans Rehabil Eng 8:320-329.

Perez-Orive J, Bazhenov M, Laurent G (2004) Intrinsic and circuit properties favor coincidence detection for decoding oscillatory input. J Neurosci. In press.

Perez-Orive J, Mazor O, Turner GC, Cassenaer S, Wilson RI, Laurent G (2002) Oscillations and sparsening of odor representations in the mushroom body. Science 297:359-365.

Pesaran B, Pezaris JS, Sahani M, Mitra PP, Andersen RA (2002) Temporal structure in neuronal activity during working memory in macaque parietal cortex. Nat Neurosci 5:805-811.

Pouille F, Scanziani M (2001) Enforcement of temporal fidelity in pyramidal cells by somatic feed-forward inhibition. Science 293:1159-1163.

Pouzat C, Mazor O, Laurent G (2002) Using noise signature to optimize spike-sorting and to assess neuronal classification quality. J Neurosci Methods 122:43-57.

Power DV (1997) Immunocytochemical detection of amino acid neurotransmitters in paraformaldehyde-fixed tissues. In: Neurotransmitter methods (Rayne RC, ed). Totowa, NJ: Humana Press.

Prut Y, Vaadia E, Bergman H, Haalman I, Slovin H, Abeles M (1998) Spatiotemporal structure of cortical activity: Properties and behavioral relevance. J Neurophysiol 79:2857-2874.

Pumphrey RJ, Young JZ (1938) The rates of conduction of nerve fibers of various diameters in cephalopods. J Exp Biol 15:453-466.

Purves RD (1981) Microelectrode methods for intracellular recording and ionophoresis. London: Academic Press.

Rein K, Zockler M, Mader MT, Grubel C, Heisenberg M (2002) The Drosophila standard brain. Curr Biol 12:227-231.

Riehle A, Grun S, Diesmann M, Aertsen A (1997) Spike synchronization and rate modulation differentially involved in motor cortical function. Science 278:1950-1953.

Ritchie JM (1995) Physiology of axons. In: The axon; structure, function and pathophysiology (Waxman SG, Kocsis JD, Stys PK, eds). New York: Oxford University Press.

Rodriguez E, George N, Lachaux JP, Martinerie J, Renault B, Varela FJ (1999) Perception's shadow: Long-distance synchronization of human brain activity. Nature 397:430-433.

Rolls ET, Tovee MJ (1995) Sparseness of the neuronal representation of stimuli in the primate temporal visual cortex. J Neurophysiol 73:713-726.

Rybak J, Menzel R (1998) Integrative properties of the Pe1 neuron, a unique mushroom body output neuron. Learn Mem 5:133-145.

Salinas E, Sejnowski TJ (2000) Impact of correlated synaptic input on output firing rate and variability in simple neuronal models. J Neurosci 20:6193-6209.

Salinas E, Sejnowski TJ (2001) Correlated neuronal activity and the flow of neural information. Nat Rev Neurosci 2:539-550.

Satou M (1990) Synaptic organization, local neuronal circuitry, and functional segregation of the teleost olfactory-bulb. Prog Neurobiol 34:115-142.

Schafer S, Bicker G (1986) Distribution of GABA-like immunoreactivity in the brain of the honeybee. J Comp Neurol 246:287-300.

Schafer S, Rosenboom H, Menzel R (1994) Ionic currents of Kenyon cells from the mushroom body of the honeybee. J Neurosci 14:4600-4612.

Schiller J, Schiller Y (2001) NMDA receptor-mediated dendritic spikes and coincident signal amplification. Curr Opin Neurobiol 11:343-348.

Schwaerzel M, Heisenberg M, Zars T (2002) Extinction antagonizes olfactory memory at the subcellular level. Neuron 35:951-960.

Sederberg PB, Kahana MJ, Howard MW, Donner EJ, Madsen JR (2003) Theta and gamma oscillations during encoding predict subsequent recall. J Neurosci 23:10809-10814.

Shadlen MN, Newsome WT (1994) Noise, neural codes and cortical organization. Curr Opin Neurobiol 4:569-579.

Shadlen MN, Newsome WT (1998) The variable discharge of cortical neurons: Implications for connectivity, computation, and information coding. J Neurosci 18:3870-3896.

Shadlen MN, Movshon JA (1999) Synchrony unbound: A critical evaluation of the temporal binding hypothesis. Neuron 24:67-77.

Sherrington CS (1906) Integrative action of the nervous system. New Haven, CT: Yale University Press.

Siapas AG, Wilson MA (1998) Coordinated interactions between hippocampal ripples and cortical spindles during slow-wave sleep. Neuron 21:1123-1128.

Singer W (1999) Time as coding space? Curr Opin Neurobiol 9:189-194.

Singer W, Gray CM (1995) Visual feature integration and the temporal correlation hypothesis. Annu Rev Neurosci 18:555-586.

Sloper JJ, Powell TP (1979) Ultrastructural features of the sensori-motor cortex of the primate. Philos Trans R Soc Lond B Biol Sci 285:124-139.

Softky WR, Koch C (1993) The highly irregular firing of cortical cells is inconsistent with temporal integration of random EPSPs. J Neurosci 13:334-350.

Solomons TWG (1988) Organic chemistry, Fourth Edition. New York: John Wiley & Sons.

Steinbrecht RA (1980) Cryofixation without cryoprotectants - freeze substitution and freeze-etching of an insect olfactory receptor. Tissue Cell 12:73-100.

Steinmetz PN, Roy A, Fitzgerald PJ, Hsiao SS, Johnson KO, Niebur E (2000) Attention modulates synchronized neuronal firing in primate somatosensory cortex. Nature 404:187-190.

Steriade M, McCormick DA, Sejnowski TJ (1993) Thalamocortical oscillations in the sleeping and aroused brain. Science 262:679-685.

Stocker RF, Lienhard MC, Borst A, Fischbach KF (1990) Neuronal architecture of the antennal lobe in Drosophila- melanogaster. Cell Tissue Res 262:9-34.

Stopfer M, Jayaraman V, Laurent G (2003) Intensity versus identity coding in an olfactory system. Neuron 39:991-1004.

Stopfer M, Bhagavan S, Smith BH, Laurent G (1997) Impaired odour discrimination on desynchronization of odour-encoding neural assemblies. Nature 390:70-74.

Strausfeld NJ (2002) Organization of the honey bee mushroom body: Representation of the calyx within the vertical and gamma lobes. J Comp Neurol 450:4-33.

Strausfeld NJ, Li Y (1999a) Organization of olfactory and multimodal afferent neurons supplying the calyx and pedunculus of the cockroach mushroom bodies. J Comp Neurol 409:603-625.

Strausfeld NJ, Li Y (1999b) Representation of the calyces in the medial and vertical lobes of cockroach mushroom bodies. J Comp Neurol 409:626-646.

Strausfeld NJ, Hansen L, Li Y, Gomez RS, Ito K (1998) Evolution, discovery, and interpretations of arthropod mushroom bodies. Learn Mem 5:11-37.

Stuart GJ, Sakmann B (1994) Active propagation of somatic action potentials into neocortical pyramidal cell dendrites. Nature 367:69-72.

Tanabe T, Iino M, Takagi SF (1975) Discrimination of odors in olfactory bulb, pyriform-amygdaloid areas, and orbitofrontal cortex of the monkey. J Neurophysiol 38:1284-1296.

Tanaka N, Awasaki T, Shimada T, Ito K (2004) Integration of chemosensory pathways in the Drosophila second-order olfactory centers. Curr Biol 14:449 - 457.

Tang S, Guo A (2001) Choice behavior of Drosophila facing contradictory visual cues. Science 294:1543-1547.

Technau G, Heisenberg M (1982) Neural reorganization during metamorphosis of the corpora pedunculata in Drosophila-melanogaster. Nature 295:405-407.

Traub RD (1982) Simulation of intrinsic bursting in CA3 hippocampal neurons. Neuroscience 7:1233-1242.

Treves A, Rolls ET (1991) What determines the capacity of autoassociative memories in the brain. Netw-Comput Neural Syst 2:371-397.

Tseng GF, Haberly LB (1988) Characterization of synaptically mediated fast and slow inhibitory processes in piriform cortex in an in vitro slice preparation. J Neurophysiol 59:1352-1376.

Tully T, Quinn WG (1985) Classical conditioning and retention in normal and mutant Drosophila melanogaster. J Comp Physiol [A] 157:263-277.

Uchida N, Takahashi YK, Tanifuji M, Mori K (2000) Odor maps in the mammalian olfactory bulb: Domain organization and odorant structural features. Nat Neurosci 3:1035-1043.

Vaadia E, Haalman I, Abeles M, Bergman H, Prut Y, Slovin H, Aertsen A (1995) Dynamics of neuronal interactions in monkey cortex in relation to behavioural events. Nature 373:515-518.

van Swinderen B, Greenspan RJ (2003) Salience modulates 20-30 Hz brain activity in Drosophila. Nat Neurosci 6:579-586.

Vinje WE, Gallant JL (2000) Sparse coding and decorrelation in primary visual cortex during natural vision. Science 287:1273-1276.

von der Malsburg C, Schneider W (1986) A neural cocktail-party processor. Biol Cybern 54:29-40.

Vosshall LB, Wong AM, Axel R (2000) An olfactory sensory map in the fly brain. Cell 102:147-159.

Vosshall LB, Amrein H, Morozov PS, Rzhetsky A, Axel R (1999) A spatial map of olfactory receptor expression in the Drosophila antenna. Cell 96:725-736.

Waddell S, Armstrong JD, Kitamoto T, Kaiser K, Quinn WG (2000) The amnesiac gene product is expressed in two neurons in the Drosophila brain that are critical for memory. Cell 103:805-813.

Wehr M, Laurent G (1996) Odour encoding by temporal sequences of firing in oscillating neural assemblies. Nature 384:162-166.

Wehr M, Laurent G (1999) Relationship between afferent and central temporal patterns in the locust olfactory system. J Neurosci 19:381-390.

Wehr M, Zador AM (2003) Balanced inhibition underlies tuning and sharpens spike timing in auditory cortex. Nature 426:442-446.

Wicklein M, Strausfeld NJ (2000) Organization and significance of neurons that detect change of visual depth in the hawk moth Manduca sexta. J Comp Neurol 424:356-376.

Williams SR, Stuart GJ (2002) Dependence of EPSP efficacy on synapse location in neocortical pyramidal neurons. Science 295:1907-1910.

Willmore B, Tolhurst DJ (2001) Characterizing the sparseness of neural codes. Network 12:255-270.

Wilson RI, Turner GC, Laurent G (2004) Transformation of olfactory representations in the Drosophila antennal lobe. Science 303:366-370.

Wong AM, Wang JW, Axel R (2002) Spatial representation of the glomerular map in the Drosophila protocerebrum. Cell 109:229-241.

Zars T, Fischer M, Schulz R, Heisenberg M (2000) Localization of a short-term memory in Drosophila. Science 288:672-675.

Zou Z, Horowitz LF, Montmayeur JP, Snapper S, Buck LB (2001) Genetic tracing reveals a stereotyped sensory map in the olfactory cortex. Nature 414:173-179.